Surface **M**odification of **P**oly(dimethylsiloxane) (**PDMS**) for **M**icrofluidic **D**evices

Jinwen **Z**hou

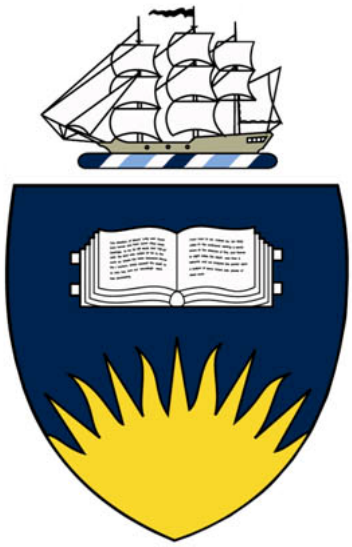

Flinders University

School of Chemical and Physical Sciences

Faculty of Science and Engineering

GPO Box 2100

Bedford Park, South Australia, 5042

Submitted November 2012

TABLE OF CONTENTS

ABSTRACT

Poly(dimethylsiloxane) (PDMS) is a popular material for microfluidic devices due to its relatively low cost, ease of fabrication, oxygen permeability and optical transmission characteristics. However, its highly hydrophobic surface is still the main factor limiting its wide application, in particular as a material for biointerfaces. This being the case, surface modification to tailor surface properties is required to render PDMS more practical for microfluidic applications.

This thesis focuses on three different PDMS surface modification techniques, including 1) thermal assisted hydrosilylation; 2) self-assembled molecule (SAM) assisted templating and 3) a combination of Soxhlet-extraction and plasma treatment. The modified PDMS surfaces were then used for a series of analytical applications, including DNA hybridization and cocaine detection. Finally, the fabrication of native and surface modified PDMS-based microfluidic devices is also presented. The content in each chapter is outlined in the following.

In Chapter 1, a comprehensive review of recent research regarding PDMS surface modification techniques is presented, including gas-phase processes, wet-chemical methods and the combination of gas-phase and wet-chemical methods. In addition, topographical and chemically patterned PDMS is discussed, as well as examples of the application of modified PDMS surfaces in microfluidics.

Chapter 2 is the methodology chapter, which describes the three PDMS surface modification techniques used in this thesis. It also describes the fabrication process involved in the making of PDMS-based microfluidic devices. Moreover, details of the surface characterization techniques used for the analysis of the PDMS surfaces are described. These techniques include water contact angle (WCA) measurements, Fourier transform infrared-attenuated total reflection (FTIR-ATR) spectroscopy, X-ray photoelectron spectroscopy (XPS), atomic force microscopy (AFM), streaming zeta-potential analysis, electroosmotic flow (EOF) measurements and fluorescence microscopy. Experimental details for the experiments involving DNA hybridization on

modified PDMS are also described.

In Chapter 3, we report on a cheap, easy and highly repeatable PDMS surface modification method by heating pre-cured PDMS with a thin film of undecylenic acid (UDA) at 80 ºC in an oven. A hydrosilylation reaction between the UDA and the PDMS curing agent was induced during heating. The results showed the modified PDMS surfaces became more hydrophilic compared to native PDMS and showed a more or less constant WCA for up to 30 d storage in air. In addition, the stability of the modified PDMS surface was further improved by reducing the weight ratio of PDMS base and curing agent from 10:1 to 5:1.

In Chapter 4, we present a chemical modification strategy for PDMS by curing a mixture of 2 wt % UDA in PDMS prepolymer on a pretreated gold coated glass slide. The pretreatment of the gold slide was achieved by coating the gold with a self-assembled monolayer of 3-mercaptopropionic acid (MPA). During curing of the UDA/PDMS prepolymer on the MPA/gold coated slide the hydrophilic UDA carboxyl moieties diffuse towards the hydrophilic MPA carboxyl moieties on the gold surface. This diffusion of UDA within the PDMS prepolymer to the surface is a direct result of surface energy minimization. Once completely cured, the PDMS was peeled off the gold substrate, thereby exposing the interfacial carboxyl groups. These groups were then available for subsequent attachment of 5'-amino-terminated oligonucleotides *via* amide linkages. Finally, fluorescently tagged complementary oligonucleotides were successfully hybridized to this surface, as determined by fluorescence microscopy.

In Chapter 5, the surface modification of PDMS was carried out by using a 2-step plasma modification with Ar followed by acrylic acid (AAc). The stability of the modified PDMS surface was further improved by Soxhlet-extracting the PDMS with hexane prior to plasma treatment. 5´-amino-terminated oligonucleotides were covalently attached to the PAAc modified PDMS surface *via* carbodiimide coupling. Results show that the covalently tethered oligonucleotides can successfully capture fluorescein-labeled complementary oligonucleotides *via* hybridization, which were visualized using fluorescence microscopy.

In Chapter 6, we report on an optical aptamer sensor for cocaine detection by first using minor groove binder based energy transfer (MBET) technique. First, a

carboxyl-functionalized PDMS was prepared using SAM assisted templating as described in Chapter 4. A cocaine sensor was then fabricated on this carboxyl-functionalized PDMS surface by covalently immobilizing DNA aptamers *via* amide linkages. The cocaine sensitive fluorescein isothiocyanate (FITC)-labeled aptamer underwent a conformational change from partial single-stranded DNA to a double stranded T-junction in the presence of the target. The DNA minor groove binder Hoechst 33342 selectively bound to the double stranded T-junction, bringing the dye within the Förster radius of FITC. This process initiated MBET, thereby reporting on the presence of cocaine. In addition, this aptamer sensor was also implemented for cocaine detection in solution.

In Chapter 7, the fabrication of microfluidic devices based on the native PDMS and/or the modified PDMS is described. First standard soft-lithography was used to produce PDMS microchannels. Then, the sealing of the microchannels was achieved with the assistance of thermal treatment or an O_2 plasma. Finally, for the modified PDMS-based devices, the presence of reactive carboxyl groups from the initial UDA or AAc plasma treatment were verified by the immobilization of Lucifer Yellow CH dye in modified PDMS microchannels.

In Chapter 8, an overall comparison between the three different PDMS surface modification methods is provided and the future perspectives are outlined.

DECLARATION

I certify that this thesis does not incorporate without acknowledgment any material previously submitted for a degree or diploma in any university; and that to the best of my knowledge and belief it does not contain any material previously published or written by another person except where due reference is made in the text.

Signed  Date 29/11/2012

ACKNOWLEDGEMENTS

I owe my deepest gratitude to my two supervisors Prof. Nicolas H. Voelcker and Ass. Prof. Amanda V. Ellis. Thank you both so very much for introducing me to this excited project and your invaluable support, advice, time, encouragement, patience and wisdom throughout my postgraduate study. This thesis would not have been possible without your great input.

I would like to thank everyone in Voelcker's group who has helped me throughout this project. Especially thanks to Steve McInnes for your time and help with my written English and experimental assistance. Thanks to Abdul Mutalib Md Jani for some discussions and suggestions. Thanks to Martin Cole for your help with XPS analysis. I also would like to thank Hilton Kobus for supplying cocaine and structural analogues.

Many thanks to those working in the mechanical and electronic workshops at Flinders University for your guidance and innovations.

I am grateful to Amit Asthana from ANFF-Q for sharing your acknowledge and skills of the fabrication of SU-8 masters.

I wish to acknowledge the National Institute of Forensic Science, Australia, and Faculty of Science and Engineering Research Award, Flinders University, for financial support.

Finally, many, many thanks for the love and support from my family. To my beloved husband Fang, who deserves special thanks for always being supportive and patient.

LIST OF PUBLICATION

Papers arising from Chapter 1

1. Zhou, J. W., Ellis, A. V., Voelcker, N. H., Recent developments in poly(dimethylsiloxane) surface modification for microfluidic devices. *Electrophoresis* 2010, *31,* 2-16. http://onlinelibrary.wiley.com/doi/10.1002/elps.200900475/abstract

2. Zhou, J. W., Khodakov, D. A., Ellis, A. V., Voelcker, N. H., Surface modification for PDMS-based microfluidic devices. *Electrophoresis* 2012, *33,* 89-104. http://onlinelibrary.wiley.com/doi/10.1002/elps.201100482/abstract

Papers arising from Chapter 3

3. Zhou, J. W., McInnes, S. J. P., Mutalib Md Jani, A., Ellis, A. V., Voelcker, N. H., One-step surface modification of poly(dimethylsiloxane) by undecylenic acid. *Proceedings of SPIE* 2008, *7267 (726719)*, 1-10. http://spie.org/x648.html?product_id=810101

Papers arising from Chapter 4

4. Zhou, J. W., Voelcker, N. H., Ellis, A. V., Simple surface modification of poly(dimethylsiloxane) for DNA hybridization. *Biomicrofluidics* 2010, *4*, 046504. http://bmf.aip.org/resource/1/biomgb/v4/i4/p046504_s1

5. Zhou, J. W., Ellis, A. V., Kobus H., Voelcker, N. H., Aptamer sensor for cocaine using minor groove binder based energy transfer (MBET). *Analytica Chimica Acta* 2012, *719,* 76-81. http://www.sciencedirect.com/science/article/pii/S0003267012000797

Papers arising from Chapter 5

6. Zhou, J. W., Ellis, A. V., Voelcker, N. H., Poly(dimethylsiloxane) surface modification by plasma treatment for DNA hybridization applications. *Journal of Nanoscience and Nanotechnology* 2010, *10,* 7266-7270. http://www.ingentaconnect.com/content/asp/jnn/2010/00000010/00000011/art00061

Papers arising from Chapter 6

7. Zhou, J. W., Ellis, A. V., Kobus H., Voelcker, N. H., Aptamer sensor for cocaine using minor groove binder based energy transfer (MBET). *Analytica Chimica Acta* 2012, *719,* 76-81.

http://www.sciencedirect.com/science/article/pii/S0003267012000797

Other papers

8. Mutalib Md Jani, A., Zhou, J. W., Nussio, M. R., Losic, D., Shapter, J. G., Voelcker, N. H., Pore spanning lipid bilayers on silanised nanoporous alumina membranes. *Proceedings of SPIE* 2008, *7267 (2670T)*, 1-10.

LIST OF ABBREVIATIONS

AA	ascorbic acid
AAc	acrylic acid
AAm	acrylamide
AFM	atomic force microscope
AHPCS	allylhydridopolycarbosilane
Ala	alanine
AMPS	2-acrylamido-2-methyl-1-propanesulfonic acid
4-AP	4-aminophenol
AP	alkaline phosphatase
APDMES	3-aminopropyldimethylethoxysilane
APTES	3-aminopropyltriethoxysilane
APTMS	3-aminopropyltrimethoxysilane
Arg	arginine
Asn	asparagine
Asp	aspartic acid
ATRP	atom transfer radical polymerization
BAS	1-butyl-3-methylimidazolium dodecanesulfonate
BGE	background electrolyte
$BMImBF_4$	1-butyl-3-methylimidazolium tetrafluoroborate
BODIPY® FL CASE	*N*-(4,4-difluoro-5,7-dimethyl-4-bora-3a,4a-diaza-s-indacen e-3propionyl)cysteic acid, succinimidyl ester
BP	benzophenone
BSA	bovine serum albumin
CAD	computer-aided design
CE	capillary electrophoresis
CEC	capillary electrochromatography
Chit	chitosan
COMOSS	collocated monolith support structure
CPTCS	3-chloropropyltrichlorosilane

CTMS	chlorotrimethylsilane
CVD	chemical vapor deposition
Cys	cysteine
3D	three dimensional
DA	dapamin
DBA	dobuamine
DDAB	didodecyldimethylammoniumbromide
DDM	n-Dodecyl-β-D-maltoside
DNA	deoxyribonucleic acid
DOC	sodium deoxycholate
dsDNA	double stranded deoxyribonucleic acid
ECM	extracellular matrix
EDAC	*N*-(3-dimethylaminopropyl)-*N´*-ethylcarbodiimide hydrochloride
EDTA	ethylenediaminetetraacetic acid
μ_{eo}	electroosmotic mobility
EOF	electroosmotic flow
EP	epinephrine
ERα	estrogen receptor α
FAM	6-carboxyfluorescein
FITC	fluorescein isothiocyanate
FRET	fluorescence resonance energy transfer
FTIR-ATR	Fourier transform infrared-attenuated total reflection
Gln	glutamine
Glu	glutamic acid
Gly	glycine
GMA	glycidyl methacrylate
GPTMS	3-glycidoxypropyltrimethoxysilane
HA	hyaluronic acid
HEPES	4-(2-hydroxyethyl)-1-piperazineethanesulfonic acid
His	histidine
HPGs	hyperbranched polyglycerols
h-PSMA	hydrolyzed poly(styrene-*co*-maleic anhydride)

HQ	hydroquinone
HSA	human serum albumin
5-HT	5-hydroxytryptamine
Ig	immunoglobulin
Ile	isoleucine
IPA	isopropyl alcohol
LBL	layer-by-layer
LPEI	linear polyethyleneimine
Lys	lysine
MA	maleic anhydride
MAAc	methacrylic acid
MALDI	matrix-assisted laser desorption/ionization
MBET	minor groove binder based energy transfer
Met	methionine
2-MP	2-mercaptopyridine
MPA	3-mercaptopropionic acid
mPEG	methyl-poly(ethylene glycol)
MPTMS	3-mercaptopropyltrimethoxysilane
MS	mass spectrometry
NHS	*N*-hydroxysuccinimide
O/W	oil-in-water
PA	phosphatidic acid
PAAc	poly(acrylic acid)
PAAm	Poly(acrylamide)
PAH	poly(aromatic hydrocarbon)
PAS	poly(4-aminostyrene)
PBS	phosphate buffered saline
PDDA	poly (diallyldimethylammonium chloride)
P(DMA-*co*-GMA)	poly(dimethylacrylamide-*co*-glycidyl methacrylate)
PDMS	poly(dimethylsiloxane)
PE	poly(ethylene)
PEG	poly(ethylene glycol)
PEGMEM	poly(ethylene glycol) methyl ether methacrylate

PEI	poly(ethyleneimine)
PEMEA	propylene glycol methyl ether acetate
PEMs	polyelectrolyte multilayers
PEO	poly(ethylene oxide)
PGA	poly(L-glutamic acid)
PGMA	poly(glycidyl methacrylate)
Phe	phenylalanine
PHMA	poly(hydromethylsiloxane)
PLLA	poly(L-lactic acid)
PMAAc	poly(methacrylic acid)
PNIPAAm	poly [*N*-isopropyl acrylamide]
P(NIPAAm-*co*-AAc)	poly(*N*-isopropyl acrylamide-*co*-acrylic acid)
p-PDA	p-phenylenediamine
PPEGMA	poly(poly(ethylene glycol)methacrylate)
PPO	poly(propylene oxide)
Pro	proline
PSCA	prostate stem cell antigenv
PSS	poly(sodium 4-styrenesulfonate)
PTX	paclitaxel
PVA	poly(vinyl alcohol)
PVA-*g*-GMA	poly(vinyl alcohol)-*g*-glycidyl methacrylate
PVC	poly(vinyl chloride)
PVP	poly(vinylpyrrolidone)
PVP-*g*-GMA	Poly(vinylpyrrolidone)-*g*-glycidyl methacrylate
QD	quantum dot
RB	rhodamine B
RGDS	Arg-Gly-Asp-Ser
RMS	root mean square
RSD	relative standard deviation
SAMs	self-assembled monolayers
SDS	sodium dodecyl sulfate
SELEX	systematic evolution of ligands by exponential enrichment
Ser	serine

SP-PCRs	solid phase-polymerase chain reactions
STB	sodium tetraborate
TAPS	*N*-tris(hydroxymethyl)methyl-3-aminopropanesulfonic acid
TBE	Tris-borate-EDTA
TEOS	tetraethyl orthosilicate
TFOS	trichloro(1H, 1H, 2H, 2H-perfluorooctyl)silane
Thr	threonine
TOF	time of flight
Tris	tris(hydroxymethyl)aminomethane
Try	tryptophan
TTE	Tris-TAPS-EDTA
Tyr	tyrosine
UDA	undecylenic acid
UV	ultraviolet
UVO	ultraviolet/ozone
Val	valine
WCA	water contact angle
W/O	water-in-oil
W/O/O	water-in-oil-in-oil
W/O/W	water-in-oil-in-water
XPS	x-ray photoelectron spectroscopy

LIST OF FIGURES

LIST OF SCHEMES

LIST OF TABLES

CHAPTER 1 INTRODUCTION

The content of this chapter is based on references [1, 2].

Abstract

Poly(dimethylsiloxane) (PDMS) is enjoying continued and ever increasing popularity as the material of choice for microfluidic devices due to its low cost, ease of fabrication, oxygen permeability and optical transparency. However, PDMS's hydrophobicity and fast hydrophobic recovery after surface hydrophilization, attributed to its low glass transition temperature of less than -120 ˚C, negatively impacts on the performance of PDMS-based microfluidic device components. This issue has spawned a flurry of research to devise longer-lasting surface modifications of PDMS, with particular emphasis on microfluidic applications. This chapter will present recent research on surface modifications of PDMS using techniques ranging from metal layer coatings and layer-by-layer (LBL) depositions to dynamic surfactant treatments and the adsorption of amphipathic proteins, as well as hydrosilylation-based surface modification. We will also discuss significant advances that have been made with a broad palette of gas-phase processing methods including plasma processing, sol-gel coatings, and chemical vapor deposition (CVD). Recent efforts to generate topographical and chemical patterns on PDMS will be also discussed. Finally, we will present examples of applications of modified PDMS surfaces in microfluidics, in areas such as molecular separations, biomolecular detection *via* immunoassays, cell culture in microchannels and emulsion formation.

1.1 Overview

In the last decade, microfluidic devices have received much attention [3-10], due to their competitive advantages, especially in regards to reduced sample and reagent consumption, analysis time and increased automation [11]. Typically, devices are fabricated from silicon, glass and polymers, or combinations of these materials. A recent review by Henares *et al.* [12] summarizes the advantages and disadvantages of these three materials. Briefly, the

main advantages of silicon lie in its superior thermal conductivity and the availability of advanced fabrication and microstructure technologies, originating from the semiconductor industry. A drawback, however, is silicon's optical opacity, which limits its applications in real-time optical detection. Glass is a far more promising alternative with well-defined surface chemistries, good electroosmotic flow (EOF) characteristics and superior optical transparency [12]. However, when considering cost, time and labor, polymers and elastomers are becoming more and more attractive for use in microfluidic devices. Some of the various polymers typically used include poly(styrene) [13], poly(propylene) [13], poly(vinyl chloride) (PVC) [14], poly(carbonate) [13, 15, 16], poly(methyl methacrylate) [15, 17, 18] and poly(dimethylsiloxane) (PDMS) [19-26]. Among these, PDMS is by far the dominant polymeric material utilized for microfluidics. This can be attributed to its numerous salient features including its elastomeric properties, biocompatibility, gas permeability, optical transparency, ease of molding into (sub)micrometer features, ease of bonding to itself and glass, relatively high chemical inertia, and low manufacturing costs [27, 28].

Although PDMS has many merits, its hydrophobicity makes introducing aqueous solutions into the microchannels of PDMS-based devices difficult. In addition, EOF, often quantitatively expressed as the electroosmotic mobility (μ_{eo}), is often unstable, and hydrophobic analytes can readily adsorb onto the PDMS surface interfering with analysis. Consequently, surface modifications are critical to successfully inhibit non-specific adsorption of hydrophobic species, improving wettability and stabilizing and improving EOF.

In this chapter, we present a review on the more recent PDMS surface modification methods, which fall squarely into three categories: gas-phase processing, wet chemical methods and a combination of both. Gas-phase processing methods include plasma oxidation, ultraviolet (UV) irradiation, chemical vapor deposition (CVD) and sputter coating of metal compounds. Wet chemical methods include layer-by-layer (LBL) deposition, sol–-gel coatings, silanization, dynamic modification with surfactants, protein adsorption and hydrosilylation-based surface modification. Finally, the combinations of gas-phase and wet chemical methods include silanization, graft polymer coating and LBL methods on PDMS pretreated by methods such as plasma oxidation or UV. A comprehensive comparison of the different PDMS surface modification methods has been

listed in Table 1-1, including the properties, advantages, limitations and relevant characterization techniques. We will proceed by discussing these surface modification methods according to the above categories. In addition, the generation of chemically or topographically patterned PDMS surfaces will also be discussed. The chapter will end by highlighting applications where modified PDMS based microfluidics have engendered analytical achievements such as biomolecular separations, capture or release of proteins, molecular detection *via* immunoassays, cell-based assays and emulsion formation. Performance will be compared between the different examples, as much as is possible.

Table 1-1. Comparison of different PDMS surface modification methods (and submethods).

Surface modification methods	Sub-methods	Properties	Advantages	Limitations	Relevant characterization techniques	Relevant references
Gas-phase processing	Plasma treatment	Employing a partially ionized gas to dissociate and react with the substrate surface and create chemical functional groups	Short treatment time and easy operation	Hydrophobic recovery or other treatments required for reducing or avoiding the hydrophobicity recovery, such as Soxhlet-extraction. The Possibility of inducing cracking or mechanically weakening of the PDMS during process	WCA, FTIR, XPS, AFM, EOF	[29-36]
	UV treatment	Employing high energy photons to attack the siloxanes backbone of PDMS to form silica-like layer and Si-OH surface structure	Much deeper modification without cracks, compared to plasma	An order of magnitude slower required to achieve the same result, compared to plasma, and hydrophobicity recovery	WCA, FTIR	[37]
	CVD	Producing a thin film on a substrate surface by means of the deposition of gaseous molecules, which chemically react on the surface	The capability of producing highly dense and uniform films with good reproducibility and adhesion at reasonably high deposition rates, and the capability of coating complex shaped components	High temperatures used for pyrolysis step in some CVD processes		[38-41]

Table 1-1. (Continued)

Surface modification methods	Sub-methods	Properties	Advantages	Limitations	Relevant characterization techniques	Relevant references
	Coating with metals and metal oxides	Sputter coating metals on PDMS surface physically	Easy operation	No strong covalent bonding between metal layer and the native PDMS, and cracks induced easily during processing	WCA	[42-45]
Wet chemical methods	LBL deposition	Alternating adsorption of polyanions and polycations onto any substrate surface to produce polyelectrolyte multilayers	Simplicity, efficiency and thickness control at the nanoscale	No strong covalent bonding between the layers, and the modifier and the native PDMS. Organic solvent-free during modification process is required to avoid swelling of PDMS.	WCA, EOF,	[25, 46-55]
	Sol-gel coating	A polymerization process based on the phase transition of a liquid state, the "sol" containing suspended particles, to a solid-like state, the "gel."	High density and homogeneous	Swelling problem caused by the precursor solution and cracking problem during the gelation process	WCA, EOF	[56-59]

Table 1-1. (Continued)

Surface modification methods	Sub-methods	Properties	Advantages	Limitations	Relevant characterization techniques	Relevant references
	Silanization	React alkoxysilanes with hydroxyl groups on PDMS surface to form covalent Si–O–Si bonds	Simplicity and introduction of various functional groups onto the PDMS surface using amine, thiol or carboxyl terminated alkoxysilanes	Long time (over hours) wet-chemical oxidation required to generate reactive sites for silanization	WCA, XPS	[60-62]
	Dynamic surface modification	The hydrophobic tails of the amphiphilic surfactant molecules or ionic liquid were physisorbed onto the PDMS surface while the hydrophilic heads stick out into the buffer, thereby changing the PDMS surface properties	Faster, cheaper and simpler	No strong covalent bonding between the modifier and the native PDMS	WCA, EOF,	[22, 63-72]
	Deliberate protein adsorption	Self-assembly at the water-PDMS interface, rendering the PDMS surface hydrophilic	Biocompatibility and the molecular recognition properties	No strong covalent bonding between the protein and the native PDMS	EOF	[73, 74]
	Hydrosilylation-based PDMS surface modification	React vinvl-terminated molecules (with functional groups) with Si-H on PDMS surfaces	Capability of introducing various functional groups into the PDMS	Require extra work before real surface modification, such as preparing Si-H rich PDMS surfaces or SAMs coated templates	WCA, FTIR, XPS, zeta-potential	[28, 75-78]

Table 1-1. (Continued)

Surface modification methods	Sub-methods	Properties	Advantages	Limitations	Relevant characterization techniques	Relevant references
Combinations of gas-phase and wet chemical methods	Combination of UV or plasma treatment and silanization	Use UV or plasma to oxidize the PDMS surface in order to generate silanol groups, then react alkoxy or chlorosilanes with specific head-groups with these silanol groups thereby introducing the desired chemical functionality	Covalent bonding between the modifiers and the native PDMS and reduction of the modification time compared to solely silanization method in wet chemical section	--	WCA, EOF	[20, 79-90]
	Combination of UV or plasma treatment and graft polymer coating	Grafting-from: create radical sites as initiators on the surface for subsequent surface-initiated polymerization by means of UV exposure or plasma pretreatment or using surface-initiated ATRP reagent; grafting-to: use plasma treatment to generate reactive sites, then prepolymerized polymers are grafted onto these sites.	covalent bonding between the modifiers and the native PDMS	Gel could be formed inside microchannel when BP was added into monomer solution as a photoinitiator.	WCA, FTIR-ATR, EOF	[19, 91-108]

Table 1-1. (Continued)

Surface modification methods	Sub-methods	Properties	Advantages	Limitations	Relevant characterization techniques	Relevant references
	Combination of plasma treatment and LBL assembly	Use plasma to activate the PDMS surface and then alternating adsorption of polyanions and polycations onto the PDMS surface to produce polyelectrolyte multilayers	Simplicity, efficiency and thickness control at the nanoscale, and more stable than using solely LBL methods due to the plasma pretreatment	No strong covalent bonding between the layers, or need special treatment for bonding the layers covalently after deposition of layers	WCA, EOF, AFM	[68, 109-112]

1.2 PDMS surface modification methods

1.2.1 Gas-phase processing

1.2.1.1 Plasma treatment

A plasma is a partially ionized gas, in which a certain proportion of electrons and ions are free rather than being bound to an atom or molecule and in which radical species abound [113]. Plasma surface modification employs gases, such as oxygen, nitrogen and hydrogen, which dissociate and react with the substrate surface, creating chemical functional groups. This method of surface treatment is by far one of the most commonly used methods for PDMS surface modification today due to its short treatment times and easy operation [29, 32, 34, 114].

An ongoing and formidable challenge with oxidation (and other surface modifications) of PDMS is hydrophobic recovery caused by the migration of uncured PDMS oligomers from the bulk to the surface and the rearrangement of highly mobile polymer chains featuring Si-OH bonds toward the bulk at room temperature [115-117]. These effects are acerbated by the low glass transition temperature of PDMS, which is in the order of -120 ˚C [118]. Vickers *et al.* [29] have overcome this problem by employing a successive three solvent extraction sequence, involving triethylamine, ethyl acetate and acetone, to remove the oligomers before oxidizing the PDMS surface in an air plasma. After storage in air for 7 d, the water contact angle (WCA) of the solvent extracted oxidized PDMS increased from 30° to 40°, while native oxidized PDMS that had not been solvent extracted had initially a less wetting surface with a WCA of 58°, which increased to 110° after 7 d. This indicates that solvent extraction renders the plasma oxidized PDMS firstly more hydrophilic and secondly more stable. Alternatively, plasma processing has been used to graft hydrophilic polymers onto the surface of PDMS. Barbier *et al.* [30] first pretreated a PDMS surface with an Ar plasma, which leads to partial oxidation of the topmost layer and improved adhesion of further layers. Then an acrylic acid (AAc) plasma was deposited and finally the surface was exposed to a He plasma in order to generate cross-links. This had the effect of producing a hydrophilic PDMS surface, which was stable in air for several days. Zhou *et al.* [31] studied the effect of plasma processing on hexane pre-extracted PDMS. They employed a 2-step plasma modification with Ar followed by AAc on hexane

extracted PDMS. This method stabilized the WCA between 50° and 60° after 1 d exposure to air, while hydrophobic recovery on Ar and AAc treated samples without hexane extraction occurred readily. Another alternative method to preserving hydrophilicity after O_2 plasma oxidation was performed by Ren *et al.* [32] who found that a stable μ_{eo} of 4×10^{-4} cm^2/Vs could be maintained for over 14 d by keeping the surface in contact with water. They also found that after 14 d storage in air the immersion of the surface in NaOH for 3 h reinstated the μ_{eo} back to 4×10^{-4} cm^2/Vs implying that uncured PDMS oligomers are being removed or the –OH groups are being reoriented to the surface after exposure to base.

It should be noted that all the above mentioned plasma modifications were applied on open PDMS surfaces. It is therefore envisaged that the direct modification of a PDMS surface inside an enclosed microchannel will simplify the whole process of microfluidic device fabrication and also avoid damaging the modified surfaces during the fabrication processing. Based on this consideration, Martin *et al.* [33] performed the plasma processing *in situ* within a PDMS microchannel by placing the microchannel parallel to the gas flow with Ar pretreatment and subsequent AAc plasma processing. They noted that the WCA decreased from 113° to 65° with a 17 % larger μ_{eo} after modification. Unfortunately, the μ_{eo} value in the modified channel returned back to that of native PDMS after 3 d storage in air. Tan *et al.* [34] employed a more innovative plasma-based technique using a scanning radical microjet approach with an oxygen microplasma. This affords many advantages including the formation of a localized pattern without the need for a mask, higher surface treatment rates and lower damage compared with normal plasma treatment. By increasing the scanning speed, the surface hydrophilicity was improved (WCA decreased from 112° for native PDMS to 70° for treated PDMS) and roughness decreased significantly (from a root mean square (RMS) of 2.9 nm for native PDMS to 1.4 nm for treated PDMS). In order to reduce the hydrophobic recovery inside a microchannel, Tan *et al.* [35] used an initial O_2 plasma treatment of PDMS, followed by heating for 2 h at 150 ºC, to bond PDMS slides together. Then, a second O_2 plasma treatment was applied inside the microchannel using a scanning radical microjet. The long plasma treatment time (300 s to 500 s) resulted in a longer hydrophobic recovery time, and a more hydrophilic surface (WCA approximately 50° - 60°). Furthermore, surface analysis using atomic force microscope (AFM) showed that the roughness of the PDMS surface decreased with increasing O_2 plasma exposure time. More recently, Priest *et al.* [36] reported an entirely

new approach to the selective plasma oxidization of a PDMS surface within a microchannel. In this work molten gallium electrode pads were placed inside bulk PDMS along a bonded microchannel in order to create patterned electrodes for plasma production, as shown in Figure 1-1. This local plasma activation differed from previous approaches where typically an entire microchannel is exposed to a plasma [33]. In Priest *et al*'s [36] work using patterned electrodes not only localized the plasma spatially by tuning the applied voltage and frequency, but also required shorter treatment time.

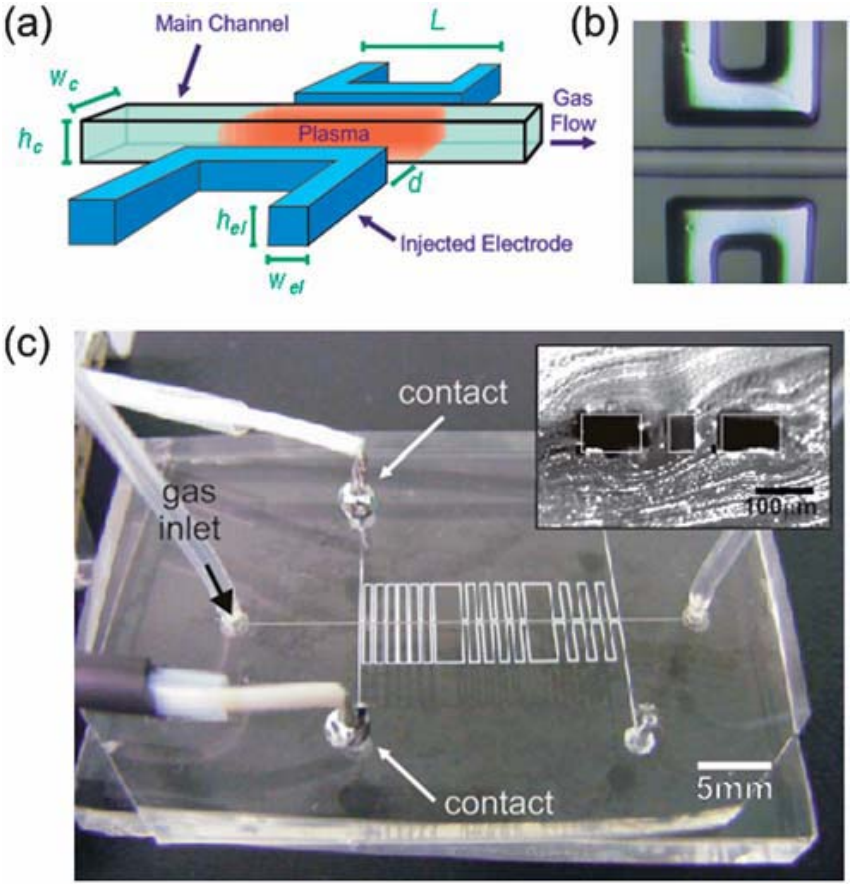

Figure 1-1. PDMS microchip with injected electrode pads for generating localized plasma in main channel. (a) Chip design, showing the injected electrodes, the main channel and the localized plasma. (b) Injected gallium electrodes adjacent to main channel. (c) PDMS microchip with patterned gallium electrodes adjacent to main channel. Cross-section of main channel and gallium electrodes is shown in the inset [36].

1.2.1.2 UV treatment

UV treatment is based on high energy photons that attack the siloxane backbone of PDMS

to form a silica-like layer and an Si-OH surface structure [119, 120]. In comparison to oxidizing PDMS with a plasma, UV treatment is nearly an order of magnitude slower in terms of the time required to achieve the same result [37]. However, the advantage of UV treatment methods is that they facilitate much deeper modification of the PDMS surface without, at the same time, inducing cracking or mechanically weakening of the PDMS [121].

Efimenko *et al.* [37] have assessed the effect of oxygen during UV treatment. They compared the contact angles of UV modified surfaces (with or without oxygen) using distilled water and diiodomethane and calculated the respective surface energies. They observed that UV modified surfaces (up to 60 min treatment time) in the presence of oxygen had higher surface energies (72 mJ/m^2) compared to UV treated surfaces in the absence of oxygen (26 mJ/m^2). This indicates that higher densities of hydrophilic functionalities were formed during oxygen exposure. Furthermore, Fourier transform infrared-attenuated total reflection (FTIR-ATR) spectroscopy showed spectral evidence of –OH moieties on the UV modified samples in the presence of oxygen but not in its absence.

1.2.1.3 CVD

CVD is a chemical process used to produce a thin film on a substrate surface by means of the deposition of gaseous molecules, which chemically react on the surface [113]. The sequence of events during deposition in CVD is typically sublimation under vacuum, pyrolysis into reactive species and deposition onto the PDMS surface. The advantages of CVD have been summarized by Choy *et al.* [122], including the capability of producing highly dense and uniform films with good reproducibility and adhesion at reasonably high deposition rates, and the capability of coating complex shaped components due to the gaseous molecules used as reactants.

Chen *et al.* [38] have deposited poly(4-benzoyl-*p*-xylylene-*co*-*p*-xylylene) on PDMS *via* CVD and subsequently wet-chemically patterned the resulting reactive coating of a microchannel with poly(ethylene oxide) (PEO). This was achieved by exposing the light-reactive carbonyl groups to UV light through a photomask generating free radicals,

which readily reacted with PEO *via* C–H abstraction. The PEO-functionalized regions of the micro-channel resisted fibrinogen adsorption. More recently, Chen *et al.* [39] have reported CVD polymerization of a range of functionalized poly(*p*-xylylenes) within PDMS microchannels with complete coating of the entire channel length. However, the coating was thicker at the inlet and outlets compared to the center, demonstrating the need for further optimization.

To facilitate improved bonding in the formation of microchannels, Chen *et al.* [40] used two complementary poly(*p*-xylylenes), poly(4-aminomethyl-*p*-xylylene-*co*-*p*-xylylene) and poly(4-formyl-*p*-xylylene-*co*-xylylene), to form Schiff base cross-links, as shown in Figure 1-2. The bonding strength for the modified sample (2.44 ± 0.15 MPa) was comparable to that between two plasma oxidized PDMS surfaces (2.34 ± 0.27 MPa). More recently, another two complementary polymers, poly(4-aminostyrene) (PAS) and poly(glycidyl methacrylate) (PGMA) were used to modify PDMS, Si wafers, and glass *etc*, also using the CVD technique [41]. Here, the bonding of microfluidic devices was formed *via* a ring-opening curing reaction between amino groups from PAS and epoxy groups from PGMA. In the two above examples, active amino groups were demonstrated to be available in the formed microchannels by the attachment of *N*-hydroxysuccinimide activated fluorescent dye Atto-655 on the poly(4-aminomethyl-*p*-xylylene-*co*-*p*-xylylene) modified PDMS surface and carboxylic acid functionalized CdSe/Zns on the PAS modified PDMS surface. After bonding, these unreacted amino groups could be used for further surface modifications [40, 41].

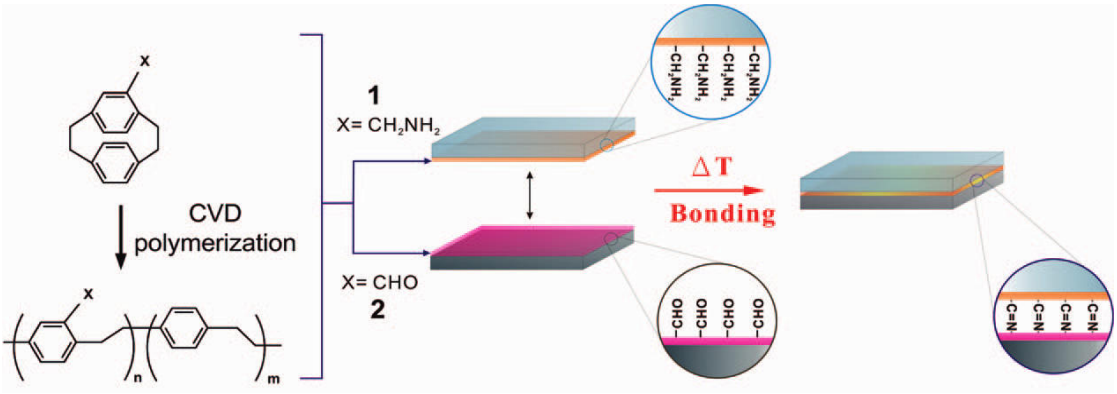

Figure 1-2. Schematic illustration of the bonding process between two complementary reactive CVD coatings 1 (poly(4-aminomethyl-*p*-xylylene-*co*-*p*-xylylene)) and 2 (poly(4-formyl-*p*-xylylene-*co*-xylylene)) [40].

From the above examples, it is clear that a wide range of chemical compounds can be deposited onto the PDMS surface *via* the CVD technique. However, high temperatures (above 700 ºC) were often employed during the pyrolysis step in some CVD processes [38, 40], which are often unsuitable for structures already fabricated on PDMS.

1.2.1.4 Coating with metals and metal oxides

Recently, it has been demonstrated that coatings with certain metals and metal oxides can effectively tailor the surface energy of a PDMS surface [42-44]. Niu *et al.* [42] have sputter-coated TiO_2 onto PDMS and demonstrated that the WCA decreased from 105° to 25°. Although the coated material maintained its transparency, severe cracking of the surface rendered this an ineffectual method for microfluidic devices [42]. Feng *et al.* [43] reported that by sputtering gold (< 1.0 nm) onto PDMS the WCA decreased by 25° with no cracking of the gold layer observed. More recently, Zhang *et al.* [44] have reported a wet chemical method for the *in situ* fabrication of gold nanoparticle films on PDMS *via* incubating cured PDMS in $HAuCl_4$ aqueous solution. The addition of metal nanoparticles to the PDMS changed the wetting behavior, however, at the same time caused loss of optical transparency.

Metal coatings have also been employed to maintain the hydrophilicity of the underlying PDMS surface after plasma oxidation. This strategy permits extended times between surface processing of a PDMS sheet and microfluidic device manufacture, usually *via* bonding of different PDMS sheets. Patrito *et al.* [45] have reported on firstly activating a PDMS surface with an Ar plasma then immediately afterwards sputter coating this surface with an Al film (44 nm thick). The Al capping layer was easily removed by immersing the surface in orthophosphoric acid to re-expose the underlying hydrophilic surface (created by the Ar plasma treatment). In this fashion, the hydrophilicity of the PDMS was prolonged (WCA of 39 ± 3°; up to 30 d storage in air).

1.2.2 Wet chemical methods

1.2.2.1 LBL deposition

LBL deposition is an emerging strategy for surface modification in microfluidics. The LBL assembly technique is generally described as the alternating adsorption of polyanions and polycations that can be accomplished on virtually any substrate surface to produce polyelectrolyte multilayers (PEMs) [111]. There are many advantages of the LBL assembly technique, including simplicity, efficiency and thickness control at the nanoscale. However, the PEM structure, surface functionality and stability are dependent on many factors, for example, polyelectrolyte ionic strength and concentration, type of solvent, temperature and pH of the solution, particularly for weak polyelectrolytes [24]. These factors have limited the widespread use of LBL coatings. Further studies are needed to improve the stability of LBL films for use in microfluidics, for example, by using chemical cross-linking after assembly [111].

Some successful examples of LBL films in the context of PDMS coatings are outlined here. Polycations poly(diallyldimethylammonium chloride) (PDDA) [46-49] and chitosan (Chit) [25, 50, 51] have been widely used as the first layer in LBL assembly on PDMS. Their ability to strongly adsorb to PDMS through hydrophobic interactions, and doing so without any pretreatment of the PDMS surface, make them highly attractive. Qiu *et al.* [47] have used alternating layers of PDDA and poly(sodium 4-styrenesulfonate) (PSS) in a phosphate buffered saline (PBS) buffer to produce a $(PDDA/PSS)_2$ modified PDMS microchannel. By performing this modification *in situ*, a microchannel with a stable μ_{eo} of $\sim 3.5 \times 10^{-4}$ cm^2/Vs was produced in addition to a surface with reduced non-specific adsorption compared to native PDMS. Schmolke *et al.* [52] used an automated dipping robot to deposit PEMs of PDDA/PAAc or poly(aromatic hydrocarbon) (PAH)/PAAc onto a PDMS surface pretreated with HCl/H_2O_2. Subsequently, a custom made PAAc-*g*-poly(ethylene glycol) (PEG, lower molecular weight of PEO, less than 20 000 Da) was successfully grafted onto the PEMs as a top layer, resulting in a hydrophilic surface (decreasing the WCA by more than 65° in comparison with native PDMS). One of the problems with the LBL technique is the use of organic solvents such as hexane, toluene and benzene, which are well known to cause swelling of PDMS [123]. To avoid this potential swelling effect, Wang *et al.* [51] used Chit and attached the linker

O-[(*N*-succinimidyl)succinyl]-*o'*-methyl-PEG in aqueous solution to obtain a Chit-*g*-methyl-poly(ethylene glycol) (mPEG) modified PDMS microfluidic device, which again produced a stable μ_{eo} of ~2 × 10^{-4} cm^2/Vs and reduced the surface adsorption of bovine serum albumin (BSA).

Compared with other PEMs, proteins in particular are more favorable due to their high biocompatibility and their molecular recognition properties. Wang *et al.* [50] prepared a bilayer of lysozyme and albumin proteins, as well as an albumin and glucose oxidase coating adsorbed on a pre-layer of Chit, within a microchannel for neurotransmitter separations. Schrott *et al.* [53] successfully combined the LBL deposition technique with protein adsorption to produce multilayers of dextran sulfate/human immunoglobulin G (IgG) on a IgG pretreated PDMS surface and glutaraldehyde was then used to crosslink the antibodies. Likewise, deoxyribonucleic acid (DNA) has been used by Qiu *et al.* [25] to modify the inside of microchannels coated with a pre-layer of Chit. An almost twofold improvement in μ_{eo} and enhanced stability was observed over the pH range of 4.5 – 6.5. In addition, Kuo *et al.* [54] produced a polybrene/dextran sulfate bilayer within a microchannel using LBL for pre-concentration and separation of DNA.

Wang *et al.* [46] used LBL assembly by firstly applying a pre-layer of polyelectrolyte (PDDA, linear poly(ethyleneimine) (LPEI), poly(allylamine hydrochloride) or Chit). Subsequently, citrate-stabilized gold nanoparticles were attached onto the polyelectrolyte modified PDMS surface (Figure 1-3) demonstrating improved μ_{eo} stability.

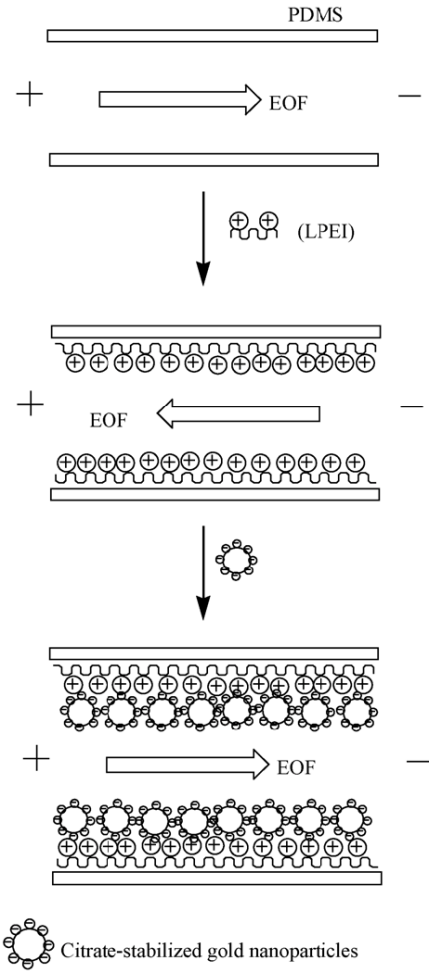

Figure 1-3. Schematic of a PDMS microchannel modified with LPEI and citrate-stabilized gold nanoparticles using LBL assembly [46].

However, all these LBL procedures involved the manual injection and removal of solutions both for layer formation and the washing steps, which made the whole process rather cumbersome. More recently, Bauer *et al.* [55] have presented a relatively automated LBL modification method by using a poly(ethylene) (PE) tube for introducing solutions into a microchannel. A PAH solution in NaCl, NaCl washing solution and PSS solution in NaCl separated by air plugs were loaded into a PE tube in sequence prior to introducing the segment into a microchannel. This sequence was repeated in the PE tube when multilayer modification was required. The treatment time of each solution within the microchannel was easily adjusted by the flow rate and the length of the respective segment. Although no surface characterization was performed on this LBL modified PDMS surface, high stability was verified by the production of a monodisperse emulsion with high reproducibility in the modified PDMS device after months of storage.

1.2.2.2 Sol–gel coating

Sol–gel methodology refers to a polymerization process based on the phase transition of a liquid state, the ‘‘sol’’ containing suspended particles, to a solid-like state, the ‘‘gel’’. Sol–gel coatings are advantageous for PDMS surface modifications due to the high density and homogeneous distribution of cross-linked ‘‘gel’’ particles near the surface stabilizing the surface chemistry [57]. However, the disadvantages of sol-gel coatings, such as swelling caused by the precursor solution and cracking during the gelation process, should be resolved before the widespread use of this technique [120].

Roman *et al.* [56] have immersed a microfluidic chip in tetraethyl orthosilicate (TEOS), then in ethylamine, and finally heating the chip at 95 ºC to form a SiO_2-PDMS surface. Whilst there was only a moderate decrease in WCA from 108.5° to 90.2°, the μ_{eo} doubled from $4.21 \pm 0.09 \times 10^{-4}$ cm^2/Vs to $8.3 \pm 0.2 \times 10^{-4}$ cm^2/Vs and remained stable for up to 60 d in dry storage. The same group [57] also modified PDMS with particles of oxides of zirconium, titanium and vanadium. The WCAs were 90°, 61° and 19° for PDMS-ZrO_2, PDMS-TiO_2 and PDMS-VO_2, respectively. Interestingly, the μ_{eo} values were reversed compared to SiO_2 modification, giving negative values. The PDMS-TiO_2 surfaces were further modified with either PEG, amino, perfluoro or mercapto groups using silanol condensation chemistry. WCAs were measured as 23°, 45°, 120° and 76° for the PEG, amino-, perfluoro-and mercapto-modified surfaces, respectively, demonstrating the value of this approach in tuning wettability of PDMS. A mixture of TEOS and trimethoxyboroxine was used as a precursor by Orhan *et al.* [58] for *in situ* coating of a PDMS microchannel on borosilicate glass. The entire modification process involved two fundamental steps, firstly flushing the precursor solution through the microchannel and secondly thermal treatment at up to 160 ºC. This resulted in a modified surface with no cracks that was resistant to swelling in the presence of toluene. However, no WCA measurements were recorded in order to confirm an increase in surface hydrophilicity.

Abate *et al.* [59] used a combination of TEOS and methyltriethoxysilane; however, this mixture can swell and dissolve PDMS. To avoid PDMS swelling, they added HCl to catalyze condensation and hydrolysis reactions of the monomeric precursors to induce the formation of larger oligomer precursors, which are less miscible with PDMS. Figure 1-4 shows a microchannel cross-section initially rectangular transformed to a rounded channel

as a result of the thick sol–gel coating.

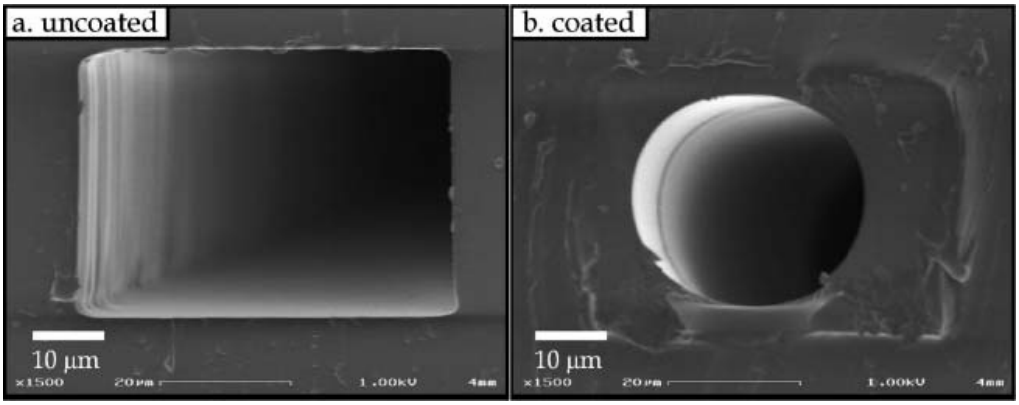

Figure 1-4. Scanning electron micrographs of cross-sections of (a) uncoated and (b) coated PDMS channels by mixture of TEOS and methyltriethoxysilane using the sol–gel method [59].

1.2.2.3 Silanization

Surface silanization can be performed on various substrates provided they contain surface hydroxyl groups, which will react with alkoxysilanes to form covalent Si–O–Si bonds to the underlying substrate. By using amine, thiol or carboxyl terminated alkoxysilanes various functional head-groups can be introduced onto the surfaces following surface oxidation [60, 61]. There is an abundance of literature on the topic of silanization of plasma-based oxidation, but comparatively little on *in situ* wet-chemical oxidation. One limitation of the silanization technique is the long oxidation time (over hours) required to generate reactive sites for silanization reaction [60, 61].

Slentz *et al.* [60] oxidized a PDMS surface by immersing it in 1 M NaOH for 24 h. They then reacted the newly formed silanol groups with three different alkoxysilanes, namely 3-aminopropyltriethoxysilane (APTES), *N*-octyldimethylchlorosilane, and methoxydimethyloctadecylsilane. The latter two alkoxysilanes required 3 % sodium dodecyl sulfate (SDS) to disperse them in aqueous solution. Sui *et al.* [61] have performed *in situ* PEG surface modification of PDMS microchannels by first using a mixture of $H_2O/H_2O_2/HCl$ to oxidize the PDMS microchannel and then incubating with 2-[methoxy(polyethylenoxy)propyl]trimethoxysilane. After 2 - 3 d, the WCA stabilized at 40° lower than that of native PDMS. Successful APTES coating was demonstrated using

the same method [61].

Sofla *et al.* [62] have reported an interesting surface modification technique using tridecafluoro-1,1,2,2-tetrahydrooctyltrichlorosilane vapor on non-pretreated PDMS and glass surfaces for permanent or non-permanent bonding between PDMS and glass, depending on the deposition time. They found that all the samples were permanently bonded using a 24 h deposition time, while no permanent bonding was obtained using deposition times of 3 h or less.

1.2.2.4 Dynamic surface modification

This technique involves the use of surfactants or ionic liquids to modify the PDMS surface. Using this method, the surface modifiers are used to pretreat the PDMS surface or added into the running buffer of an analytical separation to render the PDMS surface hydrophilic. The hydrophobic tails of the amphiphilic surfactant molecules were physisorbed onto the PDMS surface while the hydrophilic heads stick out into the buffer, thereby changing the PDMS surface properties. In this fashion, surface modification can be accomplished faster, cheaper and simpler. The fact that there is no strong covalent bonding between the surfactants and the native PDMS, and that desorption can take place, does not negatively impact on the surface properties as long as dynamic replenishment of the desorbed species occurs from excess surfactants in the running buffer during analysis [68].

To date, many surfactants have been used for dynamic PDMS coatings, including SDS [22, 63, 64], Brij35 [65], sodium deoxycholate (DOC) [22], phosphatidic acid (PA) [22], poly(vinylpyrrolidone) (PVP) [66], n-Dodecyl-β-D-maltoside (DDM) [67], didodecyldimethylammoniumbromide (DDAB) [68, 69] and Triton X-100 [70]. Roman *et al.* [64] observed that the addition of SDS inside PDMS micro-channels greatly improved the μ_{eo} by approximately 340 % to 7.1 x 10^{-4} cm^2/Vs, compared to that of native PDMS. Additionally, they found that the rhodamine B (RB) dye adsorption was effectively inhibited [64]. The effects of SDS, DOC and PA on μ_{eo} have been compared and SDS shows the highest μ_{eo}, then PA and DOC [22]. DDM [67] and Triton X-100 [70], in particular, have shown encouraging results in the reduction of non-specific protein adsorption in dynamically coated PDMS microchannels.

Whilst dynamic surface modification within PDMS microchannels using surfactants is widely used, there has been recent progress in adding the surfactant to the PDMS prepolymer prior to curing. Wu *et al.* [124] have added a non-ionic surfactant Pluronic F127 ($(PEO)_{100}$(poly(propylene oxide) $(PPO))_{65}$ $(PEO)_{100}$) into PDMS prepolymer before curing. Figure 1-5 shows that when the microchannel was filled with water, the Pluronic F127 molecules embedded in the PDMS migrate towards the water/PDMS interface to minimize surface energy. This results in the hydrophobic interaction between the PPO segments and PDMS causing the hydrophilic PEO to extend outwards from the surface. The WCA of the Pluronic F127 modified PDMS surface changed from 99° to 63° after immersing the sample in water for 24 h, compared to a WCA of 104° for native PDMS. Furthermore, this Pluronic F127 modified PDMS was shown to significantly suppress the non-specific adsorption of a fluorescein isothiocyanate (FITC) labeled IgG antibody due to the improved hydrophilicity, compared to native PDMS.

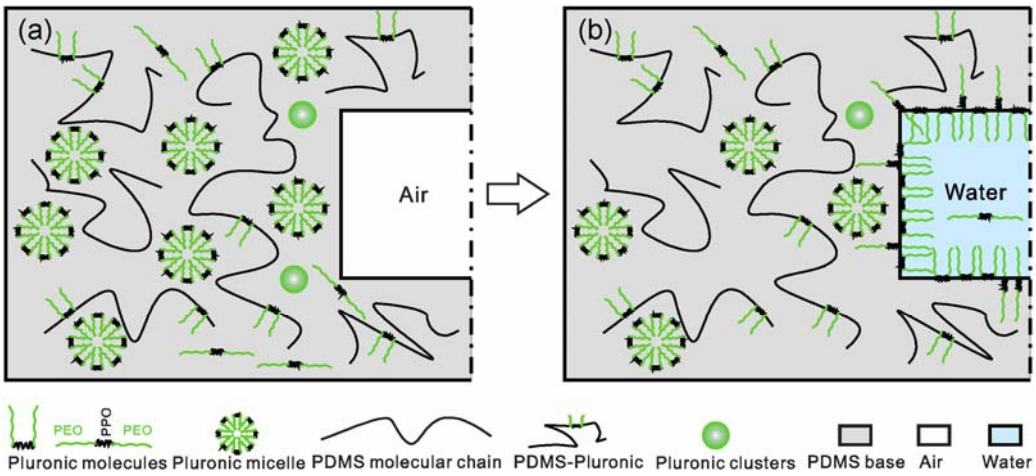

Figure 1-5. Schematics of the process of surface modification of PDMS with Pluronic F127. (a) The microchannel based on Pluoonic F127 embedded PDMS; (b) when the microchannel based on Pluronic F127 embedded PDMS was filled with water, Pluronic F127 molecules migrated to the water interface with hydrophilic PEO towards to water and hydrophobic PPO towards to PDMS [124].

To improve protein separation within a microfluidic device, ionic liquids have been successfully used including, 1-butyl-3-methylimidazolium dodecanesulfonate (BAS) [71] and 1-butyl-3-methylimidazolium tetrafluoroborate ($BMImBF_4$) [72], which act as both supporting electrolyte and surface modifier. The WCA of the BAS modified surface decreased from 114.8° for native PDMS to 47.7° and the μ_{eo} increased almost 10 times to 4 $\times$ 10^{-4} cm^2/Vs compared to native PDMS in PBS at pH 7.4 [71]. However, the μ_{eo} after

modification with $EMImBF_4$ only increased slightly [72]. Following this, a hybrid mobile phase of $EMImBF_4$ and the nonionic surfactant Triton X-100 was developed, which has shown the effective inhibition of RB adsorption, improved μ_{eo} and protein separation [72].

1.2.2.5 Deliberate protein adsorption

In comparison to other PDMS surface modification procedures, deliberate non-specific protein adsorption to PDMS offers many distinct advantages, in particular in relation to the proteins' intrinsic biocompatibility, but also their molecular recognition properties [74]. Of particular recent interest is the use of hydrophobins as surface modifiers. Hydrophobins are a class of small, cysteine-rich proteins similar to surfactants [63] which can self-assemble at the water-PDMS interface, rendering the PDMS surface hydrophilic [73, 74]. Wang *et al.*'s group [73, 74] used hydrophobin II to improve the wettability of PDMS. This was confirmed by a decrease in the WCA from 123.9 ± 0.7° on native PDMS to 51.0 ± 0.5° on hydrophobin II modified PDMS, which was stable in air for 20 d. Furthermore, this modified PDMS surface was shown to be suitable for the covalent immobilization of chicken IgG inside microfluidic channels (Figure 1-6).

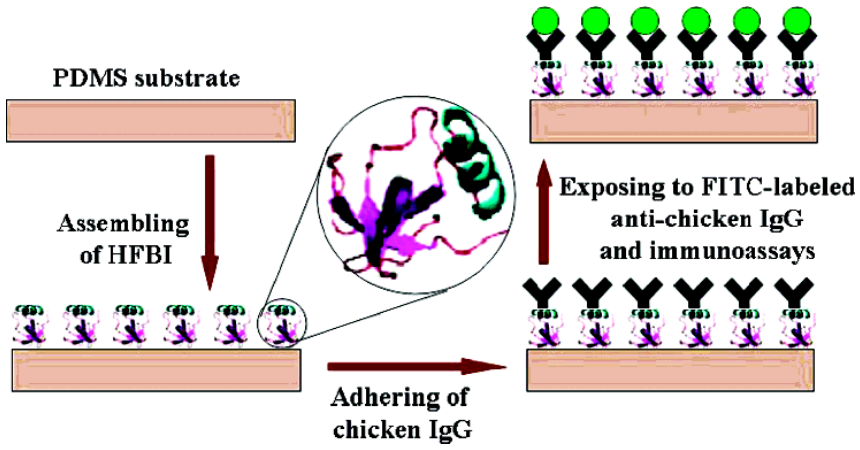

Figure 1-6. PDMS surface modification with hydrophobins followed by covalent immobilization of chicken IgG and demonstration of immunogenicity using FITC-labeled anti-chicken IgG [74].

1.2.2.6 Hydrosilylation-based PDMS surface modification

The Brook group prepared Si–H rich PDMS surfaces using pre-curing and post-curing

methods, involving adding additional SiH-containing poly(hydromethylsiloxane) (PHMA) into the PDMS prepolymer prior to curing [75], and by exchanging dimethylsiloxane units on pre-cured PDMS surface with hydromethylsiloxane ones using triflic acid catalysis [75, 76], respectively. Allyl-PEG-OH was successfully grafted onto these two SiH-rich PDMS surfaces *via* hydrosilylation in the presence of a Pt catalyst, following NSC functionalization by treatment with *N*,*N*′-dihydroxysuccinimidyl carbonate [75]. *α*-Allyl-*ω*-tosylethyl-PEG was also immobilized onto the Si–H rich PDMS surface *via* hydrosilylation. Amino-PEG modified PDMS surfaces were obtained by immersing the tosylethyl-PEG modified PDMS in diethylenetriamine solution. Finally, hyaluronic acid (HA) was grafted onto the surface *via* amide linkage [76]. PEG-OH, amino-PEG and HA modified PDMS, all showed improved wettability and inhibited nonspecific adsorption of fibrinogen, compared to native PDMS [75, 76].

Aside from the previously mentioned PDMS surface modifications based on hydrosilylation, many researchers have focused on using self-assembled monolayers (SAMs) to coat substrates as a template for curing PDMS prepolymers mixed with vinyl-terminated moieties, atom transfer radical polymerization (ATRP) initiators or acrylates [28, 77, 78]. In particular, SAMs of 1-octadecanethiol and 11-hydroxy-1-undecanethiol on gold substrates were used to drive 1H, 1H, 2H-perfluorodecene or dec-1-en-10-yl hexa(ethylene glycol) monomethyl ether impregnated within the cured PDMS to the water/PDMS interface, *via* interfacial free energy minimization [28, 78]. For the hexa(ethylene glycol)-modified PDMS the advancing WCA reduced to 88° from 106° for the native PDMS, and then increased again to 96° after 5 d of storage in air. Using the same modification technique, a carboxylic functionalized PDMS surface was also fabricated by simply curing a mixture of 2 wt % undecylenic acid (UDA) and PDMS prepolymer on a gold coated glass slide, which had been previously pretreated with a hydrophilic SAM of 3-mercapotopropionic acid [77]. This successful PDMS modification was verified by the decrease in WCA from 91° on UDA modified PDMS, compared to 110° on native PDMS and the appearance of carboxylic acid stretching bands (1715 cm^{-1} and 1730 cm^{-1}) in the FTIR-ATR spectra of UDA modified PDMS.

In an interesting approach, van Poll *et al.* [28, 78] trialed mixing an ATRP initiator, 2-bromo-2-methylpropionate, into a PDMS prepolymer, which was again cured against the

thiol modified gold template. The ATRP initiator was shown to migrate to the water/PDMS interface where it could be used to graft poly(oligo(ethylene glycol) methacrylate) chains from the initiator modified PDMS surface.

Zhou *et al.* [125] also demonstrated that adding poly(ethylene glycol) methyl ether methacrylate (PEGMEM) into PDMS prepolymer before curing improved PDMS surface wettability, even without a hydrophilic template. The WCA of PEGMEM modified PDMS decreased from 112° on native PDMS to ~ 75°. The non-specific adsorption of BSA was also effectively suppressed on this surface.

1.2.3 Combinations of gas-phase and wet chemical methods

1.2.3.1 Combination of UV or plasma treatment and silanization

Here, energy produced by physical techniques, such as a plasma [79-81] or a Tesla coil [20, 82] are used to oxidize the PDMS surface in order to generate silanol groups, which can then react with alkoxy or chlorosilanes with specific head-groups thereby introducing the desired chemical functionality. Compared with solely the silanization method (See section 1.2.2.3), the combination of both plasma treatment and silanization reduced the time of the surface modification due to the use of short plasma treatment times, rather than long solvent treatment times for generating silanol groups. APTES has been successfully attached onto PDMS surfaces pretreated with a Tesla coil [20, 82], air or oxygen plasma [20, 79, 82, 83], or ozone [84]. In addition, O-[(*N*-succinimidyl)succinyl]-*o'*-mPEG [81], poly(dimethylacrylamide-*co*-glycidyl methacrylate) (P(DMA-*co*-GMA)), poly(vinylpyrrolidone)-*g*-glycidyl methacrylate (PVP-*g*-GMA) and poly(vinyl alcohol)-*g*-glycidyl methacrylate (PVA-*g*-GMA) [85] have been covalently grafted onto APTES modified PDMS surfaces. The modified channels were suitable for the separation of amino acids, peptides and proteins [81, 85].

Aside from APTES, 3-glycidoxypropyltrimethoxysilane (GPTMS) [86, 87], 3-chloropropyltrichlorosilane (CPTCS) [88], 3-aminopropyldimethylethoxysilane (APDMES) [80], 3-aminopropyltrimethoxysilane (APTMS) [89] and 3-mercaptopropyltrimethoxysilane (MPTMS) [89] have been covalently attached to PDMS

after UV or plasma pretreatment. GPTMS, in particular, can be further modified with PEG to produce a surface with epoxy groups suitable for biomolecule coupling [87] or NH_2-PEG for separation of amino acids [86]. In addition, CPTCS modified PDMS can be further grafted by alkyne-PEG for separation of amino acids mixture and proteins mixture [88]. On APDMES modified PDMS, poly(L-glutamic acid) (PGA) was grafted *via* carbodiimide coupling. The PGA-APDMES modified PDMS surface showed an μ_{eo} of 5×10^{-4} cm^2/Vs compared to native PDMS (1×10^{-4} cm^2/Vs) at pH 5 – 10 [80]. PEG silanes were also directly grafted on air plasma treated PDMS giving a WCA of less than 20°, showing the lowest WCA reported by a silanization method [126].

O_2 plasma pretreated PDMS has also been used to covalently attach four different aminonaphthol silanes *via* silanization [90]. The results showed that the WCAs of two surfaces modified with two different aminonaphthols decreased from 109° for native PDMS to 83° and 79°, respectively, while WCA values for the two surfaces modified with fluorinated aminonaphthols increased from 109° to 116° and 122°, respectively.

1.2.3.2 Combination of UV or plasma treatment and graft polymer coating

Graft polymer coating is widely used for tailoring the surface chemistry and wettability of PDMS in order to introduce surface functional groups for further modification. Graft polymer coating can be divided into two main categories: 'grafting-from' and 'grafting-to' [120].

Graft polymer coating often involves the creation of radical sites as initiators on the surface for subsequent surface-initiated polymerization by means of UV exposure [91-95]. This approach is referred to as 'grafting-from'. Benzophenone (BP) is widely used as a photoinitiator in this technique [91-96] because its photochemically produced triplet state can abstract hydrogen atoms from almost all monomers, thus generating radical sites for further graft polymerization [127]. Hu *et al.* [19] have been the first to demonstrate a one step UV-induced graft polymerization of AAc, acrylamide (AAm), dimethylacrylamide, 2--hydroxylethyl acrylate and PEG acrylate on PDMS. The same method was used by Wu *et al.* [97] to modify a PDMS microchannel with a 4 nm thick layer of PAAc. Su *et al.* [92, 93] and Fiddes *et al.* [96] also hydrophilized a PDMS surface *via* a one-step UV exposure with

a mixture of BP and monomer solutions (AAc and AAm, respectively). The resulting hydrogel modified PDMS microchannel could be employed to generate both water-in-oil-in-oil (W/O/O) and water-in-oil-in-water (W/O/W) emulsions, which will be discussed in more detail further below [92, 93]. Hu *et al.* [98] have successfully immobilized BP onto PDMS in order to increase the rate of surface-tethered polymer formation and avoid gel formation inside the microchannel before UV-induced polymerization. Using this technique, polymers such as PAAc [98], PEG [98], thermal-responsive poly [*N*-isopropyl acrylamide] (PNIPAAm) [99, 100], thermal and pH-responsive poly(*N*-isopropyl acrylamide-*co*-acrylic acid) (P(NIPAAm-*co*-AAc)) [99] and a non-fouling hydrogel made from PEG diacrylate [99] have been grafted onto inner surfaces of PDMS microchannels.

Polymerization of AAc, methacrylic acid (MAAc) and glycidyl methacrylate (GMA) was also performed by thermal initiation (90 ºC) on Ar plasma pretreated PDMS surfaces [101]. The advancing WCA changed from 115° for native PDMS to 87°, 89° and 107° for PAAc, poly(methacrylic acid) (PMAAc) and PGMA modified PDMS surfaces, respectively. Additionally, the receding WCA changed from 85° for native PDMS to 39°, 58° and 24° for PAAc, PMAAc and PGMA modified PDMS surfaces, respectively. The decrease of these WCA values indicated the PDMS surfaces became hydrophilic after these three modifications.

Surface-initiated ATRP is another popular choice for ‘grafting-from’. Xiao *et al.* [102] immobilized (1-trichlorosilyl-2-m-p-chloromethylphenyl)ethane on UV pretreated PDMS as the initiator to perform ATRP of AAm within microchannels. The poly(acrylamide) (PAAm) grafted surface showed improved wettability with an advancing WCA of 70° compared to 110° on native PDMS, which remained stable for up to one month in dry air. Furthermore, the adsorption of proteins on the modified surfaces was greatly inhibited [102, 103]. Tugulu *et al.* [104] demonstrated an approach without the use of UV/ozone. A trichlorosilane containing a benzyl chloride moiety which acts as a surface-initiating ATRP reagent was vapor deposited onto native PDMS. The surface was then exposed to water, which resulted in the polycondensation of the silane, forming a surface-confined interpenetrating polymer network. Finally, poly(poly(ethylene glycol)methacrylate) (PPEGMA) brushes were grown on the surface using ATRP after a number of vapor deposition/hydrolysis cycles. The advancing WCA decreased from 105° for native PDMS

to 63° for the PPEGMA modified PDMS (three vapor deposition/hydrolysis cycles).

In contrast to 'grafting-from', prepolymerized polymers have been grafted onto reactive sites on a surface *via* a 'grafting-to' approach [120]. Lillehoj *et al.* [105] have attached PEG onto air plasma pretreated PDMS surfaces *via* a 'grafting-to' approach which resulted in ether bond formation. The PEG modified PDMS surface showed long-term stability maintaining a WCA < 22° for 47 d at room temperature under atmospheric conditions. In another 'grafting-to' approach, Geissler *et al.* [106] first treated PDMS with a maleic anhydride (MA) plasma, then hydrolyzed the MA film by immersing it in water. This was then followed by *N*-(3-dimethylaminopropyl)-*N′*-ethylcarbodiimide hydrochloride (EDAC) /*N*-hydroxysuccinimide (NHS) coupling with NH_2-functional PEG [106]. FTIR-ATR spectra of the MA film indicated hydrolysis by the disappearance of symmetric and asymmetric C=O stretching bands (1860 cm^{-1} and 1796 cm^{-1}, respectively) and the appearance of carboxylic acid stretching bands at 1710 cm^{-1}. In addition, the MA-PDMS surface was pH-responsive and showed a decrease in WCA values from ~ 100° to ~ 60° with increasing pH values from pH 9 to pH 13. After attachment of PEG molecules *via* amide linkages to the MA-PDMS surface, the now PEG-terminated PDMS surface showed a significant decrease in non-specific adsorption of fluorescently labeled proteins, compared to a MA-PDMS surface [106]. Although PEG has been widely used as a graft polymer coating [105, 106], it has limited functionality due to its linear nature. The lack of functionality can be addressed by using hyperbranched polyglycerols (HPGs). HPGs with multiple peripheral succinimidyl ester groups have been grafted onto an Ar and then allylamine plasma treated PDMS surface [107]. The resulting HPGs modified PDMS showed a lower WCA of 73° compared to native PDMS at 100°. Further, two characteristic bands at 1100 cm^{-1} and 2875 cm^{-1} were observed in the FTIR-ATR spectrum corresponding to C–O–C stretching and C–H stretching, respectively. A final example of a recent 'grafting-to' approach is that of Li *et al.* [108] who grafted allylhydridopolycarbosilane (AHPCS) onto a plasma pretreated PDMS surface, and the resulting AHPCS film was converted into a silica film *via* hydrolysis in NaOH solution. The WCA after hydrolysis was shown to decrease to 35°.

1.2.3.3 Combination of plasma treatment and LBL assembly

Wu *et al.* [109] and Xiao *et al.* [110] have modified oxygen plasma-treated PDMS with multilayers of poly(vinyl alcohol) (PVA) finding that the μ_{eo} from three layers of PVA was suppressed with a stable value of ~ 0.25×10^{-4} cm^2/Vs in 30 mM PBS buffer (pH 3–11) and the μ_{eo} from two layers of PVA was suppressed to ~ 1.5×10^{-4} cm^2/Vs from 4×10^{-4} cm^2/Vs on native PDMS in 10 mM borate buffer (pH 7.5 – 10.0). He *et al.* [68] immersed an air plasma treated PDMS surface into an aqueous solution of 2 wt % PVA and 5 wt % glycerol followed by heating in order to immobilize the PVA and glycerol. The procedure was repeated again to form a second coating. The WCA for the modified surface decreased to 6°. After 90 d storage in air the WCA only experienced a slight increase to 20°. However, AFM images showed the PVA and PVA/glycerol modified surfaces had significantly increased roughness compared to the native PDMS surface.

To date, the most hydrophilic and stable LBL deposition on PDMS was reported by Makamba *et al.* [111] who firstly exposed O_2 plasma pretreated PDMS to a layer of hydrolyzed poly(styrene-co-maleic anhydride) (h-PSMA), then carried out three different depositions: (i) deposition of four bilayers of poly(ethyleneimine) (PEI)/PAAc, which were then crosslinked using carbodiimide coupling. The PAAc terminated surface was covalently linked to PEG diamine *via* carbodiimide coupling. (ii) Deposition of four bilayers of PEI/PAAc, then one layer of PEI, which were cross-linked *via* carbodiimide coupling. The now PEI terminated surface was then covalently linked to PEG dicarboxylate *via* carbodiimide coupling. (iii) A PEI terminated surface was prepared as in (ii), then this surface was covalently linked to PEG dialdehyde *via* reductive amination. The WCAs of the h-PSMA/$(PEI/PAAc)_4$/PEG diamine, h-PSMA/$(PEI/PAAc)_4$/PEI/PEG dicarboxylate and h-PSMA/$(PEI/PAAc)_4$/PEI/PEG dialdehyde surfaces were 32°, 5.5° and 20°, respectively, and they were stable in air for 5 months. The extreme stability of these modified PDMS surface was probably due to the covalent bonding between layers, which was often not available in most cases using the LBL modification method. To our knowledge, this is the longest period reported for maintaining hydrophilicity of PDMS in air to date. Three protein layers, including BSA, anti-BSA and protein G were then grafted onto these PEMs modified surfaces resulting in surface with a high antibody binding capacity while at the same time affording low non-specific binding. Another attempt to covalently bond layers together and thus increase the stability of PEMs has been reported

by Sung *et al.* [112] who sequentially coated O_2 plasma pretreated PDMS microchannels with multiple layers of PEI and PAAc, followed by crosslinking the layers *via* EDAC/NHS coupling. Following the EDAC/NHS coupling, BP was allowed to penetrate into the outer PDMS layer. Then, an aqueous monomer precursor solution containing AAm, bis-AAm, glycerol and acrylate-PEG-protein G was introduced into the microchannel and exposed to UV light in certain regions through a microscope objective, forming hydrogel plugs with functionalized with protein G in sections along the microchannel, as shown in Figure 1-7.

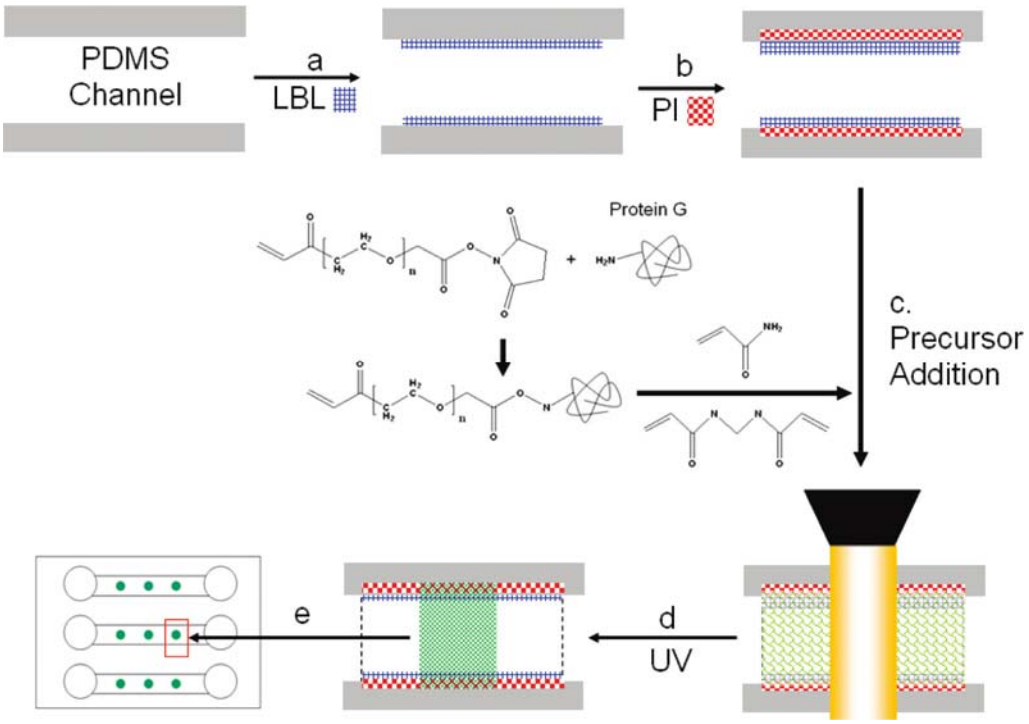

Figure 1-7. Scheme of fabricating the protein G-immobilized hydrogel chip. (a) The PDMS surface modification with PEMs (PEI/PAAc) in microchannel by layer by layer (LBL) technique; (b) absorption of photoinitiator (PI) into the PEMs-modified PDMS microchannel; (c) protein G was covalently bonded to NHS-PEG-acrylate molecules for copolymerization with the AAm/bisAAm; (d) certain region in the PEMs-modified PDMS microchannel were exposed to UV light through the microscope objective for in situ synthesis of hydrogel plugs in the PEM-modified PDMS microchannel; (e) patterned hydrogel plugs were formed within PDMS microchannels [112].

1.3 Patterned PDMS surfaces

In recent years, there has been a great deal of interest in patterning PDMS surfaces. The main reason for this interest is that patterned surfaces are of particular importance for

applications, such as cell culture [89, 128, 129], biological assays [36, 89, 96], elastomeric valves [130] and drug delivery [55, 92, 127]. We will proceed by discussing the patterned PDMS surfaces in terms of topography [128, 131] and chemistry [36, 89, 91, 96, 106, 112, 129].

1.3.1 Topographical patterning

Soft lithography is undoubtedly the most common technique for introducing controlled topography into microfluidic device surfaces due to PDMS's elastomeric properties and ease of molding into micrometer features [53, 55, 92, 93, 105]. The following highlights some additional methods of introducing topographical features. Winton *et al.* [131] employed buckling of a PDMS surface, arising from low-energy metal ion implantation, to produce three dimensional (3D) regular self-organized surface features on the micron and submicron scales. Immediately after the metal ion implantation was carried out, V-shaped cracks appeared randomly on the PDMS surface, a result of internal strain release. With increased ion implantation treatment time a sine wave-like ripple pattern of undulations, with an amplitude of just over 1 μm, was formed on the surface (Figure 1-8). The required time for this regular pattern to appear, from nearly instantaneous to several hours, was dependent upon the implanted metal ion species, presumably due to different interactions between PDMS and high energy metal ions. In addition, the buckling became disordered to form particle domains at distances further away from the V-shaped cracks. Further work on the relationship between controlled patterning and metal ion implantation conditions (ion species, ion dose and treating time) is necessary to fully understand this phenomenon.

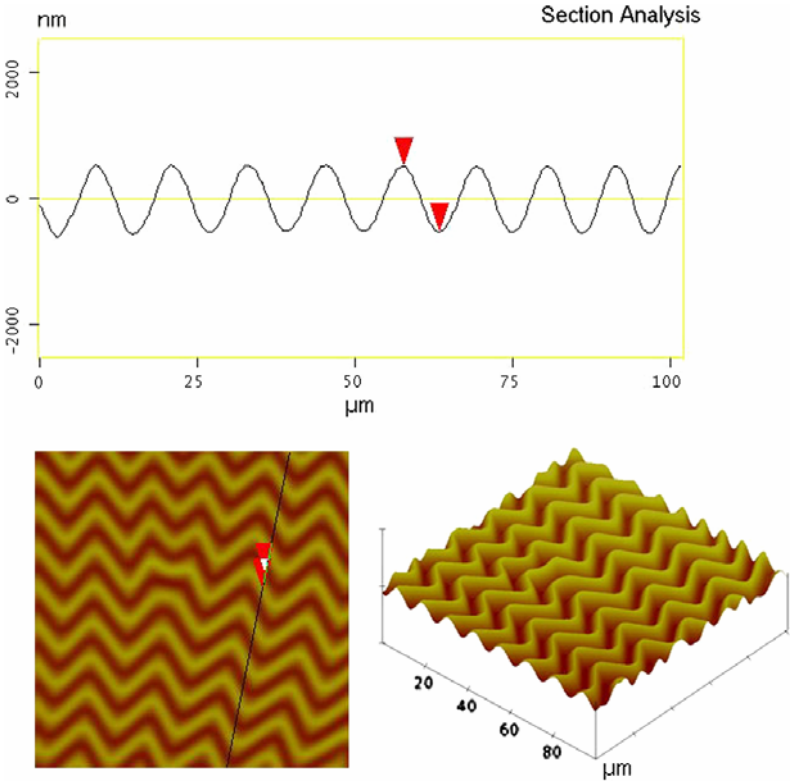

Figure 1-8. Sectional AFM scan of a sine wave-like ripple pattern that present on the PDMS surface after ion implantation [131].

In another example, PDMS samples were sputter-coated with metals and carbon to obtain topographical patterns on the surfaces [132]. The surface morphology investigations showed wavy corrugations were formed on Pt and W coated surfaces with a constant wavelength (peak to peak distance between adjacent waves) whilst random wave patterns were formed on Cr and carbon coated surfaces showing two different wavelengths. The amplitude (difference between wave peak and trough) of the corrugations correlated well with coating thickness. In addition, the effects of combined coating materials, thickness of original PDMS film and re-heating coated PDMS samples on the surface morphology were all examined. Interestingly, the surface patterns on the coated PDMS were not affected by heating the samples to 110 ˚C.

1.3.2 Chemical patterning

Due to its simplicity, UV-induced polymerization through a photomask has been the process of choice to produce a desirable chemically patterned PDMS surface within microchannels [38, 91, 93, 96, 98, 106, 129]. More recently, Su *et al.* used membrane

valves to protect hydrophobic areas on native PDMS and to control exposure of microchannels to monomer solution [93] or ethyl acetate [92]. Any non-protected areas were then exposed to UV-induced polymerization of AAc to produce patterned surfaces within a 3D microfluidic device [92, 93].

Chemical patterning within PDMS microchannels has also been demonstrated by utilizing laminar flows created within microchannels [55]. A schematic of this microfluidic device is shown in Figure 1-9 (a). The microchannel comprised of an upper narrower part and a lower wider part. For patterned hydrophilic surface modification, a fluorescently labeled polyelectrolyte sequence was loaded into a long PE tube and flushed through inlet D while inlet C was blocked and water was simultaneously injected through inlet B, and A was used as an outlet (Figure 1-9 (a)). Due to the laminar flow regime within the microchannel one side of the microchannel and the lower wider part of the device showed fluorescence and the upper narrower part of the device did not (Figure 1-9 (d) and (e)).

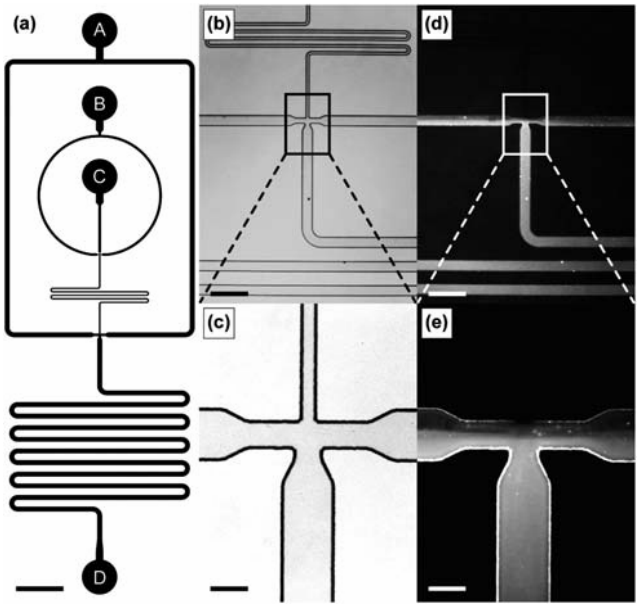

Figure 1-9. Chemical patterning in PDMS microchannel. (a) Schematic of the microfluidic device. For patterned coating in microchannel, a polyelectrolyte sequence was flushed through inlet D and water was injected through inlet B simultaneously, while Inlet C was blocked and A was used as an outlet. (b and c) Bright field micrographs of the microfluidic device after patterned coating. (d and e) Corresponding fluorescence micrographs of the microfluidic device after patterned coating. Only the lower part of the microchannel was coated with fluorescent PEMs. No deposition occurred within the upper part. Scale bars denote (a) 2 mm, (b and d) 750 μm, (c and e) 150 μm [55].

Another interesting form of lithography is bond-detach lithography. This was first shown by Thangawng *et al.* [133] in 2007. As shown in Figure 1-10 (a), an O_2 plasma treated PDMS stamp with topographical patterning was bonded and then detached from an O_2 plasma treated PDMS film on silicon. The PDMS stamp patterns were thus transferred to the PDMS film. Work by Cortese *et al.* [128] also used bond/detachment in order to transfer a pattern. As shown in Figure 1-10 (b), an O_2 plasma oxidized PDMS stamp with topographical patterning was bonded and then detached from a substrate with or without O_2 plasma pretreatment. The pattern on the PDMS stamp was successfully transferred onto the substrate. The degree of transfer from the PDMS stamp was tuned by controlling the contact time (1 to 72 h) between the PDMS and the substrate (microscope glass slide or indium tin oxide coated slide), O_2 plasma treatment or not, and the ratio of PDMS base to curing agent (10:1 or 20:1). Using the above method, a cross pattern of perpendicular PDMS lines was generated on a glass slide by placing a O_2 plasma treated PDMS stamp with parallel lines onto the substrate followed by a second stamp with lines at a 90˚ angle to the first ones. The bond-detach method was also used by Mosadegh *et al.* [130] to prepare patterns of wettability on PDMS. A plasma oxidized PDMS surface was spatially deactivated by transferring residual PDMS oligomers from a native PDMS stamp onto a plasma oxidized surface. As shown in Figure 1-11, a typical elastomeric valve consisting of two PDMS feature layers and a sandwiched PDMS membrane, was fabricated using this approach.

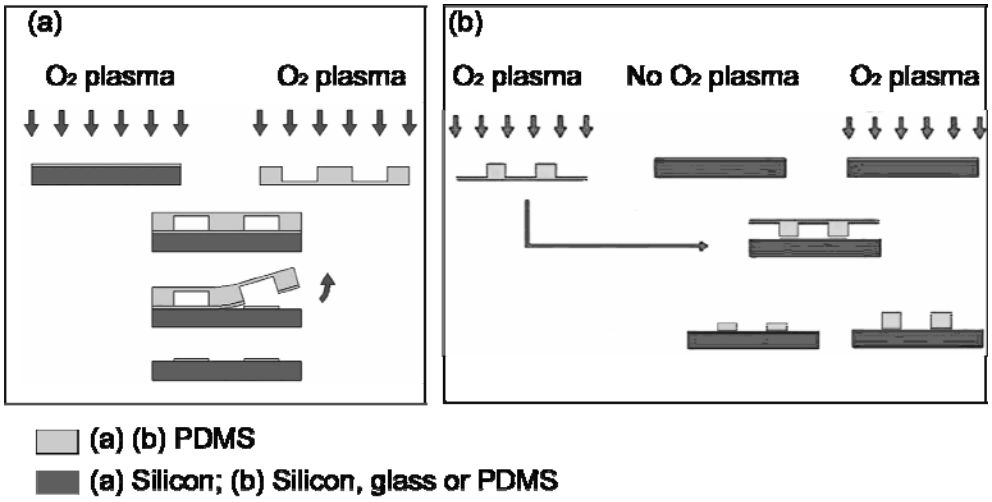

Figure 1-10. Schematic illustration of producing patterned PDMS using bond-detach lithography method. (a) PDMS patterned surface was formed *via* capturing a plasma oxidized film onto another plasma oxidized PDMS stamp corresponding to the stamp patterns [133]. (b) PDMS patterned surface was formed *via* capturing PDMS from a plasma oxidized PDMS stamp onto substrates (silicon, glass or PDMS) with/without plasma oxidization [128].

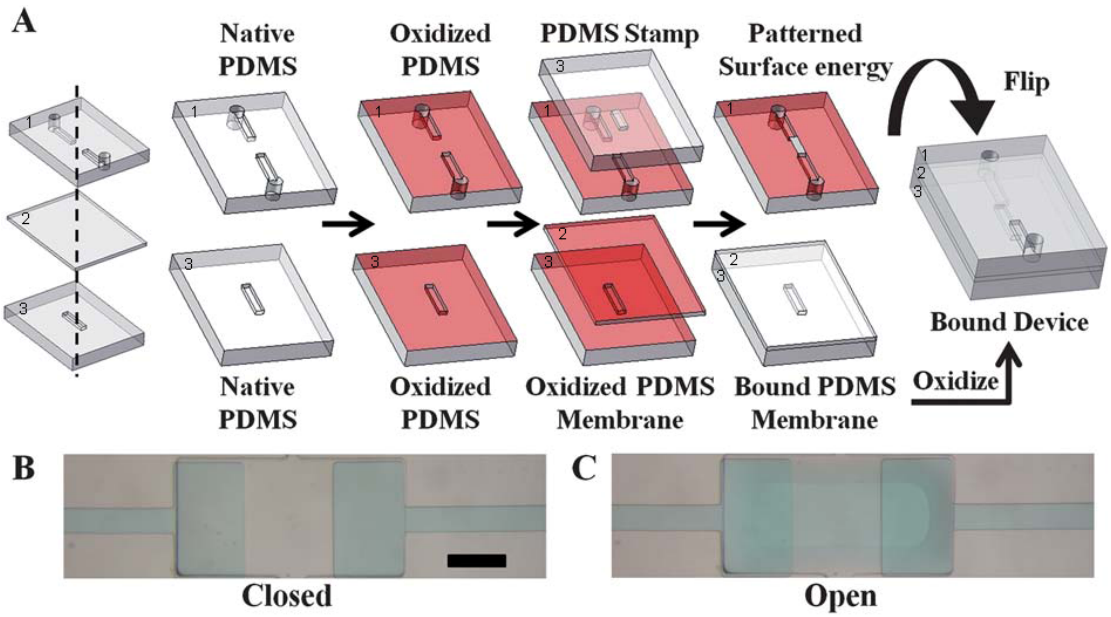

Figure 1-11. Integrated elastomeric valves. (A) Scheme for fabrication of PDMS elastomeric valve. A patterned oxidized PDMS 1, achieved by bonding and detaching an entire oxidized PDMS 1 with a native PDMS 3, was bonded with PDMS 3/PDMS 2 to form elastomeric valve. (B) Elastomeric valve in a closed position with the membrane flat. Scale bar: 0.25 mm. (C) Elastomeric valve in an open position with the membrane deflected [130].

Other methods of patterning of open PDMS surfaces with subsequent bonding to form microchannels include the use of a stainless steel mesh placed on a PDMS surface which was then exposed to an Ar plasma followed a sputter coating Al [89].

1.4 Applications

By applying suitable surface modification methods, hydrophobic PDMS surfaces can be successfully rendered hydrophilic. In particular, surfaces can be selectively equipped with functional groups, such as silanol [32, 34], carboxyl [33, 97, 98], amino [40, 57] and isothiocyanate groups [61]. This approach can greatly improve the performance of PDMS in microfluidic device and microarray applications. The most eminent application of PDMS based microfluidics is in the separation of biomolecules, including amino acids [49, 64, 80, 86, 88, 108, 110, 125], peptides [60, 85, 134, 135], proteins [63, 71, 72, 88, 103, 111], neurotransmitters [46, 48, 49] and DNA [54, 109, 136]. Furthermore, the immobilization of biomolecules with molecular recognition properties (*e.g.* antibodies or enzyme activities) inside modified PDMS microchannels is attracting much attention [61, 97, 137-141]. These bio-functionalized surfaces can be further used for genomic analysis [61, 87], immunoassays [53, 61, 112, 142] or as enzyme microreactors [97]. Spatially controlled cell attachment can be accomplished on modified PDMS surfaces rendering them beneficial in biointerfacial studies in controlled flow environments [24, 61, 89, 114, 129]. Capture-to and release-of proteins from PDMS surfaces have also been pursued [89, 95, 107]. In addition, the use of microfluidic devices to form controlled emulsions [55, 68, 91-93] is currently receiving significant attention. The following highlights some of the more recent advances in the separation of biomolecules, microfluidic immunoassays, genomic analysis, capture/release of proteins in microfluidic channels, cell culture and formation of emulsions inside microfluidic channels.

1.4.1 Separation of biomolecules

Capillary electrophoresis (CE) is commonly used for biomolecular separation in modified PDMS microchannels [46, 48-51, 56, 63, 64, 80, 81, 109]. The principal purposes of PDMS surface modification here are to reduce CE separation time, band broadening and/or increase separation efficiency *via* inhibiting non-specific adsorption of analytes and

obtaining a suitable EOF. The separation efficiency is quantitatively described by the plate number, which describes peak broadening effects. The plate number (N) is given by the following equation [143]:

$$N = 5.54 (t_r/W_{1/2})^2$$

where t_r is the retention time of the peak and $W_{1/2}$ is the peak width at half-maximum.

The separation time and efficiencies are affected by separation parameters such as the length of separation channel, background electrolyte and separation field strength [144]. Table 1-2 lists the details of the separation parameters (*i.e.* length of separation channel, background electrolyte, separation field strength and time required) for various biomolecular separations performed in microfluidic devices made from surface-modified PDMS. We will proceed by discussing these applications according to the different analyte categories.

Table 1-2. Comparison of separation conditions for different biomolecule groups in microchannels featuring surface-modified PDMS.

Analytes	PDMS microchannel surface modification	Length of the separation channel (cm)	Background buffer (pH)	Separation field strength (V/cm)	Separation time (s)	Relevant section in manuscript text and reference
Amino acids[a)]						
Arg and His	LBL (using PDDA-gold nanoparticles-Cys)	3.5	10 mM PBS (7)	229	80	Section 1.2.2.1 [49]
Arg, Pro, His, Val, Ser and Thr	LBL (using Chit-*g*-mPEG)	3.7	5.0 mM STB[b)] (9.75)	432	90	Section 1.2.2.1 [51]
Arg, Pro, His, Val, Ser, Thr and Cys	Plasma/silanization (mPEG-APTES)	3.8	5.0 mM STB (-)	421	130	Section 1.2.3.1 [81]
5-(4,6-Dichloro-striazin-2-ylamino) fluorescein-(Arg, His, Phe, Ser and Glu)	Oxygen plasma Plasma/LBL (using $(PVA)_2$)	3	10 mM borate buffer (8.0)	333	50 90	Section 1.2.3.3 [110]
FITC-(Arg, Phe, Glu and Ser)	Plasma/silanization (GPTMS)/'graft to' polymer coating (NH_2-PEG)	3.5	25 mM borate buffer (9)	300	65	Section 1.2.3.1 [86]
FITC-(Arg, Pro, Glu, Lys and Ser)	Oxygen plasma/ silanization (CPTCS)/'graft to' polymer coating (alkyne-PEG)	3.5	25 mM borate buffer (10)	300	140	Section 1.2.3.1 [88]

Table 1-2. (Continued)

Analytes	PDMS microchannel surface modification	Length of the separation channel (cm)	Background buffer (pH)	Separation field strength (V/cm)	Separation time (s)	Relevant section in manuscript text and reference
FITC-(Arg, Phe, Gly, Glu and Asp)	Plasma/'graft to' polymer coating (AHPCS)	2	2 mM borate buffer (8.8)	500	30	Section 1.2.3.2 [108]
FITC-(Arg, Ser and Glu) TAMRA-(Pro and Ser)	Sol-gel coating (using SiO_2 particles)	3.5	1 mM STB (9.5)	650	14 8	Section 1.2.2.2 [56]
TAMRA-(Try, Phe, Ser, Pro and Asp)	Dynamic (50 mM SDS)	3.65	10 mM STB (-)	650	25	Section 1.2.2.4 [64]
BODIPY® FL CASE -(Asp, Glu, Ser, Asn, Pro, Gln, Thr, Ala, Tyr, Val, Met, Ile, Phe, Lys, Try and Arg)		30 (serpentine)		750	360	
NBD-F-(His, Thr, Ser and Gly)	Plasma/silanization (PGA)	5	25 mM borate/NaOH buffer (9.0)	200	180	Section 1.2.3.1 [80]
Peptides						
FITC-BSA digest	Silanization (APTES) + poly(styrenesulfonic acid)	3.9	1 mM carbonate buffer (8.7)	256	500	Section 1.2.2.3 [60]
	Silanization (methoxydimethyloctadecylsilane) + 0.2 % SDS (dynamic)				200	

Table 1-2. (Continued)

Analytes	PDMS microchannel surface modification	Length of the separation channel (cm)	Background buffer (pH)	Separation field strength (V/cm)	Separation time (s)	Relevant section in manuscript text and reference
HSA digest	Plasma/silanization (APTES) + graft polymerization (P(DMA-*co*-GMA))	>2	10 mM PBS (9)	400	50	Section 1.2.3.1 [85]
Proteins						
TRITC-(lysozyme and cytochrome c)	UV+ATPR (PAAm)	3.5	50 mM PBS (2.15)	888	35	Section 1.2.3.2 [103]
Glucose oxidase and myoglobin	Dynamic (Brij35) + 0.01 % Brij35 pretreatment	4.3	30 mM NaOH (12)	279-325	260	Section 1.2.2.4 [65]
Insulin, cytochrome c and ovalbumin	Plasma/LBL (h-PSMA/(PEI/PAA)$_2$/PEI/PEG dialdehyde)	5.5	50 % diluted SDS gel buffer (4)	218	420	Section 1.2.3.3 [111]

Table 1-2. (Continued)

Analytes	PDMS microchannel surface modification	Length of the separation channel (cm)	Background buffer (pH)	Separation field strength (V/cm)	Separation time (s)	Relevant section in manuscript text and reference
Cytochrome c, lysozyme, ribonuclease A and myoglobin	Dynamic (25 mM SDS)	4	10 mM sodium borate and 20 % acetone (9.5)	650	20	Section 1.2.2.4 [63]
Cytochrome c, lysozyme and ribonuclease A, myoglobin and α -lactalbumin					28	
Cytochrome c, lysozyme and ribonuclease A, myoglobin, BSA and α -lactalbumin				1200	10	
FITC-myoglobin and FITC-BSA	Dynamic (5 mM SDS)	-	25 mM Tris (9)	600	-	Section 1.2.2.4 [145]
Hemoglobin, albumin and glucose oxidas	LBL (using Chit-g-mPEG)	3.7	30 mM NaOH (-)	297	80	Section 1.2.2.1 [51]
TAMRA-lysozyme and ribonuclease B	Plasma/LBL (using $(PVA)_3$)	3.5	30 mM PBS (3)	543	30	Section 1.2.3.3 [109]
BSA and β -lactoglobulin			30 mM PBS (8)	543	50	

Table 1-2. (Continued)

Analytes	PDMS microchannel surface modification	Length of the separation channel (cm)	Background buffer (pH)	Separation field strength (V/cm)	Separation time (s)	Relevant section in manuscript text and reference
Lysozyme and ribonuclease A	Plasma/silanization (APTES) + graft polymerization (PVA-*g*-GMA)	>2	30 mM PBS (3)	400	26	Section 1.2.3.1 [85, 136]
	Plasma/silanization (APTES) + graft polymerization (P(DMA-*co*-GMA))				28	
	Plasma/silanization (APTES) + graft polymerization (PVP-*g*-GMA)				25	
BSA, ovalbumin, chymotrypsinogen and lysozyme		>1	100 mM Tris-TAPS[)] buffer (8.3) (5 % PDMA and 0.1 % SDS)		20	
Cy3-extravidin and IgG	Dynamic (8 mM BMImBF4 + 4 % Triton X-100)	3.6	10 mM PBS (9.5)	417	500	Section 1.2.2.4 [72]
TRITC-IgG, Cy3-IgG and FITC-IgG			2 mM PBS (9.5)	-	-	
Cy3-extravidin and IgG	Dynamic (20 mM BAS)	4.5	20 mM BAS	222	100	Section 1.2.2.4 [71]
Cy3-IgG and FITC-IgG					-	

Table 1-2. (Continued)

Analytes	PDMS microchannel surface modification	Length of the separation channel (cm)	Background buffer (pH)	Separation field strength (V/cm)	Separation time (s)	Relevant section in manuscript text and reference
BSA and RNase A	Oxygen plasma/ silanization (CPTCS)/'graft to' polymer coating (alkyne-PEG)	3	25 mM borate buffer (10)	300	250	Section 1.2.3.1 [88]
FITC-(cytochrome C, lysozyme, lysine) and FITC	Adding modifier into PDMS prepolymer (PEGMEM) Dynamic (0.05 % SDS)		PBS buffer (7.4)	200	9	Section 1.2.2.6 [125]
Neurotransmitters[b] and environment pollutants[c]						
DA and EP	LBL (using LPEI)	3.7	30 mM PBS (7)	216	100	Section 1.2.2.1 [46]
DA, EP, p-PDA, 4-AP and HQ	LBL (using Chit-gold nanoparticles-Alb)		40 mM PBS (7)	270	140	Section 1.2.2.1 [50]
	LBL (using Lys-Alb)		30 mM PBS (7)			
5-HT, DA, EP and DBA	LBL (using PDDA-glucose oxidase)		40 mM PBS (7)	270	110	Section 1.2.2.1 [48]

Table 1-2. (Continued)

Analytes	PDMS microchannel surface modification	Length of the separation channel (cm)	Background buffer (pH)	Separation field strength (V/cm)	Separation time (s)	Relevant section in manuscript text and reference
DA and EP	LBL (using PDDA-gold nanoparticles-Cys)	3.5	10 mM PBS (7)	229	-	Section 1.2.2.1 [49]
DNA						
ϕX174 RF/Hael II	Plasma/LBL (using $(PVA)_3$)	3.5	100 mM TTE buffer (8.3)	229	400	Section 1.2.3.3 [109]
	LBL (polybrene/dextran sulfate bilayer)	4	TBE buffer (-)	250	180	Section 1.2.2.1 [54]
Others						
Glucose, penicillin, phenol and homovanillic acid	Dynamic (SDS)	5.2	5 mM boric acid buffer (12)	288	150	Section 1.2.2.4 [22]
	Dynamic (DOC)			288	125	
DA, catechol and AA	Solvent extracted and plasma oxidization	5.9	20 mM Tri-TAPS buffer (7)	170	120	Section 1.2.1.1 [29]
Doxorubicin and daunorubicin			20 mM boric acid (10)	200	70	
UA and AA	LBL (using $(PDDA/PSS)_2$)	4	20 mM PBS (7.4)	300	130	Section 1.2.2.1 [47]
UA and AA from human urine samples					-	

Table 1-2. (Continued)

Analytes	PDMS microchannel surface modification	Length of the separation channel (cm)	Background buffer (pH)	Separation field strength (V/cm)	Separation time (s)	Relevant section in manuscript text and reference
UA and AA	Chit-DNA	3.7	20 mM acetate buffer (5)	351	85	Section 1.2.2.1 [25]
UA and AA from human urine samples					-	

a) Arginine (Arg), proline (Pro), histidine (His), valine (Val), serine (Ser), threonine (Thr), cysteine (Cys), phenylalanine (Phe), glutamic acid (Glu), tryptophan (Try), aspartic acid (Asp), asparagine (Asn), glutamine (Gln), Alanine (Ala), tyrosine (Tyr), methionine (Met), isoleucine (Ile), lysine (Lys), glycine (Gly);
b) Sodium tetraborate;
c) Dapamin (DA), epinephrine (EP), 5-hydroxytryptamine (5-HT), dobuamine (DBA);
d) p-Phenylenediamine (p-PDA), 4-aminophenol (4-AP), hydroquinone (HQ)

1.4.1.1 Amino acids

Wang *et al.* [51] have successfully separated a mixture of Arg, Pro, His, Val, Ser and Thr in a Chit-*g*-mPEG modified PDMS microfluidic device (prepared by LBL technique). Devices modified with mPEG (prepared by combination of plasma and silanization) were also used to separate the same mixture, in that case also including Cys [81]. The Chit-*g*-mPEG and mPEG modified devices showed long-term stability and excellent reproducibility of separation for 2 – 4 wk [51, 81]. Wang *et al.* [49] reported successful separation of a mixture of Arg and His on a PDDA-gold nanoparticle-Cys coated channel (prepared by LBL technique). All three examples above used electrochemical detection for the analysis of the amino acids.

Using fluorescence detection, mixtures of Arg, His, Phe, Ser and Glu labeled with 5-(4,6-dichloro-striazin-2-ylamino) fluorescein were separated in both oxygen plasma treated and PVP coated PDMS microchannels (prepared by combination of plasma and LBL) [110]. Higher separation efficiencies were consistently obtained in the oxygen plasma treated channel (plate numbers: 1.03×10^6 N/m for Arg, 1.26×10^6 N/m for His, 1.37×10^6 N/m for Phe, 9.65×10^5 N/m for Ser and 7.42×10^5 N/m for Glu) compared to the PVP coated channel (plate numbers: 4.28×10^5 N/m for Arg, 5.20×10^5 N/m for His, 7.79×10^5 N/m for Phe, 6.84×10^5 N/m for Ser and 1.93×10^5 N/m for Glu). Roman *et al.* [64] separated two mixtures of amino acids labeled with *N*-(4,4-difluoro-5,7-dimethyl-4-bora-3a,4a-diaza-s-indacene-3propionyl)cysteic acid, succinimidyl ester (BODIPY® FL CASE) on serpentine PDMS channels in the presence of SDS. Having a length of 30 cm, this channel is one of the longest PDMS microchannels reported to date, which allowed the separation of 16 different amino acids [64]. Miyaki *et al.* [80] reported separation of a mixture of 4-fluoro-7-nitrobenzofurazan labeled His, Thr, Ser and Gly in a PGA modified microchannel (prepared by combination of plasma and silanization), which could still separate after 1 wk of storage. Other two mixtures of FITC labeled amino acids (mixture of Arg, Phe, Glu and Ser, and mixture of Arg, Pro, Glu, Lys and Ser) were successfully separated in NH_2-PEG and alkyne-PEG modified microchannels (both prepared by combination of plasma, silanization and 'grafting-to' polymer coating), respectively [86, 88]. A comparison was then made between the separation of amino acids (Glu, Ser and Arg) using the two PEG modified microchannels. The NH_2-PEG modified PDMS had shorter separation times and better reproducibility and

stability than the alkyne-PEG modified PDMS. In another 'grafting-to' approach, a mixture of FITC labeled amino acids (Arg, Phe, Gly, Glu and Asp) was separated in an AHPCS modified PDMS microchannel in less than 40 s [108].

The shortest amino acid separation time (8 s) was obtained when separating tetramethylrhodamine succinimidyl ester labeled Pro and Ser in a SiO_2-modified PDMS microchannel by a sol–gel method [56] while the highest reproducibility (relative standard deviation (RSD) of Arg, Pro, Val, His, Ser, Thr and Cys < 2.3 % from run to run, day to day and chip to chip, n=3) of amino acid separation was achieved in a PDMS channel modified by plasma pretreatment and functionalized with mPEG-APTES [81].

1.4.1.2 Peptides

Slentz *et al.* [60] were the first to report an efficient separation of a FTIC-labeled BSA digest by capillary electrochromatography (CEC) on a PDMS chip. The group used a collocated monolith support structure (COMOSS) column made from PDMS instead of a channel packed with a conventional particle-based stationary phase (Figure 1-12). Poly(styrenesulfonic acid) was attached to an APTES-modified PDMS surface, which resulted in a better separation efficiency for peptides from a tryptic BSA digest, compared to the unmodified COMOSS. But the best separation of the peptide mixture was obtained on methoxydimethyloctadecylsilane modified COMOSS. The separation time was reduced from 500 s to 200 s. In another example, a trypsin digest of human serum albumin (HSA) was separated in a P(DMA-*co*-GMA) modified PDMS microchannel (prepared by combination of plasma, silanization and 'grafting-to' polymer coating) [85]. Approximately 20 different peptides were resolved within 50 s by a combination of CE and mass spectrometry (MS) detection, implying that it was possible to perform rapid peptide mapping in this microfluidic device coupled with MS detection.

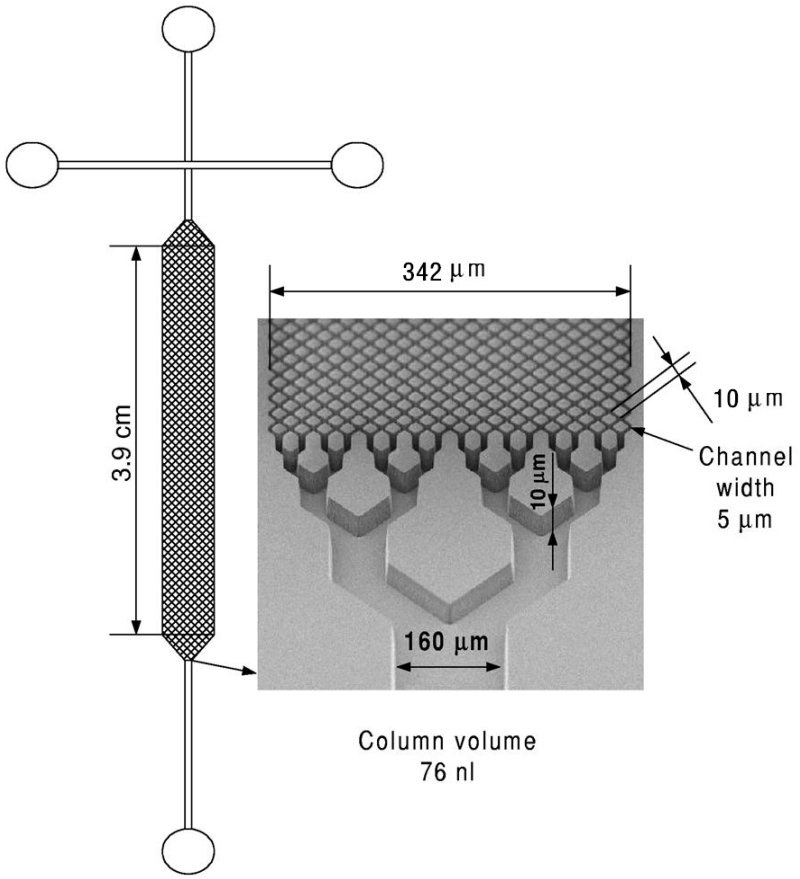

Figure 1-12. (Left) schematic of a COMOSS separation column made from PDMS and (right) scanning electron micrograph of the inlet section of the COMOSS [60].

1.4.1.3 Proteins

By using dynamic surface modification with SDS, a mixture of myoglobin and BSA both labeled with FITC has been separated [145]. Roman *et al.* [63] used SDS to modify PDMS for denatured protein separation and showed that a higher SDS concentration (25 mM) significantly improved separation efficiency. The improved efficiency was proposed to be due to the adsorption of SDS onto the proteins rendering them more negative and thus repelling them from the negatively charged PDMS surface. In this fashion, the electrostatic repulsion between the PDMS-SDS surface and the SDS-protein conjugate is the major contributor to separation efficiency. Using a combination of ionic liquid and surfactant ($BMImBF_4$/Triton X-100) as background electrolyte (BGE) buffer, protein separation efficiency was improved compared to a separation carried out with Triton X-100 only [72]. This improved separation using the $BMImBF_4$/Triton X-100 combination was attributed to

the self-assembly of the $BMImBF_4$ on the PDMS surface due to the electrostatic association between the slightly negative PDMS surface and the positively charged imidizolium groups [72]. In addition, BAS modification of PDMS has led to the prevention of protein adsorption and enabled microfluidic protein separation in a BAS containing running buffer [71]. Likewise, compared with a native PDMS microchannel (0.95×10^4 N/m plate number for myoglobin), addition of 0.01 % Brij35 in a running buffer increased the separation efficiency of myoglobin to 3.3×10^4 N/m, but the reproducibility was as low as in running buffer without Brij35 (5 - 6 runs) [65].

Besides using dynamic PDMS surface modification in the application of protein separation, Wu *et al.* [85, 109, 136] used PVA modified PDMS microchannels (using combination of gas-phase and wet chemical methods) to separate acidic and basic protein mixtures using different pHs PBS buffer. The basic proteins were separated in less than 30 s, whereas it took 50 s for acidic proteins. In another study, PEGMEM modified microchannels (prepared by simply adding PEGMEM into PDMS prepolymer before curing) showed improved separation of a mixture of FITC-labeled cytochrome C, FITC-labeled lysozyme, FITC-labeled lysine and FITC, compared with native PDMS under the same separation conditions [125]. However, when 0.05 % SDS was added to the separation buffer, better separation was achieved in the native PDMS microchannel, compared to the PEGMEM modified microchannel, presumably because more SDS was adsorbed onto the native PDMS. In addition, the alkyne-PEG modified PDMS was shown to successfully separate a mixture of BSA and RNase A [88].

Comparing reports on the PDMS-based microfluidic separation of proteins, the shortest separation time was 9 s at 200 V/cm for separating a mixture of FITC-labeled cytochrome C, FITC-labeled lysozyme, FITC-labeled lysine and FITC in PEGMEM modified microchannel or native PDMS microchannel in the presence of a dynamic modifier, SDS [125], and the best repeatability was 70 times on a PDMS microchannel modified with $(PVA)_3$ using combination of plasma and LBL technique [109].

1.4.1.4 Neurotransmitters

As signal messengers, neurotransmitters play an important role in coordinating central and

peripheral nervous systems [48]. The LBL technique was employed here for PDMS surface modifications to separate neurotransmitter mixtures [46, 48, 50]. To get high separation efficiencies, ionic strengths and field strengths were optimized. Reproducibility studies showed that the modified surfaces were stable for 2 wk if kept in contact with running buffer at 4 ºC. But similar to the work by Dou *et al.* [65], the problem of analyte adsorption onto the CE electrode required further attention since this ultimately limits repeatability when using electrochemical detection.

1.4.1.5 DNA

Using a PDMS microchannel coated with three layers of PVA, formed *via* LBL modification, 11 double stranded deoxyribonucleic acid (dsDNA) fragments (72 to ~1353 bp) from the icosahedral bacteriophage φ174 (digested by HaelII) were separated. By using a 2 % low-viscosity hydroxypropylmethyl cellulose as a separation matrix and a tris(hydroxymethyl)aminomethane (Tris) - *N*-tris(hydroxymethyl)methyl-3-aminopropanesulfonic acid (TAPS) - ethylenediaminetetraacetic acid (EDTA) (TTE) buffer separation was achieved in 400 s [109]. However, poor separation was observed when using tris(hydroxymethyl)aminomethane-borate-ethylenediaminetetraacetic acid (TBE) buffer, due to the formation of complexes by hydroxyl groups from the PVA coating with boric acid from the buffer. Kuo *et al.* [54] demonstrated the above same DNA mixture were successfully separated in microchannel coated with polybrene/dextran sulfate bilayer. The authors observed much shorter separation time (180 s) [54] when compared to a $(PVA)_3$ modified PDMS microchannel (400 s) [109]. In addition, DNA was pre-concentrated in the same polybrene/dextran sulfate bilayer coated microfluidic device with a closed valve. This closed valve with anionic surface charges forms a nanoscale channel that only allows the passage of electric current but traps the negatively charged DNA, so that the DNA are pre-concentrated. The technique showed an increasing in fluorescent intensity of the labeled DNA of up to 3 orders of magnitude with only 2 min at the pre-concentration stage [54].

1.4.1.6 Others

The separation of glucose, penicillin, phenol and homovanillic acid was performed in PDMS microchannels to compare the effect of SDS and DOC as dynamic surface modifiers in the running buffer with surfactant-free buffer [22]. Reduced separation times of 25 % and 37.5 % were achieved when DOC and SDS were added, respectively. Furthermore, the addition of these two negatively charged surfactants produced an unstable electrochemical detection response. Vickers *et al.* [29] removed uncured hydrophobic oligomers from PDMS by solvent extraction and then oxidized the PDMS surface in an air plasma. The thus prepared surface gave from four to seven times increased separation efficiencies for dopamine, catechol and ascorbic acid (AA) compared with native PDMS. The separation of doxorubicin and daunorubicin was also achieved on the same microfluidic device, albeit with increased background noise. Qiu *et al.* [25, 47] successfully separated uric acid and AA from a standard mixture and from human urine samples on PDMS microchannels modified by LBL with $(PDDA/PSS)_2$ and Chit-DNA. In terms of separation time, the Chit-DNA surface performed better (150 s for $(PDDA/PSS)_2$ PDMS modified microchannel and 85 s for Chit-DNA modified microchannel).

1.4.2 Enzyme microreactors

The immobilization of enzymes in microfluidics allows the study of enzymatic reactions in high-throughput low volume fashion. Enzyme immobilization reduces undesired auto-digestion of proteolytic enzymes, reduces the amounts of proteins required and reduces cost by re-use of the immobilized enzymes [97]. Activity of enzymes immobilized in microchannels can be maintained for extended periods of time [123]. Wu *et al.* [97] immobilized the enzyme trypsin both *via* carbodiimide covalent coupling and *via* non-covalent bonding with PDDA inside PDMS microchannels, which had been previously modified with PAAc using UV-induced graft polymerization. After trypsin immobilization, the proteins, cytochrome c, BSA or casein were introduced into the trypsin-modified microchannel, and then the digested proteins were detected by means of matrix-assisted laser desorption/ionization (MALDI) – time of flight (TOF) –MS or CE off-line, in addition to electrospray ionization MS on-line as a proof-of-principle of rapid peptide mapping of proteins. The digestion experiments were finished in 5 – 20 s and the

microreactors could be used at least 50 times in 1 wk on both the covalently and non-covalently trypsin modified surfaces. In the case of the trypsin modified surface *via* non-covalent bonding, its activity could be regenerated by acid treatment, ready for re-immobilization of fresh trypsin. In another example, trypsin covalently immobilized on PAAm modified PDMS surface *via* EDAC/NHS coupling was exposed to intramolecularly quenched BODIPY-casein complexes [96]. The fluorescence of this reporter system increased as the digestion proceeded.

1.4.3 Immunoassays

Immunoassays afford highly sensitive detection of a range of biological agents ranging from small molecules to pathogens. However, long analysis times and large amounts of expensive reagents are needed in a conventional immunoassay. The integration of immunoassay into microfluidics has the potential to provide significant reductions in terms of analysis time and cost [137, 138].

Park *et al.* [139, 140], formed carboxyl groups on PDMS surface upon permanganate-periodate oxidation of vinyl groups which had been introduced as 7-octenyltri(chloro)silane onto an oxygen plasma treated surface (Figure 1-13 (a)). This surface was further modified in two different ways for detecting IgG. In the first case, biotin-LC-PEO-amino was covalently attached to the carboxyl terminated surface *via* 1-ethyl-3-(dimethylamino)-propylcarbodiimide-*N*-hydroxysuccinimide activation (Figure 1-13 (b)). Consequently, the modified surface could capture mouse IgG fused to avidin (Figure 1-13 (c)). In a second procedure, carboxyl groups were reacted with protein G, which then served as a capture agent for the IgG antibody [140]. Alkaline phosphatase (AP)-labeled anti-IgG were detected electrochemically down to 485 pg/mL and 148 pg/mL, respectively [139, 140]. In another example, protein G was covalently immobilized onto a PDMS microchannel *via* the combination of LBL and UV-induced graft polymerization techniques [112]. Subsequently, the protein G modified PDMS microchannel was reacted with monoclonal antibody against estrogen receptor α (ERα) and a blocking solution in sequence for capturing ERα *via* a sandwich type immunoassay. Finally, the captured ERα was detected by Cy3 labeled estradiol. In addition, PDMS microchannel with bilayer of IgG incorporated into polyelectrolyte layers [53] showed a much lower detection limit (6.7

pM) than the one with monolayer adsorbed IgG, although a shorter assay time (30 min) was observed in the case of monolayer IgG adsorption [142].

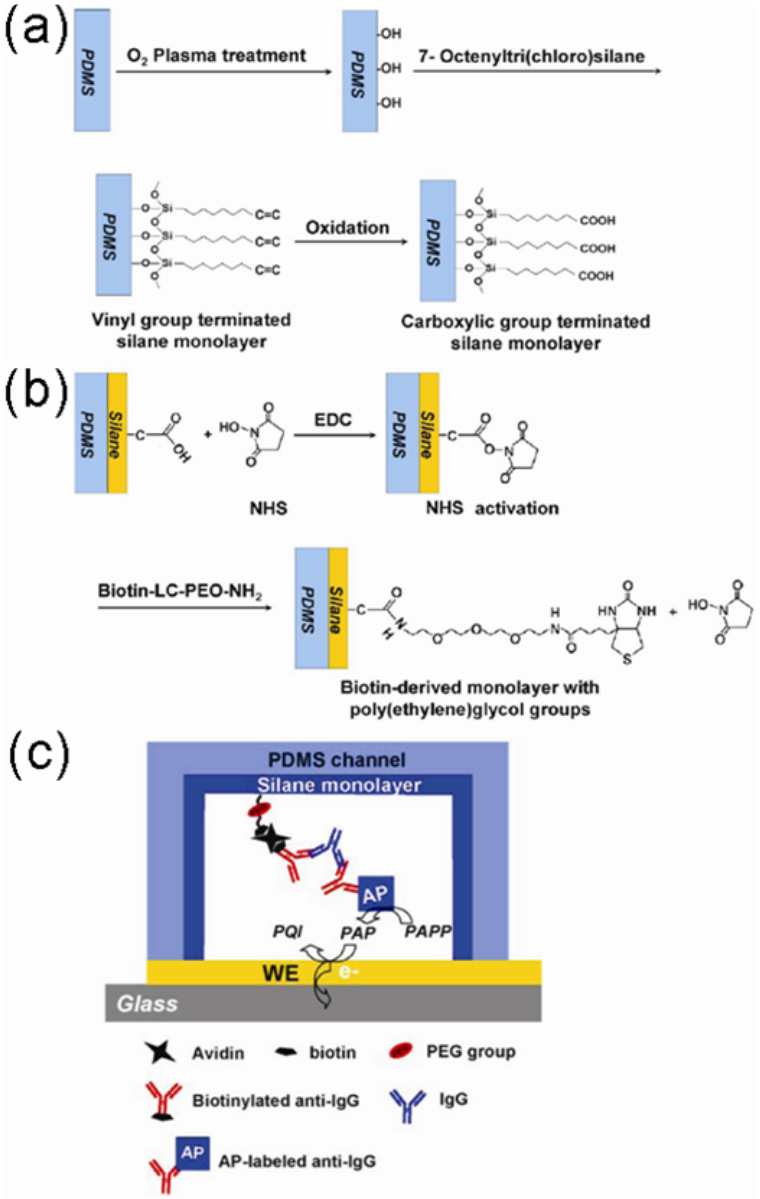

Figure 1-13. Schematic of surface functionalization and the application of an immunoassay: (a) carboxy-terminated silane monolayer derived from the PDMS surface by three steps, including oxygen plasma pretreatment, silanization of 7-octenyltri(chloro)silane and permanganate-periodate oxidation; (b) biotin-PEG-functionalized surface silane monolayer after 1-ethyl-3-(dimethylamino)-propylcarbodiimide-*N*-hydroxysuccinimide activation of the carboxy groups; (c) schematic view of on-chip immunoassay within surface-functionalized PDMS channel. Biotinylated anti-IgG was firstly immobilized on the biotin-PEG-functionalized PDMS surface *via* avidin–biotin linkage, and then used to capture IgG. Finally, AP-labeled anti-IgG was bonded to IgG for electrochemical detection [140].

Sui *et al.* [61] have reacted an aminosilanized PDMS microchannel with thiophosgen to generate isothiocyanate groups. Prostate stem cell antigen (PSCA) protein was then covalently attached onto the microchannel *via* urea bond formation. The resulting surface was used to detect a prostate cancer biomarker, anti-PSCA. Fluorescence microscopy was used to demonstrate successful molecular recognition of anti-PSCA.

It should be pointed out that microfluidic immunoassays are often carried out using native PDMS surfaces, simply exploiting antibody adsorption on the hydrophobic PDMS [137, 138, 141] as long as non-specific adsorption of analyte species can be prevented, e.g., blocking the surface with BSA.

1.4.4 Genomic analysis

An amino-terminated 21 mer oligonucleotidewas immobilized on the surface of an isothiocyanate-modified PDMS microchannel. DNA hybridization occurred inside the microchannel using a complementary dye labeled oligonucleotide, which was detected using fluorescence microscopy [61]. Similarly, an amino terminated 30 mer oligonucleotide was covalently attached onto the carboxyl group functionalized PDMS surfaces *via* amide linkages. Then, fluorescence labeled complementary strands were successfully captured *via* hybridization and were visualized using fluorescence microscopy [31, 77]. Here, PDMS surfaces functionalized with carboxylic acid groups were prepared by two different techniques. The first involved a two-step Ar and AAc plasma modification [31] and the second involved SAM assisted surface modification (adding UDA into PDMS prepolymer before curing it on a hydrophilic SAM coated substrate) [77].

In another example, hydroxy-terminated PEG was attached on PDMS which was pre-silanized with GPTMS by a UV-induced silanization method [87]. The PEG modified PDMS microchannel was loaded into an automated DNA synthesizer and both 6-mer and 21-mer DNA probes were synthesized using the channel as a solid phase. After deprotection, the surface-attached DNA could be hybridized to complementary probes. This work may have implications for other solid phase biomolecule synthesis such as those of peptides inside microfluidic channels.

1.4.5 Capture/release of proteins in microfluidic channels

Microfluidic devices have been used to purify and enrich analytes from complex biological fluids, which has important implications in clinical applications. HPGs modified PDMS microchannels with pillar arrays (prepared by a 'grafting-to' polymer coating technique) were shown to reduce non-specific adsorption of BSA and selectively capture positively charged avidin by electrostatic interaction at neutral pH [107]. The captured avidin could then be released by using a higher ionic strength buffer. Successful capture/release and enrichment of protein A has also been demonstrated on a PNIPAAm modified PDMS microchannel (prepared by a 'grafting-from' polymer coating technique) by changing the temperature [95]. As shown in Figure 1-14 (a), streptavidin-PNIPAAm conjugates were introduced into the microfluidic channel at room temperature. Then the temperature was raised to 36 ºC (above the lower critical solution temperature of the polymer), conjugates aggregated and then moved onto the surface through hydrophobic interactions. Warm buffer was applied to remove unbound conjugates. Finally, the aggregates were re-dissolved when the temperature was lowered to 25 ºC. When streptavidin-PNIPAAm conjugates were introduced into the microfluidic device heated to 36 ºC (Figure 1-14 (b)), the conjugates were immediately captured from solution onto the PNIPAAm modified PDMS surface. Compared with the previous case where the process started at room temperature, a higher concentration of conjugates was achieved using this 'hot start' procedure. Using this method, it was possible to enrich anti-p24 monoclonal IgG by up to six times.

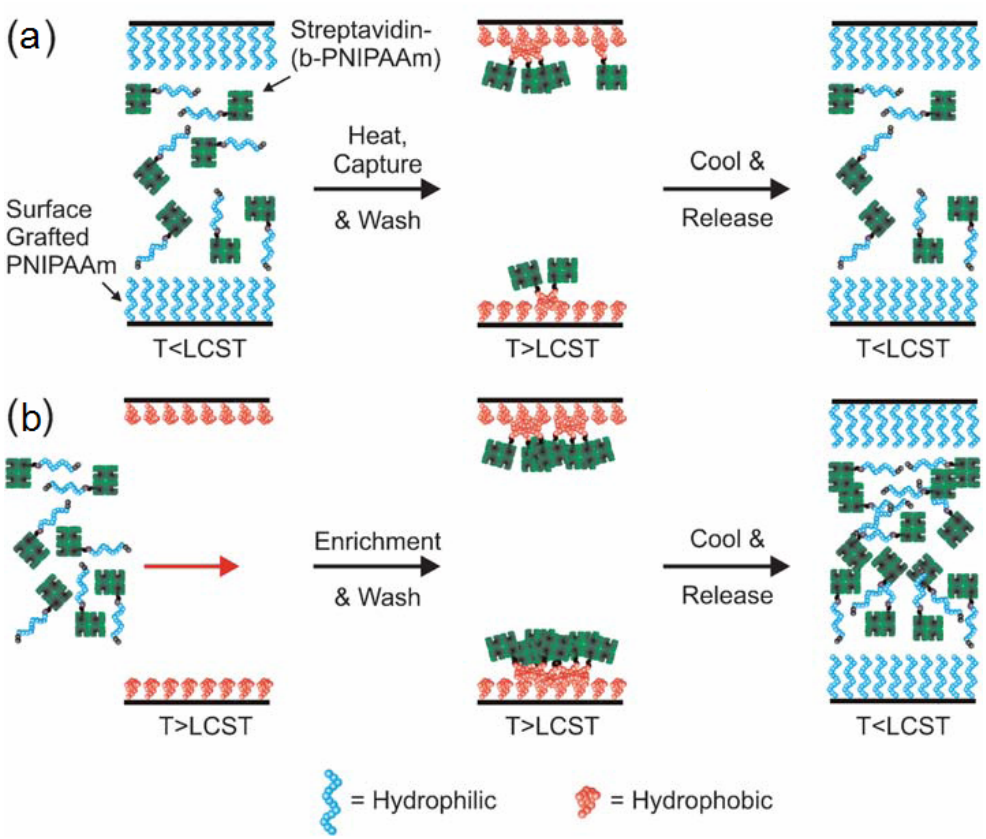

Figure 1-14. Conjugate capture schematics responding to temperatures. (a) Conjugate capture schematic (cold start). Conjugates were loaded at room temperature. When the temperature was raised above 36 ºC, conjugates aggregated and moved onto the PNIPAAm-modified surface; (b) Conjugate enrichment schematic (Hot Start). When the microfluidic device was heated above 36 ºC and conjugates were introduced into the microchannel under continuous flow, conjugates were sequentially captured onto the PNIPAAm surface as they aggregated and were concentrated. Hereafter, a cool wash was applied to release surfaces bound conjugates from the PNIPAAm surface into the solution, following a warm buffer for removing unbound conjugates in both cold start (a) and hot start (b) procedures. Conjugate solution with higher concentration than that in the original sample stream (enrichment) was obtained in hot start (b) procedure [95].

1.4.6 Cell culture

Microfluidic devices provide experimentally amenable microenvironments for cell culture with large surface-to-volume ratio and fluidic properties mimicking *in vivo* environments [21]. Controlling cell behavior in microchannels is highly advantageous for fundamental studies of cell–surface and cell–cell interactions [24, 61, 83].

Peterson *et al.* [114] found that O_2 plasma treatment of PDMS helped to increase the material's biocompatibility and decreased cell aggregate formation inside a microchannel in a glial cell culture. However, O_2 plasma treatment did not enhance cell (intestinal epithelial cells (Caco-2 cells)) adhesion [146]. Wang *et al.* [146] found by varying the base-to-curing agent ratio of PDMS also did not enhance cell adhesion. Caco-2 cells indicated favorable attachment on positively charged poly-D-lysine surfaces. In addition, two extracellular matrix (ECM) proteins, collagen and fibronectin, on the PDMS surfaces improved the cell attachment and proliferation, but the laminin protein coating on the PDMS surface enhanced the initial cell attachment, then suppressed cell proliferation. Fibronectin and collagen were also immobilized on patterned PAAc modified PDMS surfaces *via* straightforward carbodiimide coupling [129]. Both fibronectin and collagen coated surfaces showed positive effects on Chinese hamster ovary K1 cell attachment and proliferation at least for 2 d, however the fibronectin coating was more effective. Metha *et al.* [24] prepared microchannels functionalized *via* LBL deposition with 2, 4 or 7 bilayers of collagen and fibronectin on 5 bilayers of PDDA and clay showed good cell spreading, proliferation and viability of primary bone marrow stromal cells for more than 2 wk.

As an important ligand for cell adhesion through integrin interactions, the amino-terminated Arg-Gly-Asp was attached onto a isothiocyanate-modified PDMS microchannel to facilitate the adhesion of A427 cells (a colon cancer cell line) (Figure 1-15) [61]. The results showed that the cells could survive for 4 d at 37 ºC when cell culture medium was refreshed continuously (Figure 1-15 (a)), whilst very few cells were retained on a native PDMS microchannel (Figure 1-15 (b)). In another example, Arg-Gly-Asp-Ser (RGDS) peptides were covalently bonded with ester groups onto NSC modified PDMS surfaces, prepared by hydrosilylation of allyl-PEG-OH onto Si-H enriched PDMS surfaces [75]. This RGDS modified PDMS supported human umbilical vein endothelial cell adhesion. 87 % of seeded cells adhered after 6 h incubation on the modified surface, while only 17 % of seeded cells attached onto native PDMS [75]. Compared to native PDMS, HA modified PDMS surfaces, prepared by using a similar method, showed beneficial effects on mammalian cell attachment and proliferation, and the effects were more pronounced for human corneal epithelial cells in comparison to mouse 3T3 fibroblast cells [76].

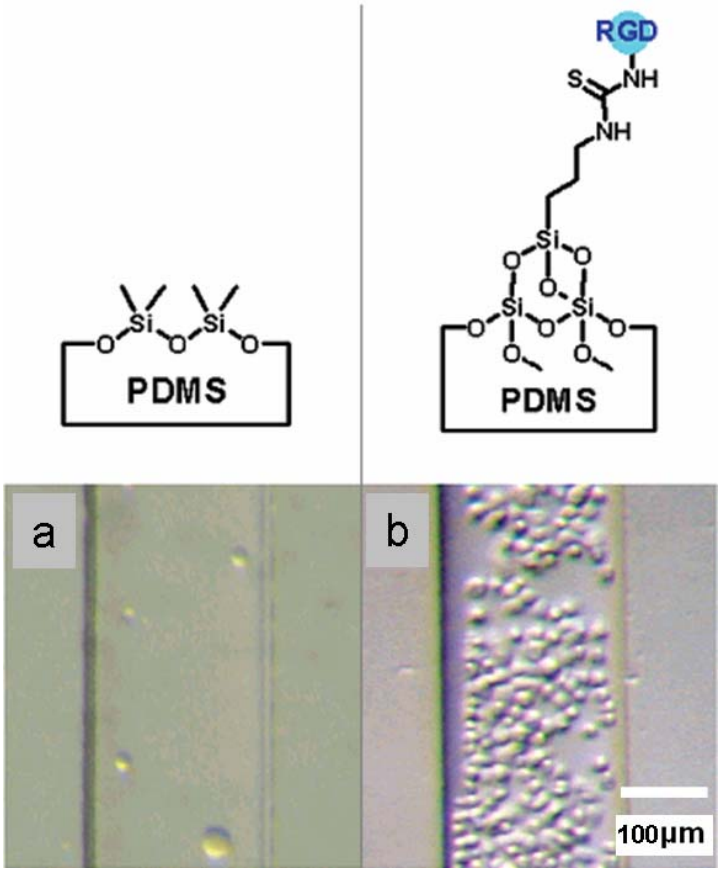

Figure 1-15. Optical micrographs of A427 colon cancer cell immobilization in microfluidic devices based on (a) native PDMS (b) Arg-Gly-Asp modified PDMS [61].

PNIPAAm modified PDMS microchannels have not only been used to capture and release proteins [95], but also to capture and release COS7 cells (African green monkey kidney fibroblast cells) in static culture mode [94]. The COS7 cells were attached onto the microchannel walls at 37 ºC and detached from the walls after 15 min incubation at room temperature. The yield of the harvested cells was improved over the traditional trypsinization method. However, it should be pointed out that a gelatin coating was applied in microchannel before cell culture to improve cell adhesion. In addition, the released cells from the modified surface were able to adhere and proliferate again downstream in the microchannel with identical surface features. To our knowledge, this is the first demonstrated thermomodulated system based on PDMS microfluidics which combines cell culture, harvest, and passage operations all together.

Likewise, mast cells were cultivated on PDMS structures, which had been surface-modified by an oxygen plasma, followed by treatment with 1 M HCl and finally

APTES [83]. The results showed that this three-step modification promoted the attachment of cells, with cell numbers being highest on the APTES-modified surface. Séguin *et al*. [89] have used an APTMS patterned PDMS surface (prepared by combination of plasma and silanization) to capture C2C12 rat endothelial cells and found that attachment only occurred at the APTMS modified spots. By using a suitably sized stainless steel mesh for patterning the surface, appropriate regions could be sized to accommodate single cells, affording a platform to monitor intercellular communications.

Schmolke *et al*. [52] demonstrated the ability of reducing the cell adhesion strength of hydrophobic yeast *S. cerevisiae* in PDMS microfluidic devices. Here, a PAAc-*g*-PEG modified PDMS surface (prepared by using a combination of LBL and 'grafting-to') showed at least two orders of magnitude less adhesion of the yeast compared to native PDMS. These surfaces may have the potential to support planktonic growth inside microfluidic devices.

1.4.7 Formation of emulsions inside microfluidic channels

Emulsions are typically formed through the mixing of immiscible fluids and have great potential in the application of drug delivery. Normally, water-in-oil (W/O) emulsions are formed in microchannels with hydrophobic properties, while oil-in-water (O/W) emulsions are formed in microchannels with hydrophilic properties.

Using a microfluidic device modified with PSS in a LBL approach, Bauer *et al.* [55] fabricated hexadecane droplets in water with diameters of 52 μm or 36 μm, produced at a droplet generation frequency of 170 Hz and 13.5 kHz, respectively [55]. Similarly, He *et al.* [68] used an LBL approach to fabricate a hydrophilic microchannel for the fabrication of stable monodisperse poly(L-lactic acid) (PLLA) droplets loaded with paclitaxel (PTX). Upon solvent evaporation, PTX loaded PLLA micropheres with a size range of 30 μm to 50 μm were fabricated [68].

A key application of the chemical/wettability patterning of PDMS microfluidic devices is the formation of double emulsions. To achieve double emulsification, a two-step breakup of droplets is required, which requires patterns of hydrophobic and hydrophilic

regions [55, 91-93]. Schneider *et al.* [91] used PAAc patterned PDMS microchannels (prepared by a 'grafting-from' polymer coating technique through a mask) to fabricate a water-in-fluorinated oil-in-water double emulsion, where droplets of W/O were produced within the hydrophobic native PDMS regions and subsequent droplets of O/W were produced within the hydrophilic PAAc modified regions. Wettability patterned PDMS microfluidic channels have also been used to produce W/O/W droplets with diameters of 85 μm and 109 μm for inner water and outer oil droplets, respectively, at a 130 Hz generation frequency [55]. Using the 'grafting-from' polymer coating technique, Su *et al.* [92, 93] have fabricated two different PAAc patterned PDMS microfluidic devices). As shown in Figure 1-16 (a), a double W/O/W emulsion consisting of water-in-ethyl acetate (containing 10 wt % PLLA, 50 wt % of trilaurin or 0.5 wt % of phosphocholine) in water was produced with one-step. The diameter of the resulting droplets was in the range of 180 μm to 280 μm with a standard deviation less than 7 %. Once the W/O/W droplets were formed, the ethyl acetate was evaporated, leaving behind solid capsules of biodegradable PLLA [92]. In another experiment, γ-Fe_2O_3 nanoparticles were embedded into the microcapsules by dispersion of the nanoparticles in the oil in order to render them responsive to external magnetic stimulation. In Figure 1-16 (b), both W/O/O and W/O/W double emulsions were fabricated using the two-step breakup method on a PAAc patterned PDMS microchannel [93]. In contrast to most emulsification schemes [55, 68, 91, 92] where the size and frequency of droplets is varied by adjusting the flow rates of syringes pumps driving the water and oil phase, here pneumatic actuated membrane valves were employed for controlling the droplet size and frequency by varying the open time and cycle time of the valves [93].

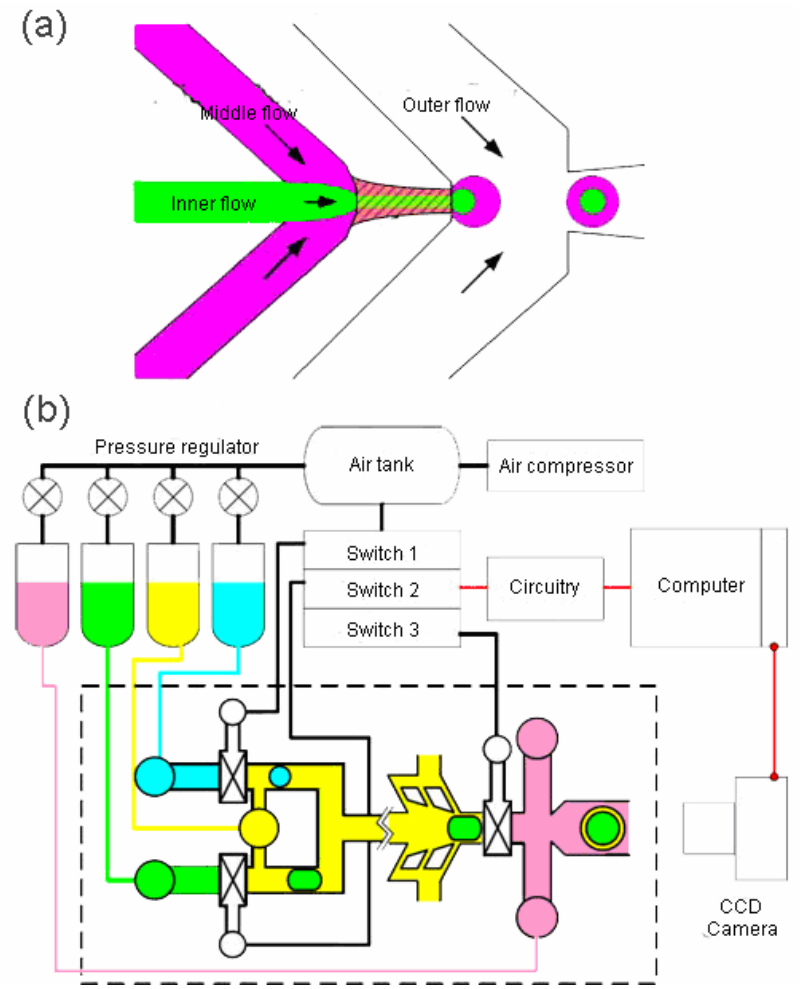

Figure 1-16. Schematic illustrations of double emulsification devices. (a) One-step breakup of droplet for double emulsion formation [92]; (b) two-step breakup of droplet for double emulsion formation [93].

1.5 Summary and future perspectives

PDMS is a versatile material with excellent properties for microfluidics. It is affordable, easily moldable and accessible to laboratories all over the world. Limiting its usefulness is its inherent hydrophobicity. This chapter has highlighted some recent surface modification techniques to render PDMS more useful for microfluidic applications by tailoring surface properties. Gas-phase processing, whilst allowing the introduction of diverse surface chemistries, easily damage the PDMS surface. In contrast, chemical compatibility is an issue when organic solutions are used in a wet chemical modification process. Deliberate adsorption of amphiphilic proteins on PDMS from aqueous solution is a promising strategy,

although long term stability of such surfaces requires sterile environments and the absence of proteases. Dynamic coatings involving surfactants and ionic liquids are becoming more and more popular for PDMS surface modification due to the simplicity of the technique, although the surface modifiers used here may interact with components of the sample solution, potentially interfering with the analytical task. Of significance is the increased use of combinations of techniques for surface modification, often involving gas-phase modification and wet chemical modification to achieve a more stable surface in a relatively short period of time.

With the advent of improved patterning techniques there has been an expansion of research into topographically and chemically patterned PDMS surfaces particularly for applications in cell culture and drug delivery, *etc.* In the past, soft lithography has been the most common method for topographical patterning of PDMS. More recent research has included metal ion implantation, UV-induced polymerization through a photomask and bond-detachment approaches.

Surface-modified PDMS microfluidics has been used in applications such as biomolecule separations, enzyme microreactors, immunoassays and cell culture studies and have allowed for a paradigm shift in the immobilization of biomolecules in microchannels for the capture/release of proteins, antifouling and cell cultures. The emergence of spatially controlled immobilization of biomolecules or cells, inside PDMS microchannels has a high trajectory of innovation in regards to bioanalytical endeavors and tissue engineering. Finally, the relatively new application of emulsion formation within surface-modified microfluidic devices is also receiving considerable attention. All of these developments are underpinned by advancements made in PDMS surface modification.

CHAPTER 2 METHODOLOGY

The content of this chapter is partly based on references [31, 77, 147].

2.1 Introduction

This chapter describes the details of the materials and chemicals used in the preparation of PDMS microfluidic devices. PDMS surface modification and characterization and the application of DNA hybridization on the modified PDMS surfaces are also described. More detailed techniques used throughout this thesis will be presented in the relevant chapters.

2.2 Material and chemical

PDMS Sylgard 184 (Dow Corning Corporation, USA) was purchased as a two-component kit, including pre-polymer (base agent) and cross-linker (curing agent) components. Gold-coated glass slides were purchased from Platypus Technologies, USA. Lucifer Yellow CH dipotassium salt and Hoechst 33342 were purchased from Invitrogen, USA. 3-mercaptopropionic acid (MPA) was purchased from Ajax Finechem Pty. Ltd., New Zealand. All other chemicals were purchased from Sigma-Aldrich, USA.

DNA synthesis reagents were bought from ABI (USA). DNA oligmers were synthesized with an ABI 394 DNA synthesizer producing the sequences as follows: Oligo1: 5′-amino AAA AAA AAA CCA CCC CTA CCA CTA ATC CCC; Oligo2: 5′-GGG GAT TAG TGG TAG GGG TGG-carboxyfluorescein (FAM) and Oligo3: TTTGGCCTAAGGTCTCGAAG-FAM.

The formulations of buffer are as follows: PBS (pH 4.8): NaH_2PO4 (30 mM); PBS (pH 7.2): KH_2PO4 (50 mM), EDTA (10 mM), NaCl (150 mM); PBS (pH 7.4): NaCl (137 mM), KCl (54 mM), Na_2HPO4 (10 mM), KH_2PO4 (2 mM); 10 mM PBS (pH 8.2): Na_2HPO4 (20 mM), KH_2PO4 (1 mM); 20 mM PBS (pH 8.2): Na_2HPO4 (20 mM), KH_2PO4 (1 mM); 4-(2-hydroxyethyl)-1-piperazineethanesulfonic acid (HEPES) buffer (pH

7.4): HEPES (10 mM), NaCl (200 mM), EDTA (1 mM); and Tris buffer (pH 8.4): Tris (25 mM), NaCl (100 mM), $MgCl_2$ (1 mM). For pH adjustment of the buffers, NaOH (0.1 M) and HCl (0.1 M) were used.

2.3 Preparation of PDMS samples

In this thesis, three different surface modification methods were performed to improve the hydrophilization on the PDMS surfaces, including 1) thermal assisted hydrosilylation; 2) SAM assisted templating and 3) combination of Soxhlet-extraction and plasma treatment. The samples prepared using these three methods are referred as MP1, MP2 and MP3, respectively, throughout the whole thesis. The corresponding native PDMS without modifications are referred as NP1, NP2 and NP3 in these three cases, respectively. The following section will describe the modification details according to the different methods.

2.3.1 Thermal assisted hydrosilylation

2.3.1.1 Preparation of NP1

The two components of PDMS Sylgard 184, base and curing agent (10:1 or 5:1 weight ratio) were thoroughly mixed and degassed by applying a gentle vacuum to remove air bubbles. As shown in Scheme 2-1, the PDMS prepolymer was then poured onto a PVP ring on a fresh microscope slide previously cleaned with Piranha solution (1:3 (v/v); H_2O_2:H_2SO_4) and cured at 80 ºC for 1 h. After curing and immersing in MilliQ water (18.2 MΩ) for 2 h, the NP1 sample was peeled off the slide, and then rinsed with MilliQ water, then ethanol and dried under a stream of nitrogen.

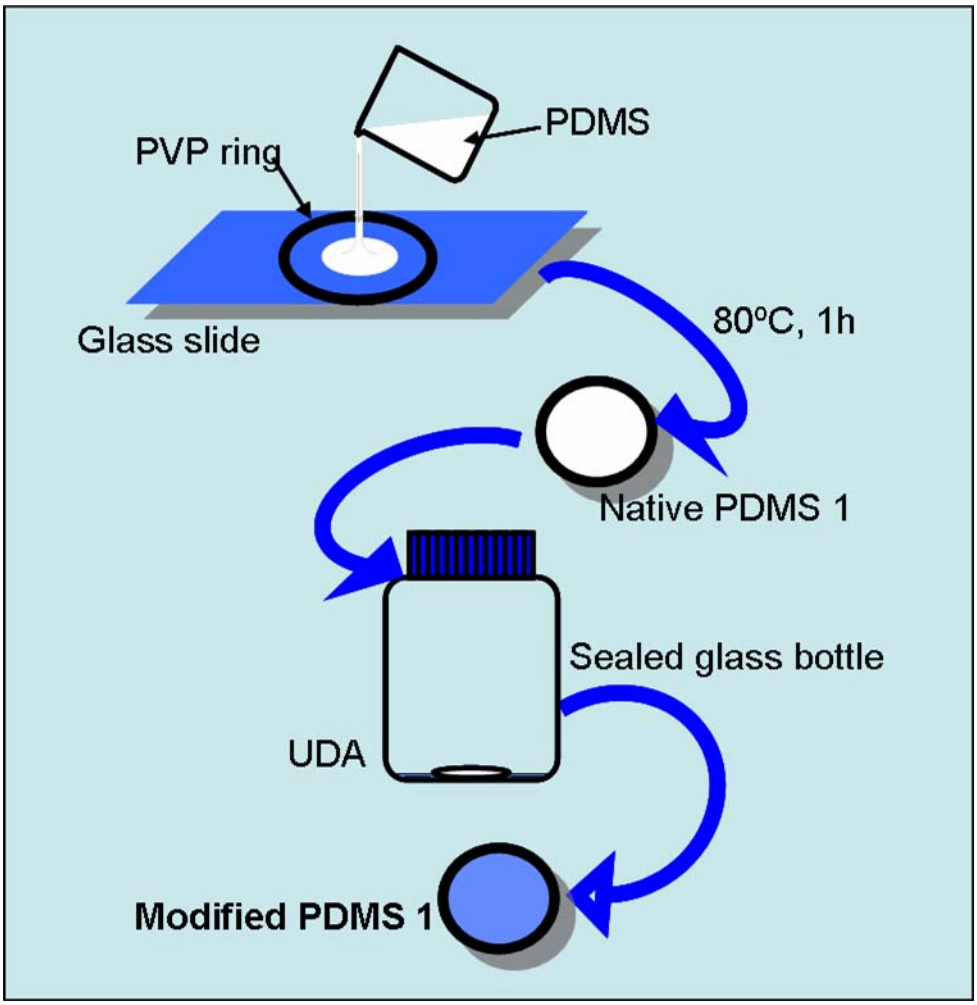

Scheme 2-1. Schematic illustration of the procedure for preparing native PDMS (NP1) and modified PDMS 1 (MP1).

2.3.1.2 Preparation of MP1 by heating NP1 with UDA

The cleaned pre-cured NP1 (10:1), prepared as described in section 2.3.1.1, was then placed in a sealed glass container with enough UDA to thinly coat the bottom surface of each sample (Scheme 2-1). The UDA coated PDMS was kept in an oven at 80 ºC for 10 min, 1 h and 1 d, and the resulting modified PDMS samples will hereafter be referred to as 10 min MP1 (10:1), 1 h MP1 (10:1) and 1 d MP1 (10:1), respectively. After modification, the samples were cleaned *via* ultrasonication for 10 min in MilliQ water, 20 min in 50 % ethanol and then a further 10 min in MilliQ water. Finally, the modified samples were dried under a stream of nitrogen.

In addition, PDMS prepolymer with 5:1 base to curing agent weight ratio was mixed,

degassed and cured at 80 ºC for 1 h. This pre-cured NP1 (5:1) sample was then reacted with UDA at 80 ºC for 1 d, referred to hereafter as 1 d MP1 (5:1). The resulting 1 d MP1 (5:1) was used to compare the surface stability with 1 d MP1 (10:1). The choice of the ratio between base and curing agent is based on the required quantity of Si-H groups for hydrosilylation with UDA, which has been outlined in Chapter 3, Section 3.3.2.

2.3.2 SAM assisted templating

2.3.2.1 Preparation of NP2

First degassed PDMS prepolymer (10:1 base to curing agent weight ratio) was prepared as detailed in section 2.3.1.1. Then the PDMS prepolymer was poured onto a blank gold slide and cured at 80 ºC for 2 h. Finally, the NP2 sample was peeled off the gold slide after immersing in MilliQ water for 1 h and sequentially rinsed with MilliQ water, ethanol (75 %) and then dried under a stream of nitrogen.

2.3.2.2 Preparation of MP2 on a MPA-modified gold surface

For preparing a MPA-modified gold slide, first gold-coated glass slides were cleaned with fresh Piranha solution (1:3 (v/v); H_2O_2:H_2SO_4) for 5 min, then rinsed with MilliQ water and dried under a stream of nitrogen. Then, the clean gold slide was immersed in 1 mM MPA in 100 % absolute ethanol for 24 h. Finally, the MPA-modified gold slides were removed and washed with absolute ethanol (Scheme 2-2).

PDMS (10:1 w:w base and curing agent) and 2 wt % UDA were thoroughly mixed and degassed by applying a gentle vacuum to remove air bubbles. The degassed UDA/PDMS prepolymer mixture was subsequently poured onto the MPA-modified gold slide and left to stand at room temperature for 24 h, followed by curing at 80 ºC for 2 h (Scheme 2-2). In order to remove the MP2 from the MPA-modified gold slide, the entire assembly was immersed in MilliQ water for 4 h, the MP2 was then peeled off the gold slide and sequentially rinsed with MilliQ water, ethanol (75 %) and then dried under a stream of nitrogen. In addition, PDMS samples with higher UDA concentration (3 wt %) were also prepared. Here, the modified sample was not as transparent as NP2. Because

transparency in a microfluidic device is always needed for analyte detection using optics, 2 wt % was selected as the UDA concentration of choice for the following work.

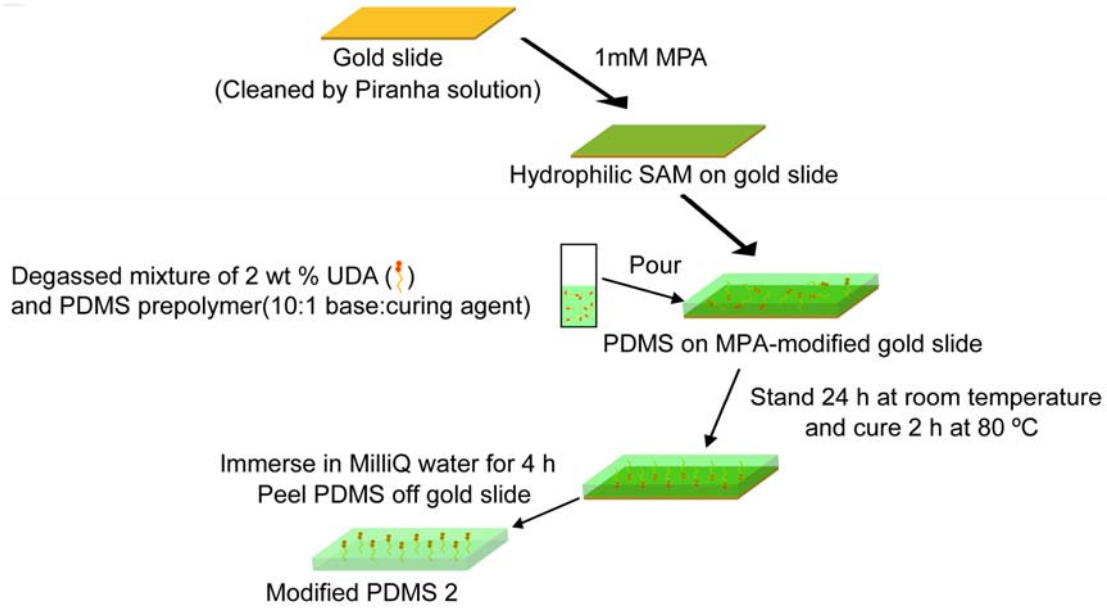

Scheme 2-2. Schematic illustration of the procedure for preparing modified PDMS 2 (MP2).

2.3.3 Combination of Soxhlet-extraction and plasma treatment

2.3.3.1 Preparation of NP3

First, degassed PDMS prepolymer (10:1 w:w base to curing agent) was prepared as detailed in section 2.3.1.1. Then, the PDMS prepolymer was poured into a glass Petri dish which had been previously treated with Piranha solution (1:3 (v/v); H_2O_2:H_2SO_4) for 5 min and subsequently silanized with chlorotrimethylsilane (CTMS) to reduce the adhesion between the PDMS and the Petri dish. After curing the PDMS at 80 ºC for 1 h, the cured NP3 was then peeled from the Petri dish.

2.3.3.2 Preparation of MP3 by 2-step plasma treatment on hexane extracted PDMS surfaces

The cured NP3 was Soxhlet-extracted with hexane at 60 ºC for 24 h [148]. Following that, the hexane was removed by evacuating the PDMS under vacuum for 24 h. After

Soxhlet-extraction, the PDMS sample was sequentially exposed to an Ar and then an AAc plasma (Plasma cleaner PDC-32G, Harrick Plasma Company, USA). As shown in Scheme 2-3 (a), Ar and AAc gas with desirable pressure can be produced by adjusting the yellow valves and then introduced into the cylindrical plasma reactor. The initial monomer pressure and deposition time used for Ar and AAc plasma were 0.7 mbar, 0.5 min and 0.2 mbar, 5 min, respectively, and a high power was used for both (Scheme 2-3 (b)). Ar plasma conditions (0.7 mbar, 0.5 min) were adopted from our group's previous work [149], and the AAc plasma conditions (0.2 mbar, 5 min) were optimized by monitoring the intensity of the COOH peak on the FTIR-ATR spectra (See chapter 5). Finally, the samples were cleaned with MilliQ water and then ethanol, followed by drying under a stream of nitrogen.

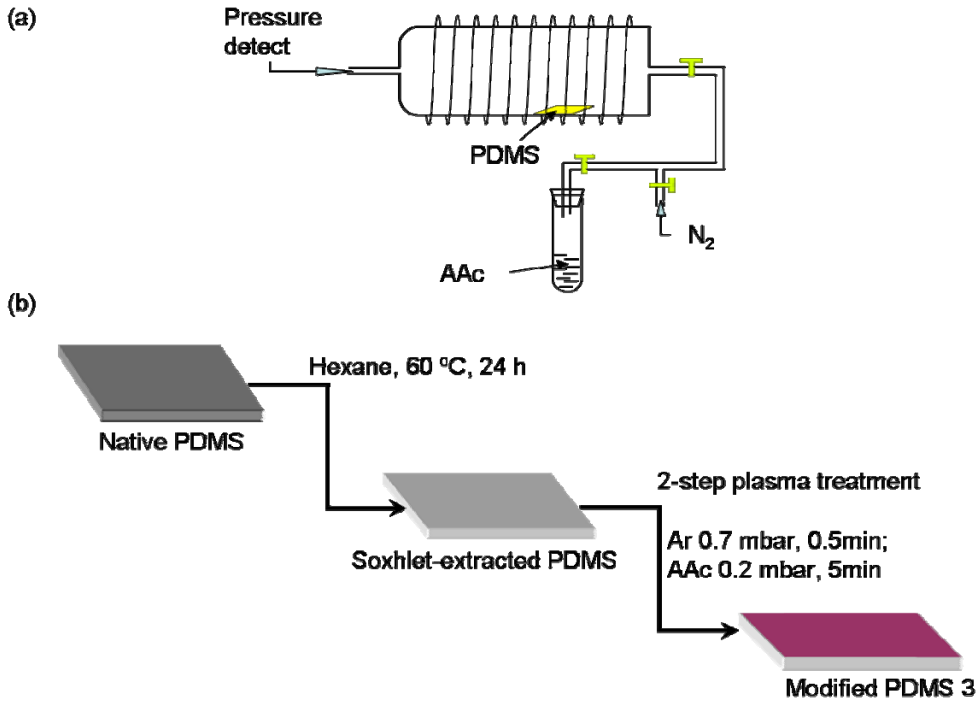

Scheme 2-3. Schematic illustration of (a) plasma system and (b) the procedure for preparing modified PDMS 3 (MP3).

2.4 Surface characterization

To verify the successful surface modifications of the native PDMS surfaces, various surface characterization methods were applied in this thesis, including WCA measurements, FTIR-ATR spectroscopy, X-ray photoelectron spectroscopy (XPS) and AFM. Table 2 lists

the kinds of surface characterization techniques used on each modified PDMS surface.

Table 2-1. Details of the surface characterization methods used on each modified PDMS surface.

Sample	Surface characterization						
	WCA	FTIR-ATR	XPS	AFM	Zeta-potential	Fluorescence labeling	Stability analysis
MP1	√	√	×	×	√	√	√
MP2	√	√	√	×	√	√	√
MP3	√	√	√	√	×	√	√

The details of each surface characterization method are described in the following.

2.4.1 WCA measurements

The contact angle is a measure of the wettability of a solid surface by a liquid. It is defined as the angle at which the solid, liquid and gas phase meet [150]. There are many methods for the measurement of contact angles such as the static sessile drop [151, 152], dynamic sessile drop [151, 152], dynamic Wilhelmy [153] and single‐fiber Wilhelmy [154] and powder contact angle [155] methods. The sessile drop method is the most common method and works *via* placing a small drop of water onto the surface and measuring the angle made at the three interfaces (Scheme 2-4).

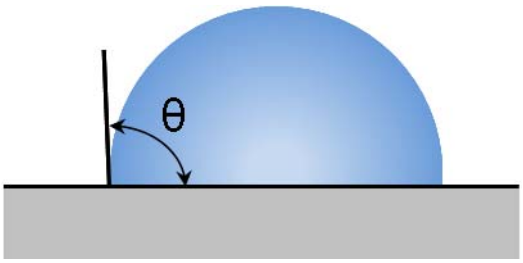

Scheme 2-4. Schematic illustration of the static sessile drop for the measurement of WCA.

The static WCA was measured using the sessile drop method by placing a small drop (2 μL) of MilliQ water onto the sample surfaces *via* a syringe, a digital image of which was taken by a Panasonic SuperDynamic WV-BP550/G camera with a macrolens. The image was processed by ImageJ software V1.34. All reported water contact angles were the

average value of five measurements on different parts of the sample.

2.4.2 FTIR-ATR spectroscopy

FTIR-ATR is a surface sensitive IR technique. When an infrared beam comes onto an optically dense crystal with a high refractive index at a certain angle, the internal reflectance creates an evanescent wave that extends beyond the surface of the crystal into the sample held in contact with the crystal. In the region of infrared spectrum where the sample absorbs energy, the evanescent wave will be attenuated or altered. The attenuated energy from each evanescent wave is passed back to the IR beam, which then exits the opposite end of the crystal and is passed to the detector in the IR spectrometer. The detection depth of FTIR-ATR usually ranges from several hundred nanometers to several microns [156], which largely exceeds the detection depth of XPS (<10 nm) [157].

FTIR-ATR spectroscopy was carried out on a Thermo-Nicolet Nexus 870 spectrophotometer. 64 scans were taken at room temperature and atmospheric pressure with a resolution of 4 cm^{-1}. The data was collected from 625 to 4500 cm^{-1}, and analyzed using OMNIC version 7.0 software.

2.4.3 XPS

XPS is a quantitative spectroscopic technique that measures the elemental composition, empirical formula, chemical state and electronic state of the elements that exists within a sample. XPS works by irradiating a material with a beam of X-rays and subsequent collection of data on the number of photoelectrons being ejected from the material and their kinetic energy (KE) within the top 10 nm of the sample. Ultra high vacuum (UHV) is required to make sure the electrons ejected from the material can reach the detector without any energy loss. The X-rays can typically penetrate up to 5 μm into a material. However, any photoelectrons generated from beyond 10 nm depth will not be detected as the electrons will be trapped. For this reason, XPS is a surface sensitive detection technique only.

XPS analysis of the PDMS samples was performed on an AXIS HSi spectrometer

(Kratos Analytical Ltd, GB), equipped with a monochromatized Al Ka source. The pressure during analysis was typically 5×10^{-9} kPa. The elemental composition of the samples was obtained from a survey spectra collected at a band-pass energy of 320 eV. High resolution spectra were collected at a pass energy of 40 eV. Binding energies were referenced to the aliphatic hydrocarbon peak at 285.0 eV.

2.4.4 AFM

AFM is a form of scanning probe microscopy. AFM consists of a cantilever with a sharp tip at its end that is used to scan the sample surface. When the tip is brought into proximity of a sample surface, the deflection of the cantilever is measured by a detector using a laser spot reflected off the cantilever. The change in laser signal detected as the tip scans over the surface can then be converted into a map of the surface. There are a variety of modes for AFM operation. However, the two most common modes are tapping and contact mode.

AFM was performed on a Nanoscope IV Digital Instruments microscope (Veeco Corp. Santa Barbara, USA) in tapping mode and in air. Silicon cantilevers, FESP (Digital Instruments, Veeco, USA), with a 50-100 KHz resonance frequency were used for the imaging. Image processing (flattening once) was performed using Nanoscope off-line software (Veeco Corp.).

2.4.5 Streaming zeta-potential analysis

The zeta-potential is a function of the surface charge which develops when the sample is placed in a liquid. The liquid layer on the sample surface exists as two parts: an inner region, called the Stern layer, and an outer region, called the diffuse layer. Within the diffuse layer, there is a notional boundary inside which the ions and the surface form a stable entity. This boundary is called the slipping plane. The potential that exists at this boundary is known as the zeta-potential. Several techniques are available for determing the zeta-potential of surfaces. Among these, streaming zeta-potential technique is most suitable for flat surfaces [158]. Experimentally, a streaming potential is generated, when electrolyte solution is forced, by means of hydraulic pressure, to flow across a channel formed by two flat samples. The fluid flow in the channel carries a net charge and gives rise to a streaming

current due to hydraulic pressure. A potential difference between two ends of the channel is then built up due to the accumulation of charges at one end of the channel. The potential difference further causes a leakage current in the opposite direction of the streaming current, due to ion diffusion and EOF. When the leakage current is equal to the streaming current, the measured potential difference is the streaming zeta-potential [159].

Zeta-potential data were obtained on a ZetaCAD instrument equipped with an RS232C bi-directional interface as well as a programmable in/out board for automation of the measurements with the aid of a Keithley 2400 high accuracy multimeter. The approach by Mizadeh *et al.* [160] was adapted where 1 mM KCl was used as a background electrolyte in all experiments. 0.1 M KOH and 0.1 M HCl was used for pH adjustment. The measured samples were immersed in the electrolyte solution overnight to equilibrate the samples prior to the measurements. The measurements were repeated three times and the results were averaged.

2.4.6 Fluorescence labeling study

For fluorescent labeling experiments EDAC and Lucifer Yellow CH dipotassium salt dye were dissolved in MilliQ water (0.4 M EDAC and 1 mg/mL dye). This concentration of dye was chosen to ensure that there was enough dye in the solution for labeling. PDMS samples were immersed into the EDAC/dye solution for 4 h at room temperature after which time they were removed and rinsed with MilliQ water, then ethanol and dried under a stream of nitrogen. The reacted samples were investigated under a fluorescence microscope (Leitz Laborlux upright fluorescence microscope or Olympus IX 81 motorized inverted fluorescence microscope).

2.4.7 Stability experiments

After exposing modified PDMS samples (MP1, MP2 and MP3) to certain environmental conditions, FTIR-ATR spectra were obtained on a Thermo-Nicolet Nexus 870 spectrophotometer (as described in section 2.4.2) to monitor the stability of the carboxyl peak (at 1715 cm^{-1}) on the modified PDMS surfaces. More details about the treatment conditions used will be presented in the relevant chapters.

2.5 DNA hybridization on PDMS surfaces

In order to perform DNA hybridization experiments PDMS samples (MP2 and MP3) were successively treated with 4 mg/mL EDAC in PBS (pH 4.8), at room temperature for 2 h, 10 μM amino-terminated Oligo1 (PBS, pH 7.4) at room temperature for 2 h and 10 μM FAM-labeled complementary Oligo2 (HEPES buffer, pH 7.4) at 4 ºC overnight (~18 h). To quantify DNA hybridisation the modified PDMS samples (MP2 and MP3) were placed on glass slides and examined under an IX 81 inverted fluorescence microscope (Olympus, Japan) through a 450-490 nm band pass excitation filter. A line scan on each sample was performed and analyzed using LS Research software (Olympus, Japan) or ImageJ software V1.34 to produce an intensity profile. For comparison, PDMS samples incubated with EDAC and then Oligo 2, or incubated with EDAC, then Oligo 1 and finally Oligo 3 were also observed under the fluorescence microscope.

2.6 Fabrication of PDMS-based microfluidic devices

2.6.1 Fabrication of SU-8 masters

First, the microfluidic devices were designed using L-Edit V14.1 software, as per the layout shown in Scheme 2-5. Then, a glass photomask with the channel pattern was generated using a photoplotting process (MIVA 1624E T3 photoplotter). Following that, a SU-8 master mold was fabricated using standard photolithography, as described in the following and shown schematically in Scheme 2-5. The silicon wafer was first rinsed with acetone and isopropyl alcohol (IPA), followed by drying under a stream of nitrogen and then in the oven at 200 ºC for 20 min. Then, a 50 μm thick layer of SU-8 2050 photoresist was spin-coated onto the silicon wafer, followed by pre-baking at 65 ºC for 3 min and 95 ºC for 9 min, exposure to 365 nm UV light at an intensity of 215 mJ/cm for 22 sec through the glass mask, and post-baking at 65 ºC for 2 min and 95 ºC for 7 min. Finally, the silicon wafer with SU-8 was developed in propylene glycol methyl ether acetate (PEMEA) for 7 min, followed by the rinsing with PGMEA and IPA, and drying with under a stream of nitrogen. In order to reduce the adhesion of PDMS to the master mold, a monolayer of trichloro(1H, 1H, 2H, 2H-perfluorooctyl)silane (TFOS) was produced on the master mold surface by placing it in a desiccator with 5 μL of TFOS inside. The desiccator with the

master and TFOS inside was vacuumed for 2 min until a sufficient amount of TFOS vapor had built up. The desiccator was kept closed overnight.

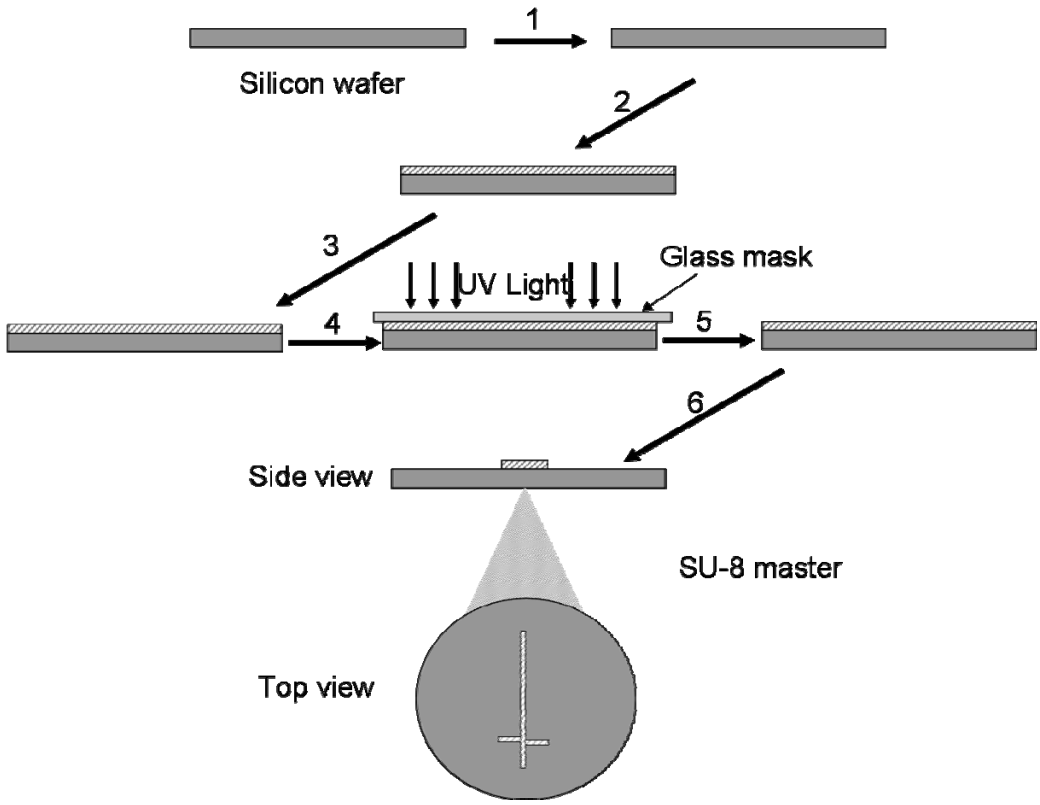

Scheme 2-5. Schematic illustration of the procedure for preparing SU-8 master. 1) Rinse with acetone IPA, then dried with nitrogen gas, and finally dehydrated at 200 ºC for 20 min. 2) Spin-coat 50 µm thick SU-8 2050 photoresist. 3) Pre-bake at 65 ºC for 3 min and 95 ºC for 9 min. 4) Exposure to UV light at an intensity of 215 mJ/cm for 22 sec through the glass mask. 5) Post-bake at 65 ºC for 2 min and 95 ºC for 7 min. 6) Develop in PEMEA for 7 min, then rinse with PGMEA and IPA, and finally dried under a stream of nitrogen. (Dimensions: main channel = 2 cm length, side channel = 0.5 cm length. Both channels are 250 µm wide and 50 µm in deep).

2.6.2 Fabrication of native PDMS-based microfluidic devices

After silanizing, the SU-8 master mold with TFOS, PDMS-based microfluidic devices were fabricated using standard soft-lithography (Scheme 2-6). For native PDMS-based microfluidic devices, the degassed PDMS prepolymer (10:1 base to curing agent weight ratio) was first prepared, as detailed in section 2.3.1.1, and was poured onto the master mold and cured at 80 ºC for 20 min. To provide fluidic access, holes were punched by a

needle into the microchannel featured PDMS slide after removal from the mold. Meanwhile, a flat native PDMS slide was prepared by curing the degassed PDMS prepolymer in a glass Petri dish with CTMS pretreatment at 80 ºC for 20 min and then peeling off. These two native PDMS slides were brought together and fixed at 80 ºC for 2 h to form the devices (Scheme 2-6 (a)).

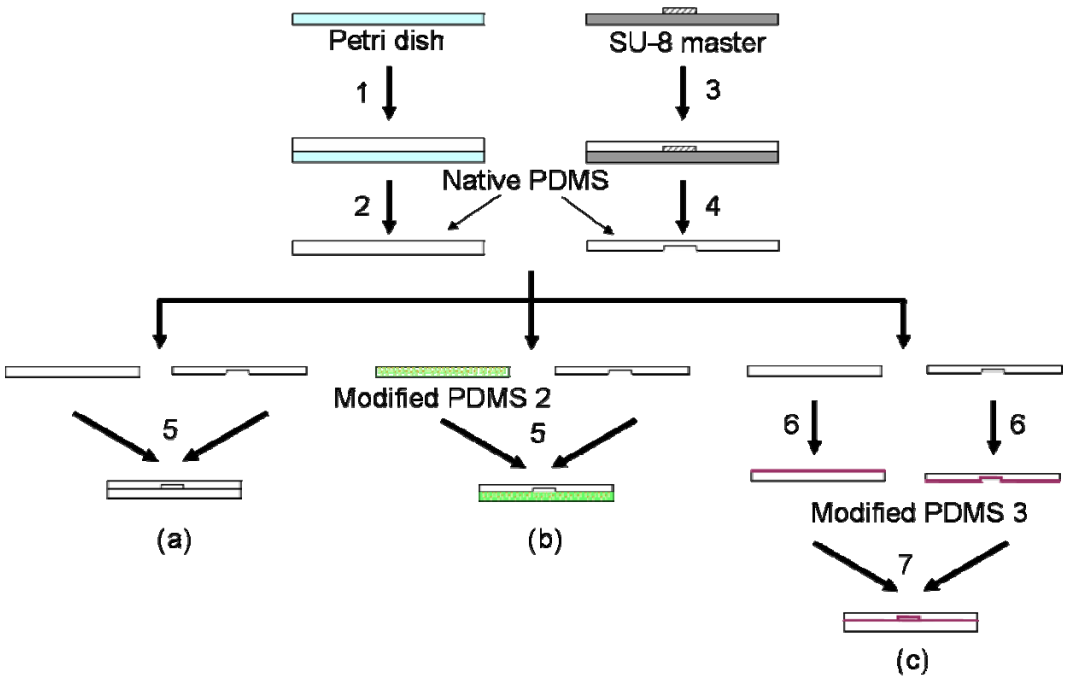

Scheme 2-6. Schematic illustration of the procedure for fabrication of (a) native PDMS-based, (b) MP2-based and (c) MP3-based microfluidic devices. 1) Pour PDMS in Petri dish and cure at 80 ºC for 20 min for (a) native PDMS-based microfluidic devices or 1 h for (c) MP3-based microfluidic devices. 2) Peel flat PDMS slides off Petri dish. 3) Pour PDMS over SU-8 master and cure at 80 ºC for 20 min for (a) native PDMS-based microfluidic devices or 1 h for (c) MP3-based microfluidic devices. 4) Peel microchannel featured PDMS slides off the master. 5) Bring two PDMS slides together and keep at 80 ºC for 2 h. 6) Soxhlet-extract native PDMS with hexane and then treat the surfaces with 2-step plasma (Ar and AAc). 7) Treat the surfaces with O_2 plasma for 10 sec, then clean with ethanol and finally apply another 10 sec of O_2 plasma for bonding the devices.

2.6.3 Fabrication of MP2-based microfluidic devices

As described in section 2.3.2.2, a flat MP 2 slide was prepared by curing a mixture of 2 wt % UDA with PDMS prepolymer on a MPA-modified gold surface. A native PDMS slide with a microchannel was prepared according to the description in section 2.6.2. For the

fabrication of native PDMS-based microfluidic devices, devices were sealed at 80 ºC for 2 h which was also used to seal the MP2 slide and another native PDMS slide to form a microchannel (Scheme 2-6 (b)).

2.6.4 Fabrication of MP3-based microfluidic devices

First, two native PDMS slides (one flat and one featuring a microchannel), were prepared as described in section 2.6.2, except the curing time was changed from 20 min to 1 h. Secondly, these two slides were Soxhlet-extracted with hexane and pretreated with a 2-step plasma (Ar and AAc) procedure, as described in section 2.3.3.2. Finally, the two slides were treated with 10 sec of O_2 plasma (0.2 mbar), cleaned with ethanol, and treated with another 10 sec of O_2 plasma (0.2 mbar), followed by bringing the slides into contact for 15 min under an applied pressure to form the devices (Scheme 2-6 (c)).

2.6.5 EOF measurements

The generation of EOF in a microchannel depends on the net charge density on the surface of the microchannel that is in contact with the electrolyte solution. This gives rise to an electrical double layer. When an electric field is applied along an electrolyte-filled microchannel, the net charge in the electrical double layer is induced to move, which results in the generation of EOF [33, 161].

The EOF was measured using a typical current monitoring method [33] in a single microchannel (3 cm length × 250 μm wide × 50 μm height). The PBS buffers used for the EOF measurements were prepared in deionized water and degassed for 10 min in a sonicated water bath (Soniclean 160HT, Soniclean Pty. Ltd.) before use. As shown in Scheme 2-7, the microchannel and the cathodic reservoir were initially filled with 20 mM PBS buffer (pH 8.2), and the anodic reservoir was filled with 10 mM PBS buffer (pH 8.2). Electrical connections to the microfluidic devices were made with two Pt electrodes placed into the reservoirs at the ends of each channel. A constant voltage of 100 V was applied using a high voltage power supply (PS 350/5000 V-25W, Stanford Research Systems Inc. USA), resulting in the migration of the lower concentration buffer into the microchannel and a further increase of the electrical resistance due to the generation of EOF in the

microchannel. Once the 10 mM buffer had reached the cathodic reservoir, the current reached a constant value. The change in current under a 100 V voltage was monitored using a 6-11/2 digit precision multimeter (Fluke 8845A, Fluke Corporation, USA). Software LabVIEW 8.2 was used to set up the parameters and collect the data. The time required to reach a current plateau was used to calculate EOF based on Equation (1), where L is the length of the separation channel (3 cm), V is the total applied voltage (100 V), and t is the time in seconds required to reach the current plateau.

$$\mu_{eo} = L^2/Vt \qquad (1)$$

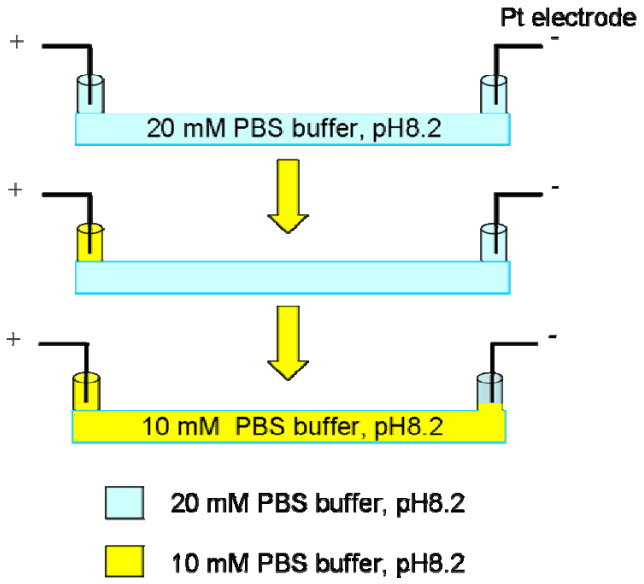

Scheme 2-7. Schematic illustration of the procedure for EOF measurements.

2.6.6 Fluorescence labeling in microchannels

The process of fluorescence labeling within microchannels used the same procedure as described in section 2.4.6 for the open surfaces. The fluorescently-labelled microchannels and the control microchannels were investigated under a fluorescence microscope (Olympus IX81 motorized inverted microscope).

CHAPTER 3 HYDROPHILIZATION OF PDMS BASED ON THERMAL ASSISTED HYDROSILYLATION

The content of this chapter is partly based on reference [147].

3.1 Introduction

The advantages and disadvantages of PDMS as the main material of microfluidic devices, have been described in Chapter 1. Briefly, PDMS has various advantages over other materials, including biocompatibility, gas permeability, optical transparency, ease of molding into (sub)micrometer features and bonding, relative chemical inertness and low manufacturing costs which allows the material to be disposable [27, 28]. One significant problem that must be overcome for most life science applications is the hydrophobic nature of native PDMS surfaces.

There are various surface modification techniques available to render the PDMS surface more hydrophilic, as detailed in Chapter 1. One of these techniques makes use of the fact that during PDMS curing, olefins can be covalently bonded within the PDMS matrix *via* hydrosilylation in the presence of a Pt catalyst [28]. For example, UDA was added into PDMS prepolymer before curing as an additive by Luo *et al.* [162]. The 0.5 wt % UDA modified PDMS showed a twofold increase in μ_{eo} (7.6×10^{-4} cm^2/Vs) compared to native PDMS. But no significant difference in WCA was observed on native and modified PDMS surfaces, indicating that this method did not greatly alter the hydrophobicity of PDMS. It seems reasonable to postulate that increasing the amount of UDA on the PDMS top surface, rather than in the bulk PDMS, would increase the hydrophilicity of the PDMS surface.

In this work, we present a cheap, easy and highly repeatable surface modification technique for PDMS, which involves coating pre-cured PDMS (10:1 base to curing agent weight ratio) with a thin film of UDA with subsequent heat treatment to induce hydrosilylation. Modified PDMS surfaces were characterized by means of WCA measurements, FTIR-ATR specroscopy and zeta-potential analysis. Fluorescence labeling and stability experiments were also performed. The results showed that MP1 surfaces became more hydrophilic compared to NP1 and that carboxylation of the PDMS surface was achieved. Furthermore, the stability and reactivity of carboxylic acid groups on modified PDMS surface were improved by decreasing the weight ratio of PDMS base to curing agent from 10:1 to 5:1 for preparing the pre-cured PDMS.

3.2 Experimental section

The details of the materials and chemicals, preparation of PDMS samples and surface characterization applied on PDMS surfaces were all detailed in Chapter 2, except for the experiments described below.

3.2.1 WCA measurements

The WCA measurements were performed on all PDMS surfaces as described in Chapter 2. The NP1 and MP1 samples were stored in air or MilliQ water in order to observe the effects of aging times on the WCA value. In addition, the WCA was also determined on a pure UDA covered NP1 surface prepared by spin-coating.

3.2.2 Stability experiment

1 d MP1 (10:1) samples were kept in MilliQ water at 50 ºC, and in PBS buffer (pH 7.2) at room temperature and 50 ºC, to investigate the stability of the surface modification. FTIR-ATR spectra were obtained after 3 h and 17 h to analyze the carboxyl group peak on the surfaces. MP1 (10:1) were also characterized by FTIR-ATR spectroscopy after storage in a desiccator for 5.5 h and 19.5 h, respectively.

For 1 d MP1 (5:1) samples, the stability of the modified surfaces was investigated using FTIR-ATR spectroscopy after immersing the samples in 1 mM KCl (pH 4 and pH 12) for 1 d at room temperature, and PBS buffer (pH 7.2) at room temperature and 50 ºC for 3 h and 17 h, respectively.

3.3 Result and discussion

3.3.1 PDMS samples with 10:1 base/curing agent weight ratio

3.3.1.1 WCA measurements

Figure 3-1 shows the WCA of the NP1, 10 min, 1 h and 1 d MP1 (10:1), which were kept in air or MilliQ water. NP1 shows a WCA of ~110º in both air and MilliQ water, which remained constant even after the surface was aged for up to 30 d in both environments. After 10 min, 1 h and 1 d UDA modification, the WCA decreased to ~93º, ~86º and ~77º, respectively. The large decrease in the WCA value is due to the incorporation of oxygen-containing functionalities on the surface [163]. In addition, the WCA of every sample was measured after 5 d, 10 d, 20 d, 25 d, and 30 d of storage in air or MilliQ water. Over this timeframe, the WCA stayed relatively constant, even in air. Whilst not as hydrophilic as PDMS modified by oxygen plasma [164], the MP1 (10:1) surface was significantly more stable in both air and MilliQ water. This implies that in all cases little surface rearrangement had taken place. Compared with previous work [162], in which 0.5 wt % UDA was added into the PDMS prepolymer before curing as an additive, a higher wettability was obtained using our thermal-assisted hydrosilylation method.

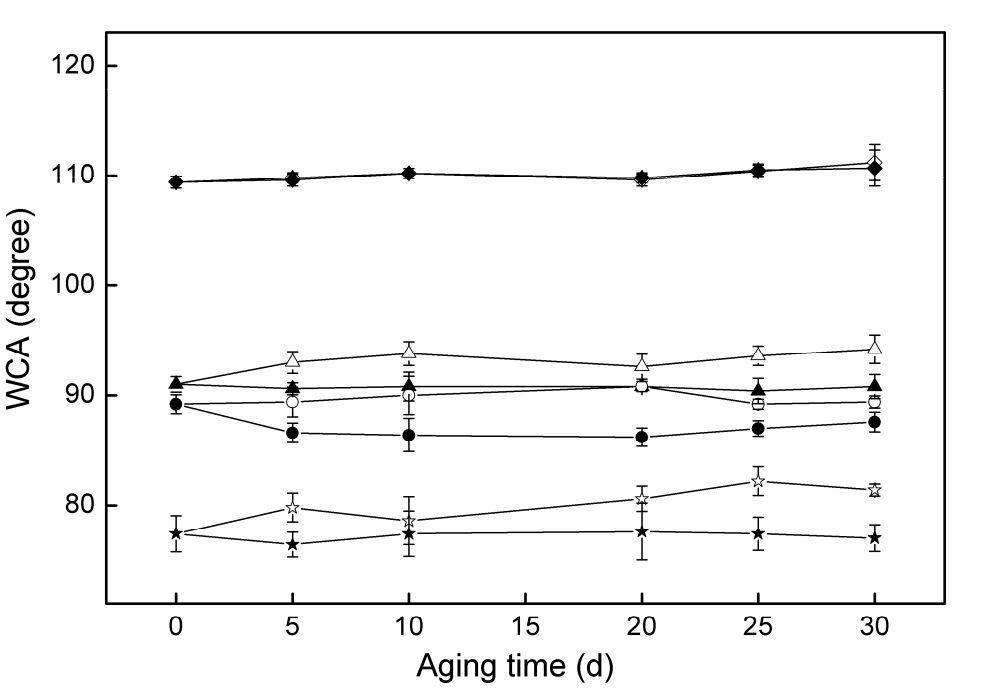

Figure 3-1. WCA vs. aging time for NP1 and MP1 (10:1). The samples were stored in air (filled symbols) and in MilliQ water (empty symbols). Diamond: NP1; triangle: 10 min MP1 (10:1); circle: 1 h MP1 (10:1); pentagram: 1 d MP1 (10:1).

3.3.1.2 FTIR-ATR spectroscopy

FTIR-ATR spectroscopy was carried out to interpret the outcomes of the WCA measurements and to confirm the presence of carboxyl groups on the PDMS surfaces. Figure 3-2 shows the spectra of NP1, 10 min, 1 h and 1 d MP1 (10:1). The spectrum of NP1 (Figure 3-2(a)) is in accordance with previous publications [37, 164]. From Figure 3-2, it is very clear that NP1 (Figure 3-2(a)) and MP1 (10:1) (Figure 3-2 (a, b and c)) have distinct spectral features in the region 1600-1800 cm^{-1}. A characteristic peak at 1715 cm^{-1} corresponding to carboxyl groups [19] is observed in the spectrum of MP1 (10:1). The large reduction in WCA after modification is therefore due to the introduction of carboxyl groups onto the modified PDMS surface. In addition, the intensity of the COOH peak increases with the treatment time (Figure 3-2 inset), which reveals that more carboxyl groups were introduced onto the surface with increased treatment time, resulting in lower WCA values.

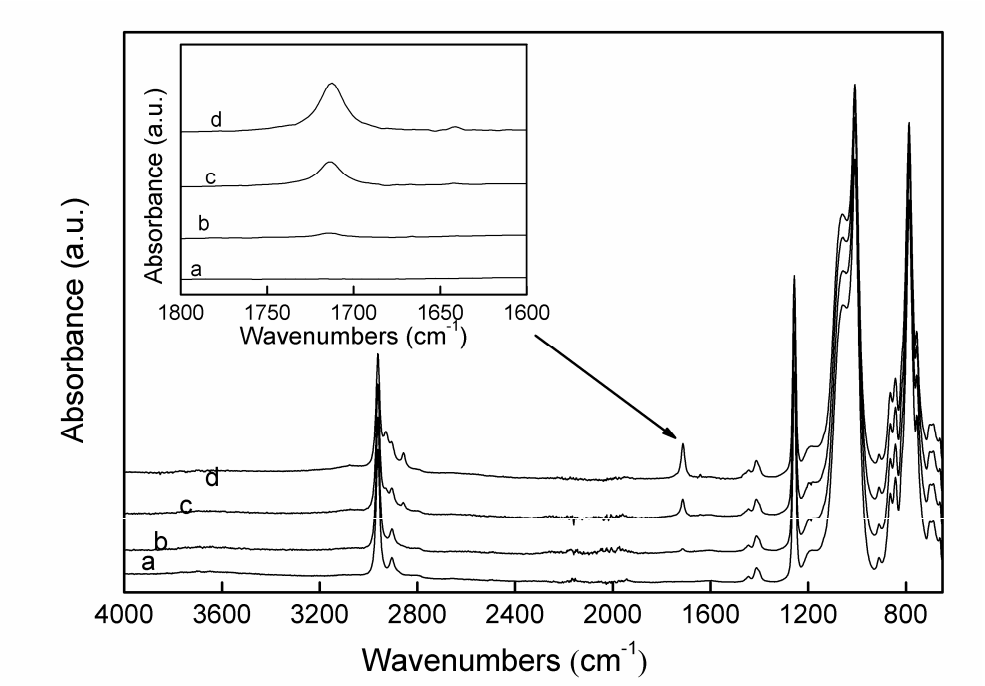

Figure 3-2. FTIR-ATR spectra of (a) NP1, (b) 10 min MP1 (10:1), (c) 1 h MP1 (10:1), and (d) 1 d MP1 (10:1).

3.3.1.3 Streaming zeta-potential analysis

Figure 3-3 shows the results of the average zeta potential at pH 4 and pH 12 for NP1 and 1 d MP1 (10:1). For NP1, the zeta potential changed from -26.70 ± 0.43 mV at pH 4 to -38.30 ± 1.35 mV at pH 12. A similar trend has been observed before [165]. Although NP1 does not contain any surface ionizable functional groups for the generation of zeta-potential, anions were found to approach more closely to the hydrophobic surfaces because they were less hydrated than cations [166], and the physisorbed anions within the Stern layer may have been an important contributor to the negative zeta-potentials observed on the NP1 sample at pH 4 and pH 12 [165]. In addition, this was also explained to be due to the surface Si-OH groups from fumed silica [20]. For 1 d MP1 (10:1), the zeta potential at pH 4 was -18.88 ± 1.35 mV, which is less negative than the value measured on NP1 (-26.70 ± 0.43 mV) at the same pH. The pKa of the carboxyl acid in UDA is closed to 5 [167]. So at pH 4, the carboxyl-terminal moieties from the UDA on the modified PDMS surface are presumably protonated, which explains the reason why a less negative zeta-potential was measured on MP1, compared to NP1. Figure 3-4 shows the FTIR-ATR spectra of the 1 d MP1 (10:1) before and after zeta potential analysis, respectively. The

surface appears to be stable at pH 4 with the carboxyl groups clearly being retained (Figure 3-4 (a and b) inset). At higher pH, that is pH 12 (Figure 3-3) the zeta potential became more negative than at pH 4, changing from -18.88 ± 1.35 mV to -34.24 ± 1.42 mV. It would be expected that the carboxyl groups still remaining were deprotonated at high pH, which would result in a far more negative zeta potential than NP1 at the same pH [160]. However, the value measured on the modified PDMS surface was slightly less negative than that of NP1 (-38.30 ± 1.35 mV) at pH 12, indicating that most carboxyl groups might no longer be present at this pH. To verify the loss of carboxyl groups at pH 12, a FTIR-ATR spectrum was acquired. The spectrum in Figure 3-4 (c) shows a substantially diminished carboxyl peak at pH 12, suggesting that the surface modification is unstable at highly alkaline pH.

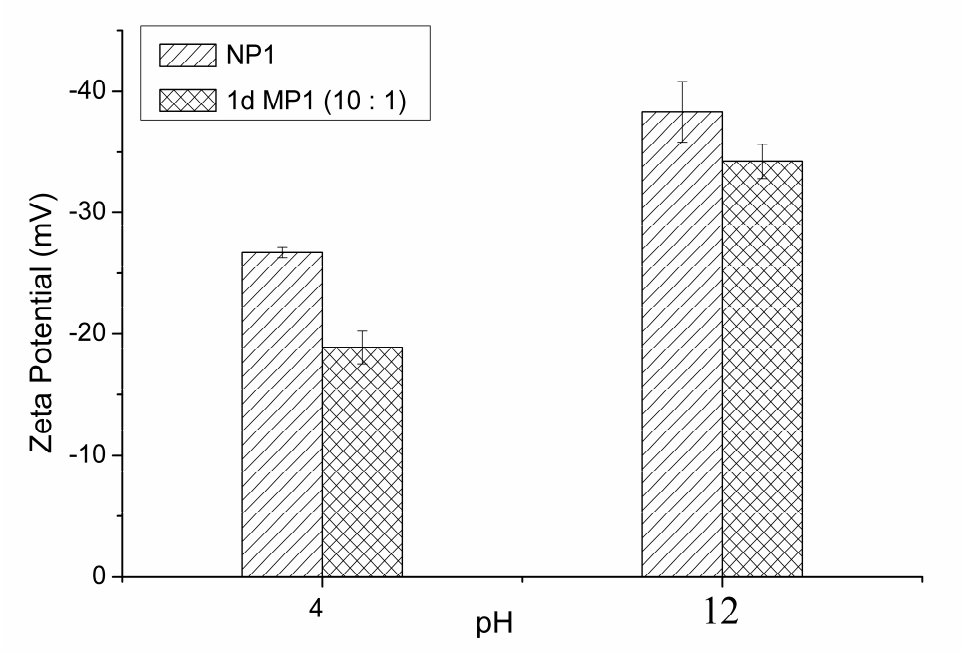

Figure 3-3. Zeta potential measurements of NP1 and 1 d MP1 (10:1) at pH 4 and pH 12. (n=3).

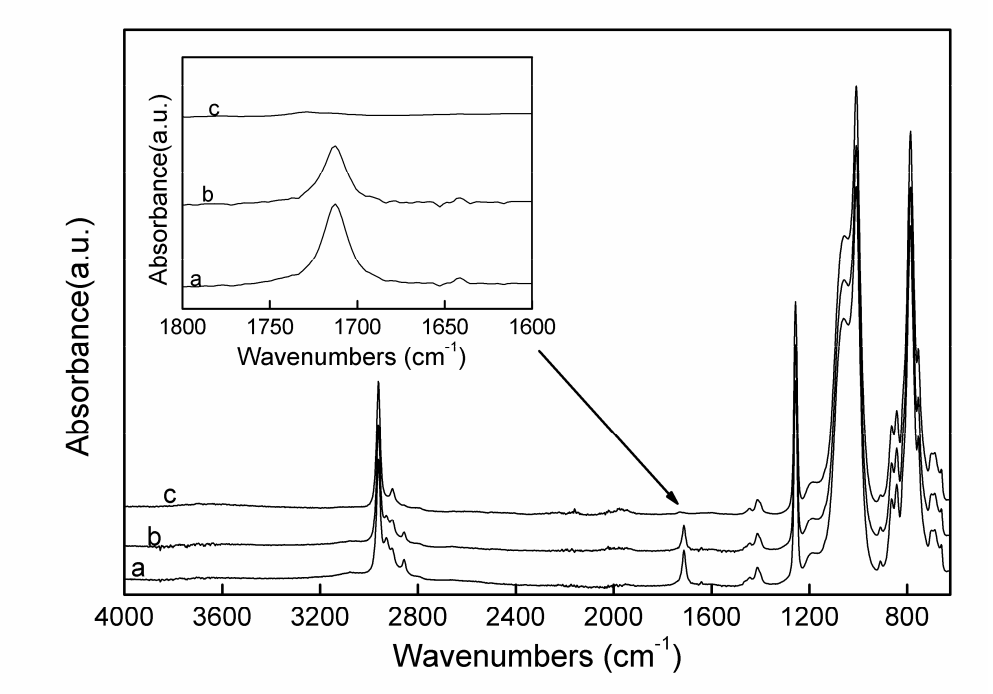

Figure 3-4. FTIR-ATR spectra of (a) 1 d MP1 (10:1) before zeta potential analysis, (b) 1 d MP1 (10:1) after zeta potential analysis at pH 4, and (c) 1 d MP1 (10:1) after zeta potential analysis at pH 12.

3.3.1.4 Stability experiments

Stability experiments were performed on 1 d MP1 (10:1). First, the stability of the samples in MilliQ water at 50 ºC and PBS buffer (pH 7.2) at 50 ºC and room temperature was determined. From the FTIR-ATR results (Figure 3-5(a)), it was very clear that 1 d MP1 (10:1) was stable in MilliQ water at 50 ºC for 17 h, as evidenced by the retention of the carboxyl peak in each spectrum. However, the intensity of the carboxyl group peak decreased dramatically after PBS buffer treatment not only at 50 ºC (Figure 3-5(b)), but also at room temperature (Figure 3-5(c)), indicating the surface modification was not stable in PBS buffer. The reduced stability of 1 d MP1 (10:1) in PBS buffer was most likely caused by the increased ionic strength, compared to MilliQ water. Further work is required to fully understand the phenomenon, but this is beyond the scope of this work. The 1 d MP1 (10:1) sample was also kept in a desiccator and investigated by means of FTIR-ATR after 5.5 h and 19.5 h. The longer testing times used in a desiccator were just based on considering lower temperatures used here, compared to in water or PBS buffer. The result (Figure 3-5(d)) shows the carboxyl group still remained on the 1 d MP1 (10:1) surface.

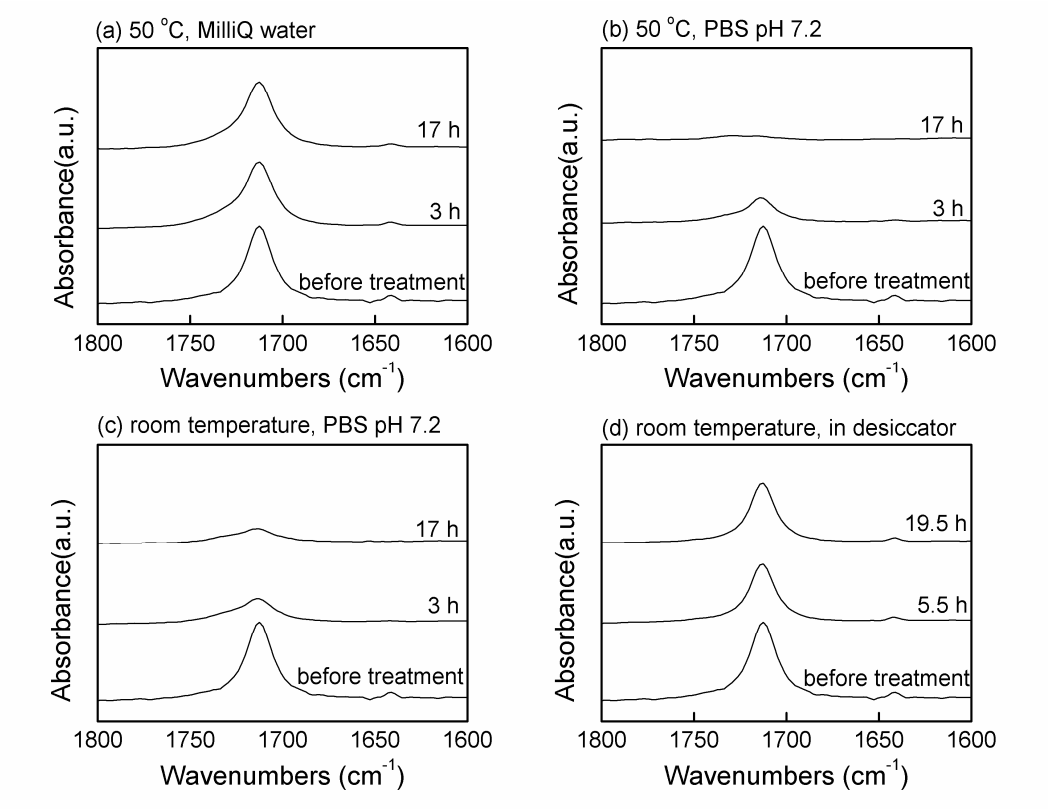

Figure 3-5. Stability of the carboxyl peak in FTIR-ATR spectra of 1 d MP1 (10:1) surfaces: of (a) immersion in MilliQ water for 3 h and 17 h at 50 ºC; (b) immersion in PBS buffer (pH 7.2) for 3 h and 17 h at 50 ºC; (c) immersion in PBS buffer (pH 7.2) for 3 h and 17 h at room temperature; (d) stored in a desiccator for 5.5 h and 19.5 h at room temperature.

3.3.2 Comparison of MP1 samples with different weight ratio of base to curing agent in PDMS prepolymer

According to the stability study of 1 d MP1 (10:1) in PBS buffer, even though a thorough cleaning process was used to remove the physically adsorbed UDA molecules, it was evident that the sample was not stable, which implied that most carboxylic groups were not covalently bonded onto the PDMS matrix. This could be the result of a suboptimal density of SiH groups from the curing agent on the PDMS surface available for hydrosilylation with UDA. Based on this consideration, another 1 d MP1 sample with 5:1 base to curing agent was prepared aiming to supply more reactive SiH sites for covalently bonding UDA and further improve the stability of MP1 sample.

3.3.2.1 WCA measurements

The wettability of 1 d MP1 (10:1) and 1 d MP1 (5:1) was compared by monitoring the WCA on surfaces. As shown in Figure 3-6, decreasing the weight ratio of PDMS base to curing agent from 10:1 to 5:1 resulted in a slight decrease of WCA value from 77 ± 2º to 71 ± 0.5º. In addition, the WCA of 1 d MP1 (5:1) was also measured after 5 d, 10 d, 20 d, 25 d, and 30 d of storage in air or MilliQ water. The result shows the WCA of 1 d MP1 (5:1) stayed relatively constant over this observed timeframe, which was similar to 1 d MP1 (10:1). In addition, the WCA of the pure UDA surface was measured to be ~60 º, which is a lower value than on any MP1 surface. This result indicates that the coverage of UDA on MP1 surfaces might be less than 100%.

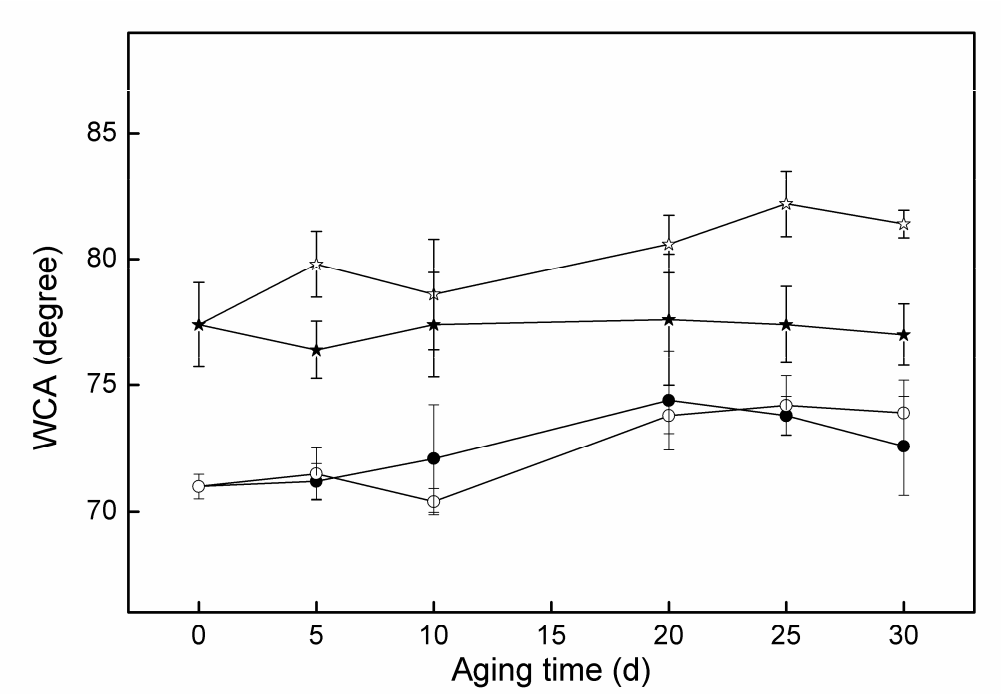

Figure 3-6. WCA vs. aging time for 1 d MP1 (10:1) and 1 d MP1 (5:1). The samples were stored in air (filled symbols) and in MilliQ water (empty symbols). Pentagram: 1 d MP1 (10:1); circle: 1 d MP1 (5:1).

3.3.2.2 FTIR-ATR spectroscopy

From Figure 3-7, it is obvious that MP1 (5:1) shows the same characteristic peak at 1715 cm^{-1} corresponding to carboxylic groups, as the spectrum of MP1 (10:1). The intensity of

the two COOH peaks is very close, indicating the amount of carboxyl groups on these modified PDMS surfaces is similar. This may explain why there is only a very slightly difference in WCA values obtained on MP1 (5:1) and MP1 (10:1).

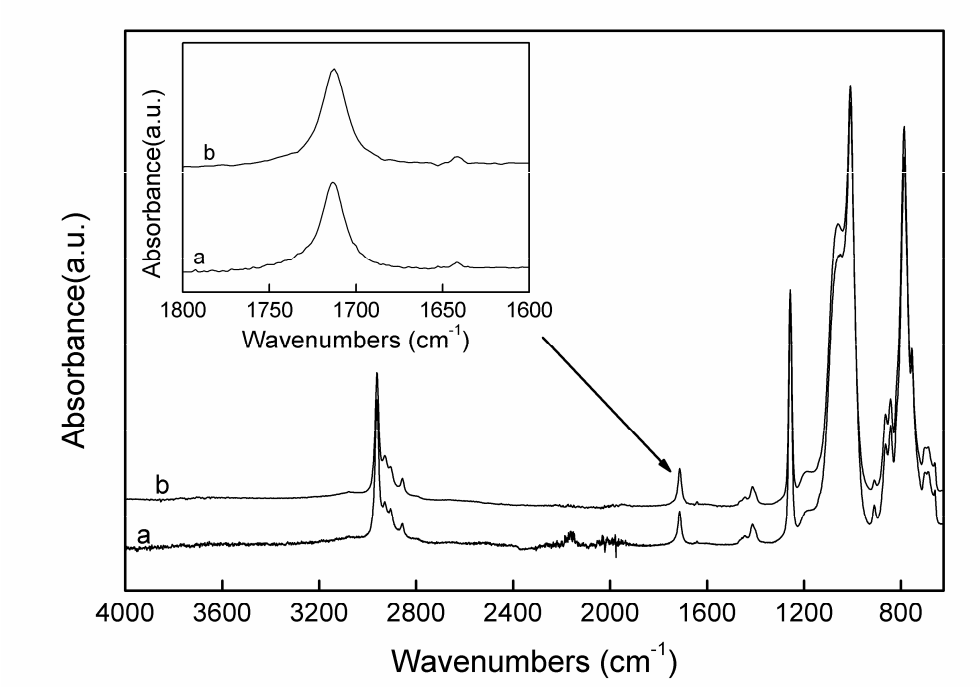

Figure 3-7. FTIR-ATR spectra of (a) 1 d MP1 (5:1) and (b) 1 d MP1 (10:1).

3.3.2.3 Stability experiments

According to the FTIR-ATR analysis of the 1 d MP1 (10:1) surface, it was observed that this sample was not stable in PBS buffer or at alkaline pH. For comparison, the carboxyl peaks in the FTIR-ATR spectra of 1 d MP1 (5:1) and 1 d MP1 (10:1) were monitored after immersing the samples in PBS buffer and in KCl buffer. First, the stability of the samples in 1 mM KCl solution at room temperature for 1 d was determined. It was clear that both 1 d MP1 (5:1) and 1 d MP1 (10:1) surfaces were very stable in pH 4 KCl solution, as shown by the retention of the carboxyl peak in each spectrum (Figure 3-8). However, the intensity of the carboxyl group peak of the 1 d MP1 (10:1) surface disappeared after treatment in KCl solution at pH 12 (Figure 3-8(b)). In contrast, the peak was still present in the 1 d MP1 (5:1) spectra (Figure 3-8(a)), indicating 1 d MP1 (5:1) was much more stable than the 1 d MP1 (10:1) sample at highly alkaline pH.

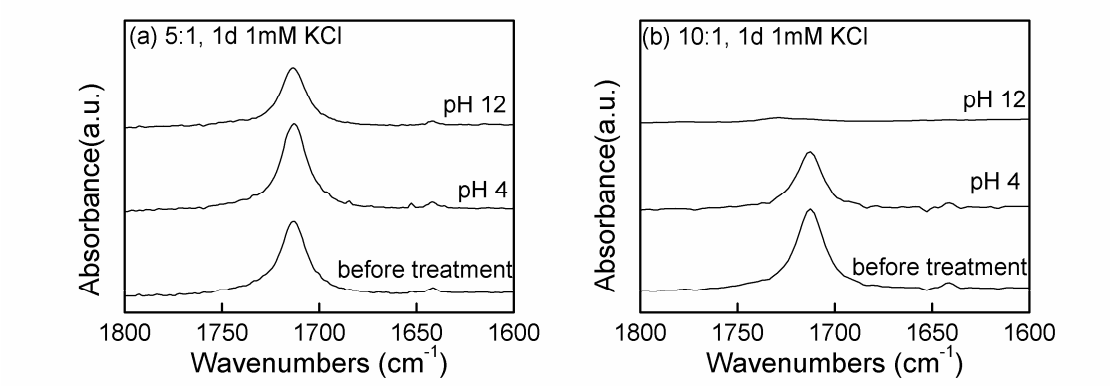

Figure 3-8. Stability of the carboxyl peak in the FTIR-ATR spectra of (a) 1 d MP1 (5:1) and (b) 1 d MP1 (10:1) after immersing in 1mM KCl at pH 4 or pH 12 for 1 d at room temperature.

In addition, the improved stability of the 1 d MP1 (5:1) surface was confirmed by the presence of carboxyl peaks in the FTIR-ATR spectra after immersing the sample in PBS buffer (pH 7.2) for 3 h and 17 h, not only at 50 ºC, but also at room temperature (Figure 3-9 (a)). However, the carboxyl peak decreased dramatically for the 1 d MP1 (10:1) surface.

As expected, the stability of the modified PDMS surface in PBS buffer and in KCl buffer is markedly improved by reducing the base to curing agent from 10:1 to 5:1 in order to supply more reactive Si-H sites for hydrosilylation with UDA. This implies that after surface modification, more covalent bonding to UDA is acheivable on 1 d MP1 (5:1), compared to 1 d MP1 (10:1).

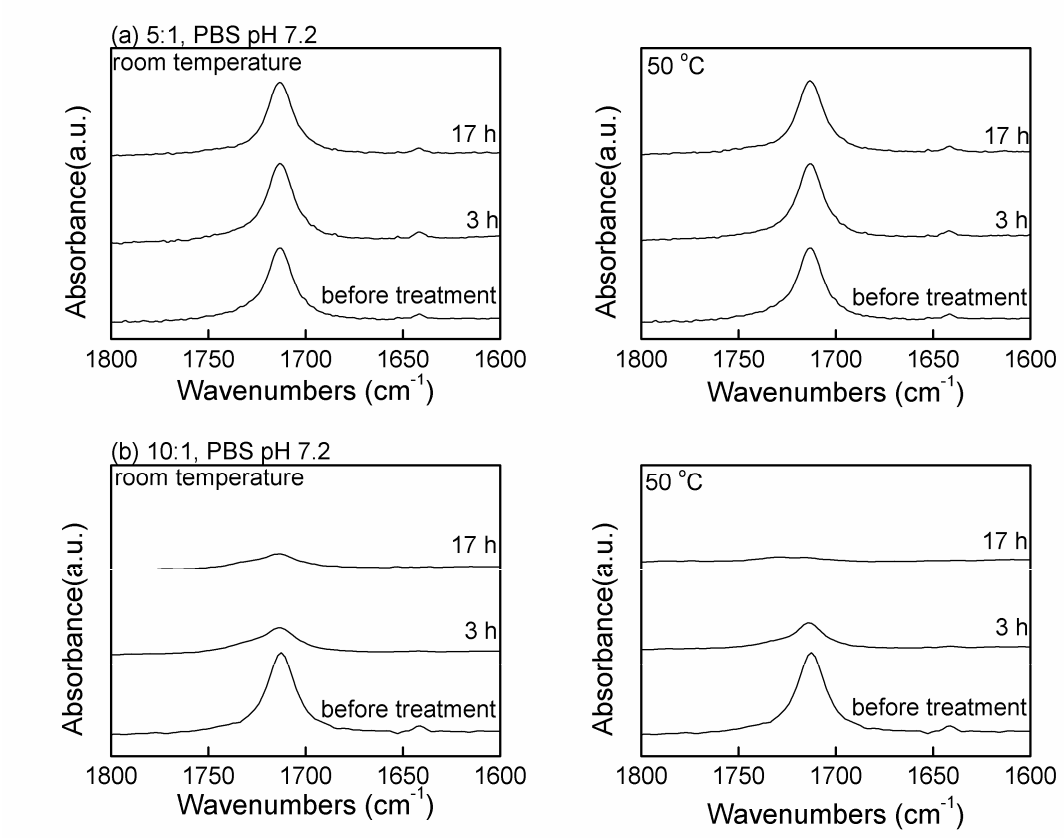

Figure 3-9. Stability of the carboxyl peak in the FTIR-ATR spectra of (a) 1 d MP1 (5:1) and (b) 1 d MP1 (10:1) after immersing in PBS buffer (pH 7.2) for 3 h and 17 h, at 50 ºC and room temperature.

3.3.2.4 Fluorescence labeling study

To demonstrate the presence and reactivity of the carboxyl functional groups on the modified PDMS surfaces, Lucifer Yellow CH was covalently coupled to the carboxyl groups [168]. Scheme 3-1 depicts the reaction scheme of Lucifer Yellow CH attachment on the carboxyl functionalized PDMS surface. Carboxyl groups on the 1 d MP1 (5:1 and 10:1) surfaces were reacted with amino groups on Lucifer Yellow CH dipotassium salt *via* carbodiimide coupling using EDAC.

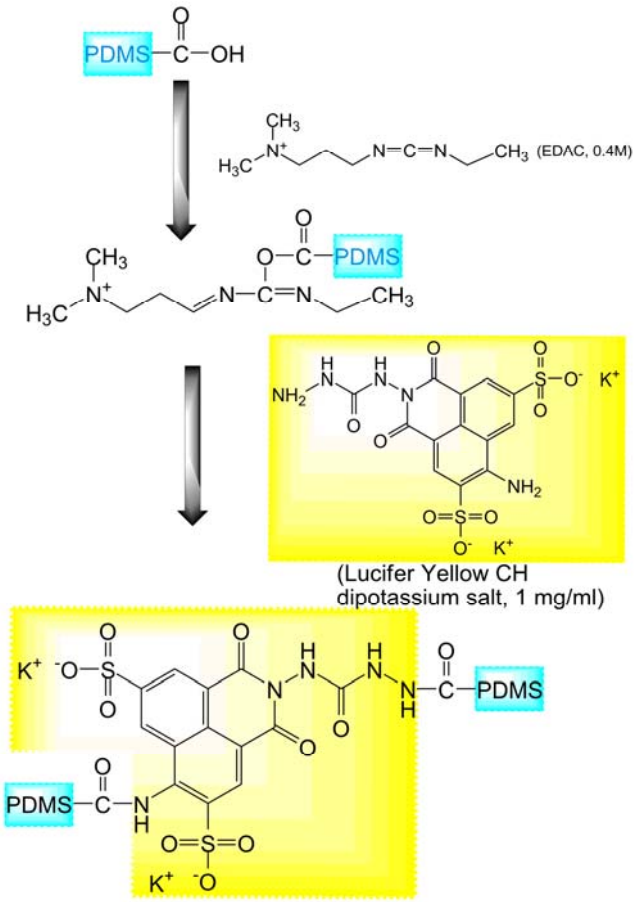

Scheme 3-1. Immobilization of Lucifer Yellow CH dipotassium salt dye on carboxyl functionalized PDMS surface.

Figure 3-10 (a) shows NP1 and 1 d MP1 (10:1) with Lucifer yellow CH after cleaning the surface with MilliQ water. Clearly, the dye has successfully attached to the carboxyl functionalized PDMS surfaces. The fluorescence signal decreased significantly after ethanol washing, perhaps due to the removal of loosely adsorbed dye (Figure 3-10 (b)). In addition, Lucifer Yellow CH was also successfully attached onto the 1d MP1 (5:1) surface after MilliQ water and ethanol washing (Figure 3-10 (c)). By comparing the fluorescence signal on Figure 3-10 (b) and (c), it is evident that the 1 d MP1 (5:1) surface showed brighter fluorescence than the 1 d MP1 (10:1) surface. This suggests that there were more reactive carboxyl groups on 1 d MP1 (5:1) surface, which is consistent with the outcome of the stability study. No fluorescence was detected on the NP1 (5:1 or 10:1) control surfaces after incubation with Lucifer Yellow CH and EDAC.

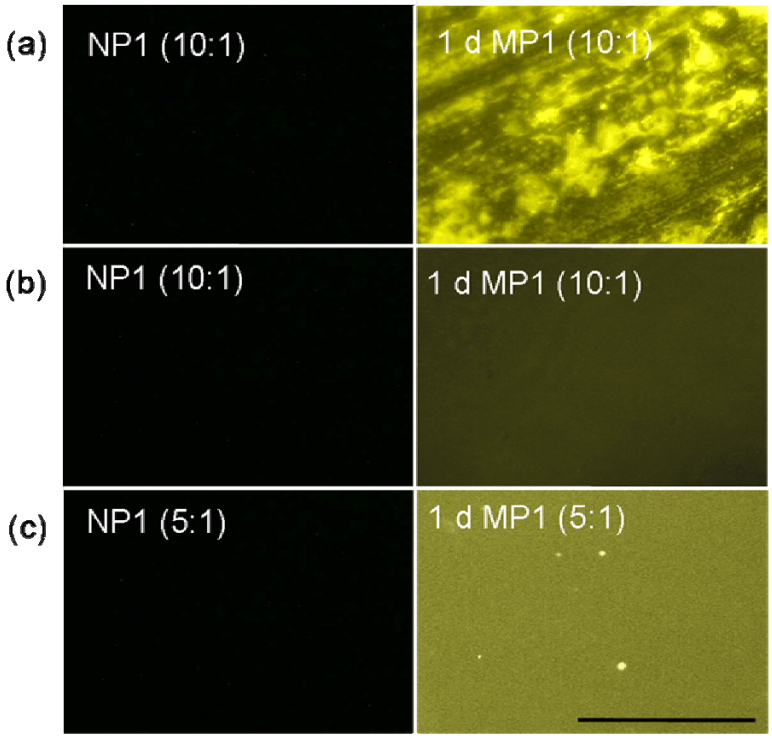

Figure 3-10. Fluorescence microscopy images: (a) NP1 and 1 d MP1 (10:1) with Lucifer Yellow CH after cleaning with MilliQ water; (b) NP1and 1 d MP1 (10:1) with Lucifer yellow CH after cleaning with MilliQ water and ethanol; (c) NP1 and 1 d MP1 (5:1) with Lucifer Yellow CH after cleaning with MilliQ water and ethanol. (Scale bar: 100 μm)

3.4 Conclusion

In this study, a simple one-step surface modification of PDMS was demonstrated. The increase in hydrophilicity of the MP1 (10:1) was confirmed by water contact angle data, indicating a change in the surface chemical properties, which was confirmed by the presence of the characteristic vibrational band corresponding to the carboxyl stretch of carboxylic acids at 1715 cm^{-1} in the FTIR-ATR spectrum of the MP1 (10:1) sample. The difference in the streaming zeta potential at pH 4 between native PDMS and 1 d MP1 (10:1) further confirmed UDA attachment to the PDMS surface, however this attachment was not stable at highly alkaline pH. The fluorescence labeling with Lucifer Yellow CH further demonstrated carboxyl functionalization of PDMS, however this attachment was unstable in ethanol. The surface was shown to be stable for up to 30 d in MilliQ water but not in PBS buffer based systems or at high pH.

By increasing the curing ratio in the PDMS prepolymer, we were able to supply more Si-H sites for the covalently bonding UDA. Consequently, 1 d MP1 (5:1) showed higher stability in PBS buffer based systems or at high pH than 1 d MP1 (10:1). In addition, the attachment of Lucifer Yellow CH suggested that there was a higher proportion of carboxyl groups available on the 1 d MP1 (5:1) surface compared to the 1 d MP1 (10:1) surface.

CHAPTER 4 HYDROPHILIZATION OF PDMS USING SAM ASSISTED TEMPLATING

The content of this chapter is based on references [77, 169].

4.1 Introduction

PDMS is a moldable silicon-based elastomeric polymer with numerous advantages over other polymeric systems. These advantages include biocompatibility, gas permeability, relative chemical inertness, readily disposable, optical transparency, ease of bonding and molding into (sub)micrometer features, and low manufacturing costs [27, 28]. However, the most problematic issue with native PDMS is its hydrophobicity. Therefore in order to improve the surface wettability of PDMS for, in particular, microfluidic applications it is necessary to modify the surface chemically.

There are various surface modification techniques available to render the PDMS surface more hydrophilic, as detailed in Chapter 1. Aside from these surface modification techniques, the bulk modification of PDMS is also critical in the fabrication of stable hydrophilic surfaces and in particular surfaces that do not undergo hydrophobic recovery. This has been achieved by the addition of a nonionic surfactant (TX-100) [170], an amphiphilic biocompatible copolymer poly(lactic acid)-poly(ethylene glycol) [171] or UDA [162] into the PDMS prepolymer. Pertinent to the work presented here Luo *et al.* [162] used 0.5 wt % UDA in PDMS prepolymer and cast this onto a silicon wafer. However, they found no reduction in the WCA of the UDA/PDMS modified surface. In addition, SAM coated gold slides were used as a template for curing PDMS prepolymer mixed with vinyl-terminated moieties, which could drive the moieties impregnated within the cured PDMS to the water/PDMS interface, *via* interfacial free energy minimization [28].

As shown in Scheme 4-1, here we generate a PDMS surface with decreased hydrophobicity by adding 2 wt % UDA into the PDMS prepolymer. This mixture was then cast onto a SAM of hydrophilic MPA-modified gold slide. The UDA carboxyl moieties then migrate to the hydrophilic SAM modified gold surface *via* interfacial free energy minimization [28]. Once the UDA/PDMS is peeled off the gold, the new MP2 surface had a WCA 20° lower than NP2. In addition, FTIR-ATR spectroscopy showed the presence of carboxyl groups on the MP2 surface. These carboxyl groups remained stable at room temperature in PBS buffer for 3 h and 17 h. In addition, XPS and streaming zeta-potential analysis on the MP2 surface also proved successful PDMS surface modification by UDA. Once the presence of the carboxyl groups had been verified 5'-amino terminated oligonucleotides were attached to the carboxylated UDA-modified PDMS surface *via* amide linkages. FAM-labeled complementary oligonucleotide strands where then passed over the modified surface and the fluorescence measured using a fluorescence microscope (Scheme 4-1).

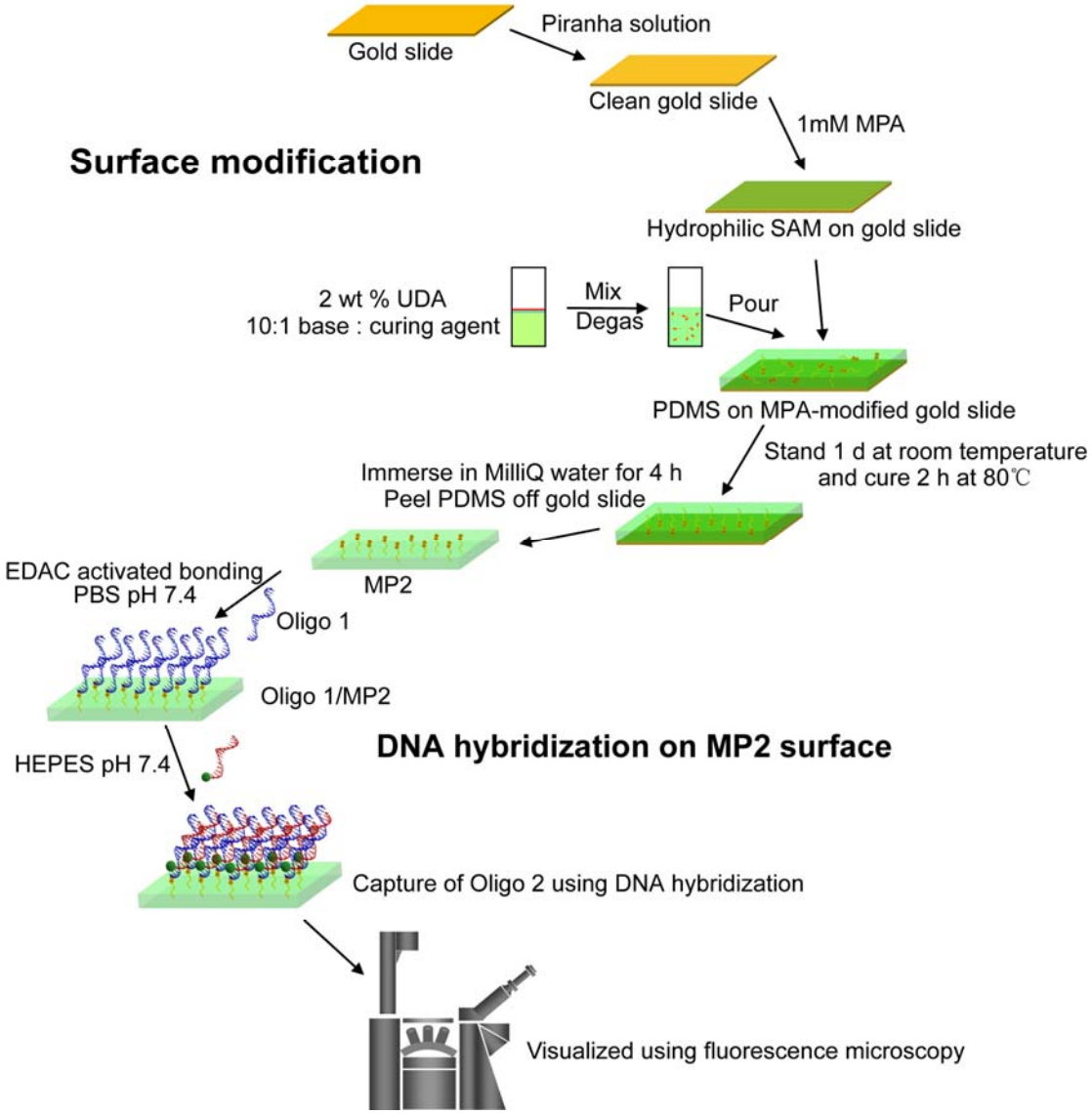

Scheme 4-1. Process of PDMS surface modification by UDA and DNA hybridization on MP2 surface.

4.2 Experimental section

The details of materials and chemicals used, preparation of PDMS samples, surface characterization on open PDMS surfaces and the application in DNA hybridization are all detailed in Chapter 2, except for the stability experiment.

4.2.1 Stability experiment

The stability of the MP2 surfaces was tested in MilliQ water and PBS (pH 4.8 or pH 7.4) at

room temperature and/or at 50 ºC for 3 h and 17 h. These conditions were chosen as they are typical of normal hybridization conditions. Each surface was then analyzed using FTIR-ATR spectroscopy.

4.3 Results and discussion

4.3.1 Surface characterization on PDMS surfaces

4.3.1.1 WCA measurements

To characterize the hydrophilicity of MP2 surfaces, static WCA measurements were performed. The WCA of blank gold slide was ~72 ± 1° (Figure 4-1 (a)), and the WCA value decreased to ~20 ± 1° when a SAM of hydrophilic MPA was formed on the gold slide (Figure 4-1 (b)). After standing on the resulted substrate for 1 d in air, a mixture of PDMS prepolymer and 2 wt % UDA was cured at 80 ºC for 2 h. The WCA of MP2 after removal from the MPA-modified gold was measured at 91 ± 2° (Figure 4-1 (d)), which is 18° lower than the WCA of NP2 (110 ± 1°) (Figure 4-1 (c)) and close to the WCA value obtained when 3 wt % undec-11-enylhexaethylene glycol was used as an additive [28]. This decrease of WCA indicates that the wettability of the PDMS surface has been improved by adding UDA into the PDMS prepolymer. In addition, in order to confirm that the UDA carboxyl moieties preferentially migrate to a hydrophilic MPA-modified gold slide, a mixture of UDA/PDMS was also cured on a hydrophobic 2-mercaptopyridine (2-MP)-modified gold slide which had been previously prepared by immersing the gold slide in 2 % (w/v) 2-MP: 100 % absolute ethanol for 24 h. The UDA/PDMS sample removed from the hydrophobic 2-MP-modified gold slide was measured at 104 ± 2°, which is only 5° lower than the WCA of NP2. This result showed the UDA carboxyl moieties preferentially migrate onto the hydrophilic surface to minimize the interfacial free energy.

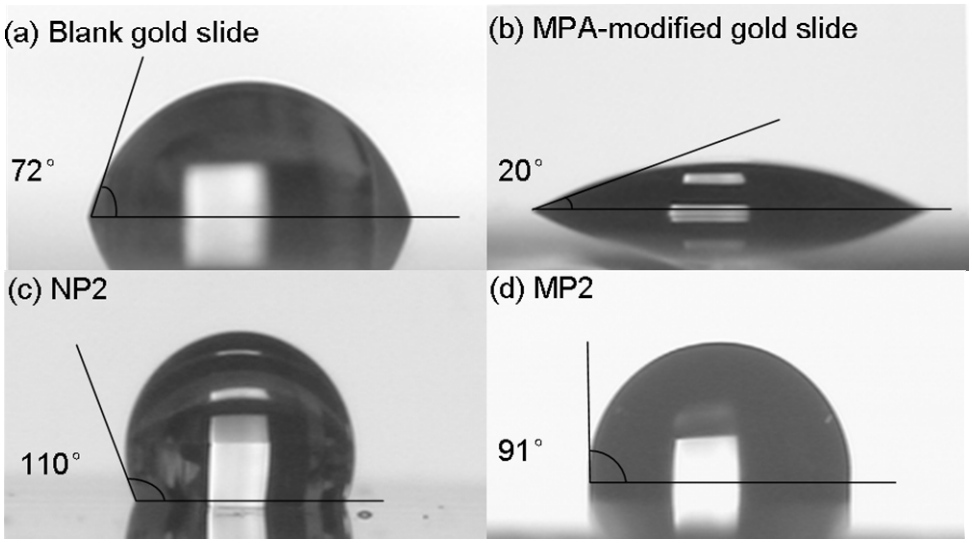

Figure 4-1. WCA measured on the surfaces of (a) blank gold slide; (b) MPA modified gold slide; (c) NP2 and (d) MP2.

4.3.1.2 FTIR-ATR spectroscopy

FTIR-ATR spectroscopy was carried out to confirm the presence of carboxyl groups on the PDMS surfaces. Figure 4-2 (a) shows the FTIR-ATR spectrum of NP2 between 1600-1800 cm^{-1} indicating the absence of carboxyl moieties in this region, which is in accordance with literature [37, 164]. From Figure 4-2 (b), it is obvious that the MP2 has different spectral features with the appearance of two characteristic carboxyl peaks one at 1715 cm^{-1} due to hydrogen bonded carboxylic groups and the other at 1730 cm^{-1} due to free carboxylic acid [172]. This clearly indicates the presence of UDA on the surface. The reduction in WCA after modification is therefore attributed to these introduced carboxylic groups.

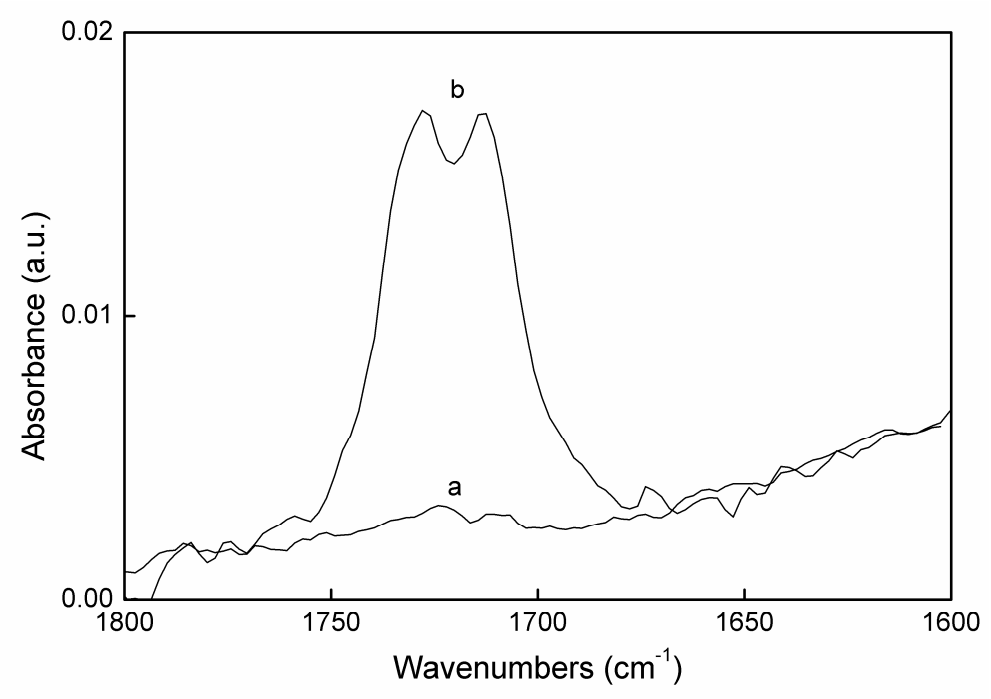

Figure 4-2. FTIR-ATR spectra of (a) NP2 and (b) MP2.

4.3.1.3 XPS

XPS was also used to investigate the change in the PDMS surface chemistry after UDA modification. The XPS C 1s and O 1s signals are increased by approximately 1 % and 2 %, respectively, after UDA modification, while Si 2p signal is decreased by approximately 3 % (Table 4-1.). This change in chemical composition is in good agreement with the literature [28], where 3 wt% undec-11-enylhexaethylene glycol was used as an additive.

Table 4-1. Chemical compositions of the surfaces of NP2 and MP2 within the depth of information of XPS.

	C (%)	O (%)	Si (%)
NP2	45.9	26.0	28.1
MP2	47.0	28.0	25.0

Figures 4-3 (a) and (b) show a fit of the C 1s peaks taken from a high resolution XPS scan of the NP2 and the MP2 surface, respectively. The XPS results indicate only one peak at 285.00 eV, corresponding to C-H/C-C on the NP2 surface (Figure 4-3 (a)). However, after UDA modification, an additional C 1s high-resolution peak at 290.0 eV

corresponding to O–C=O groups [33, 173] appeared in the spectrum for MP2 (Figure 4-3 (b)), showing that carboxylic acid groups are available on the surface, which is consistant with the presence of characteristic carboxyl peaks in the FTIR-ATR spectrum of MP2.

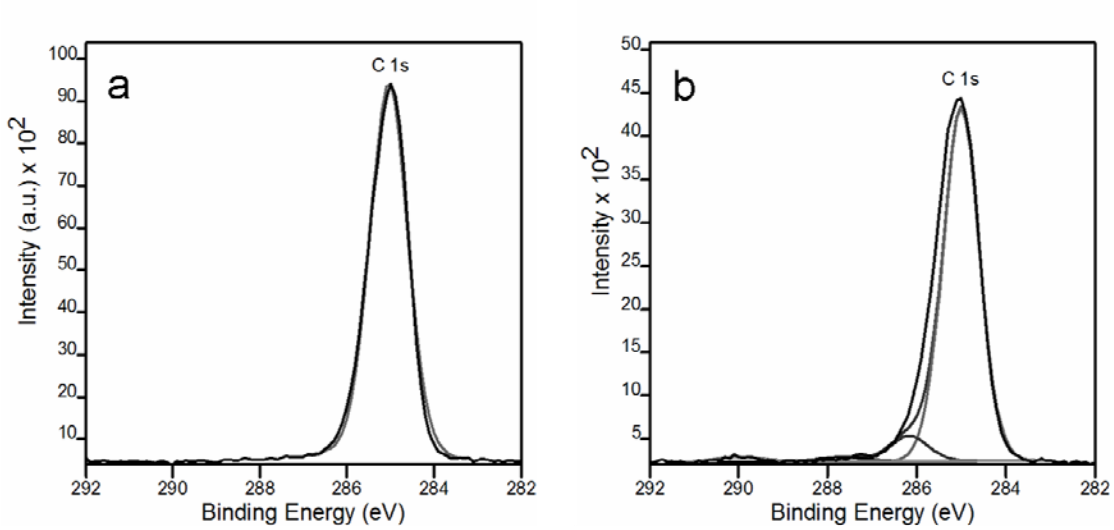

Figure 4-3. High resolution XPS C 1s spectra of (a) NP2 and (b) MP2.

4.3.1.4 Streaming zeta-potential analysis

The change of PDMS surface chemistry after UDA modification was also verified by the comparison of the zeta potential on NP2 and MP2 surfaces over the pH range from 4 to 12 (Figure 4-4). For MP2, the zeta potential was -14.1 ± 3.0 mV at pH 4, compared to -24.3 ± 1.7 mV for NP2. This difference was attributed to the presence of protonated carboxylic acid moieties from the UDA on the surface. As the pH increased, the zeta potential on the MP2 decreased more rapidly than for NP2. At pH ≥ 8, more negative zeta potentials were measured on the MP2 (-43.4 ± 4.0 mV at pH 8, -51.0 ± 0.8 mV at pH 10 and -55.9 ± 1.8 mV at pH 12) compared to NP2 (-30.0 ± 2.0 mV at pH 8, -33.2 ± 1.7 mV at pH 10 and -38.3 ± 2.0 mV at pH 12), due to the deprotonated carboxylate functionalities present on the surface at higher pH. The slow decrease of zeta potential on NP2 with the increase of pH might result from the deprotonation of the surface Si-OH groups on the NP2 surface at high pH [20] and/or physisorbed anions within the Stern layer [165].

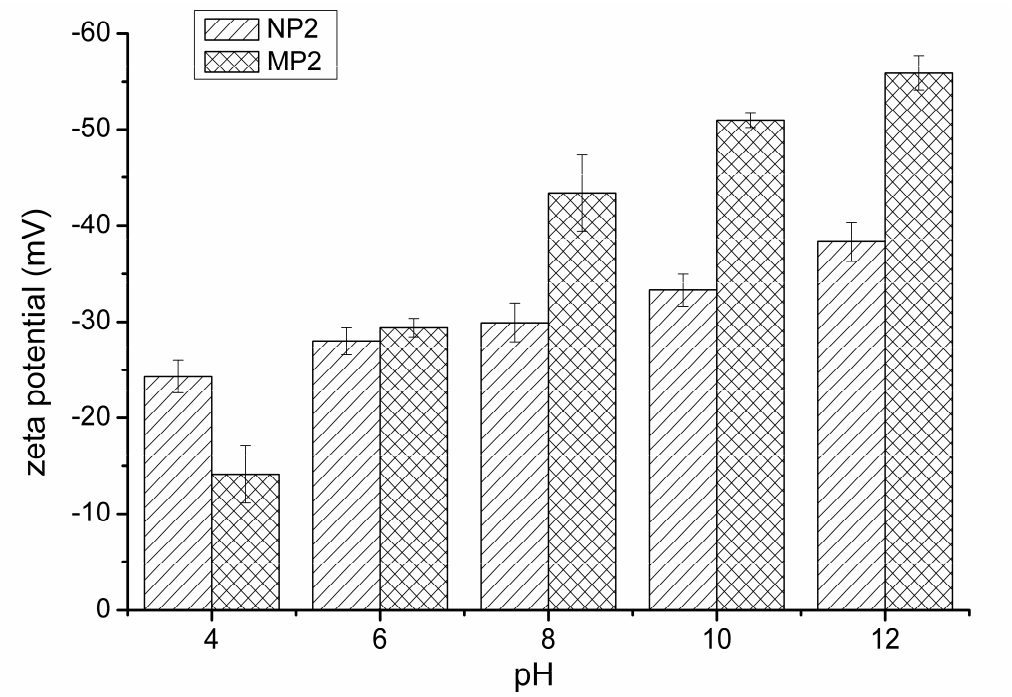

Figure 4-4. Streaming zeta potential measurements for NP2 and MP2 at pH 4, 6, 8, 10 and 12; (n=3).

4.3.1.5 Stability experiments

Stability experiments were performed on MP2. FTIR-ATR spectroscopy results (Figure 4-5(a)), demonstrate that the carboxyl groups remain on the surface after storage of the samples in MilliQ water (Figure 4-5 (a)), PBS buffer (pH 4.8) (Figure 4-5 (b)) and PBS buffer (pH 7.4) (Figure 4-5 (c)) at room temperature and/or 50 ºC for 3 h and 17 h. Clearly, the diffusion of the UDA to the interface has resulted in immobilized carboxyl groups, which do not undergo the typical hydrophobic recovery observed in traditional oxidized PDMS. These groups are then available for attachment of Oligo1 *via* amide coupling. It should also be noted that the peak at 1715 cm^{-1} corresponding to hydrogen bonded carboxylic groups is stable, but the peak at 1730 cm^{-1} corresponding to free carboxylic acid is reduced slightly, which is likely due to the diffusion of unbound UDA into the PBS.

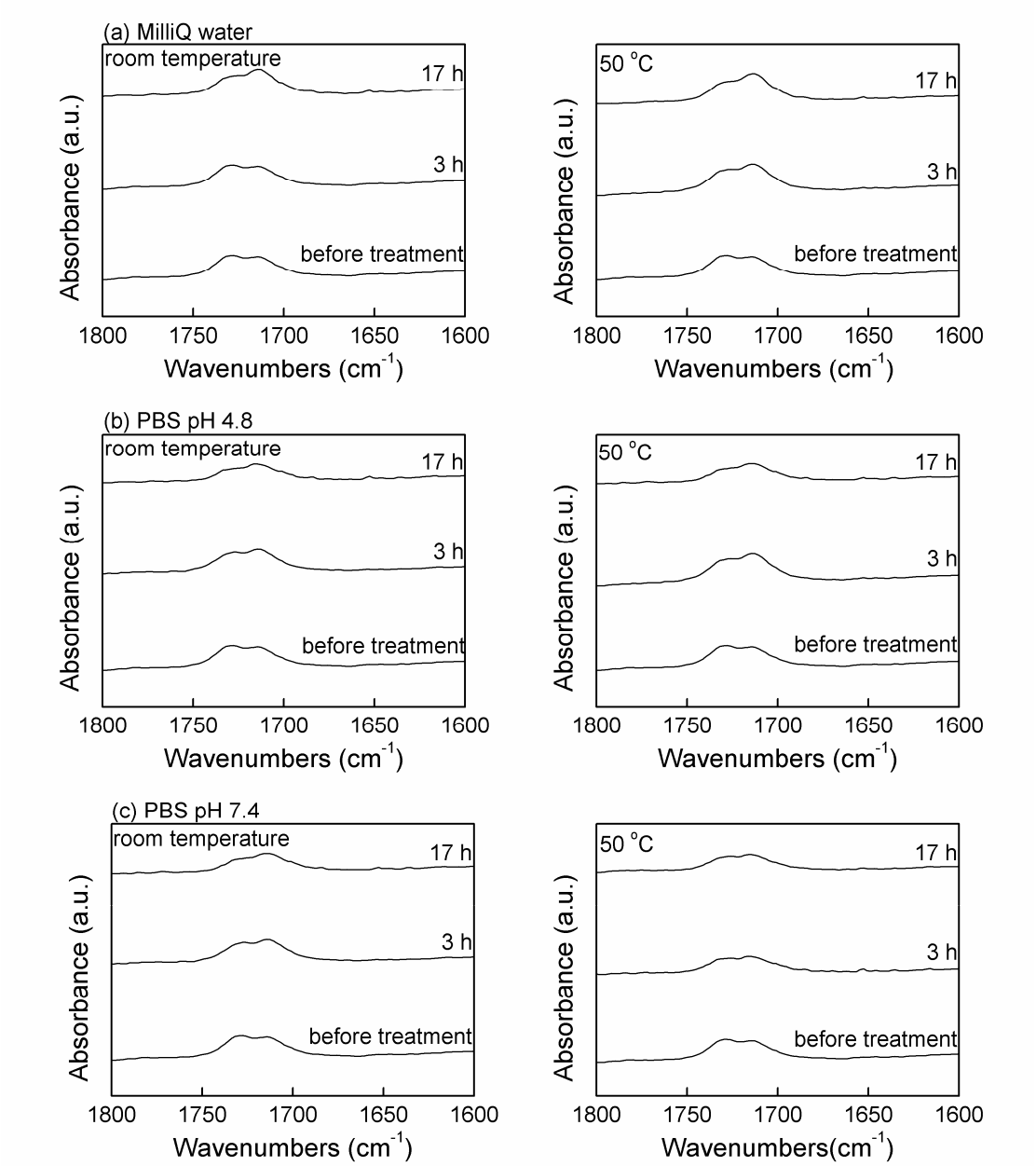

Figure 4-5. Stability of the carboxyl peak in FTIR-ATR spectra of MP2 immersing in: (a) MilliQ water, (b) PBS (pH 4.8) and (c) PBS (pH 7.4) for 3 h and 17 h at room temperature and/or 50 ºC.

4.3.1.6 Fluorescence labeling study

To demonstrate the reactivity of carboxylic acid groups on the MP2 surface, Lucifer Yellow CH was coupled to the carboxylic acid groups *via* EDAC carbodiimide coupling. The reaction process has been illustrated in Scheme 3-1. The fluorescence microscopy images clearly demonstrate rather homogenous yellow fluorescence across the MP2 surface (Figure 4-6 (b)), indicating that the dye has successfully been attached to the

carboxy-functionalized PDMS surface. However, no fluorescence was detected on the NP2 surface (Figure 4-6 (a)) after incubation with EDAC and Lucifer Yellow CH.

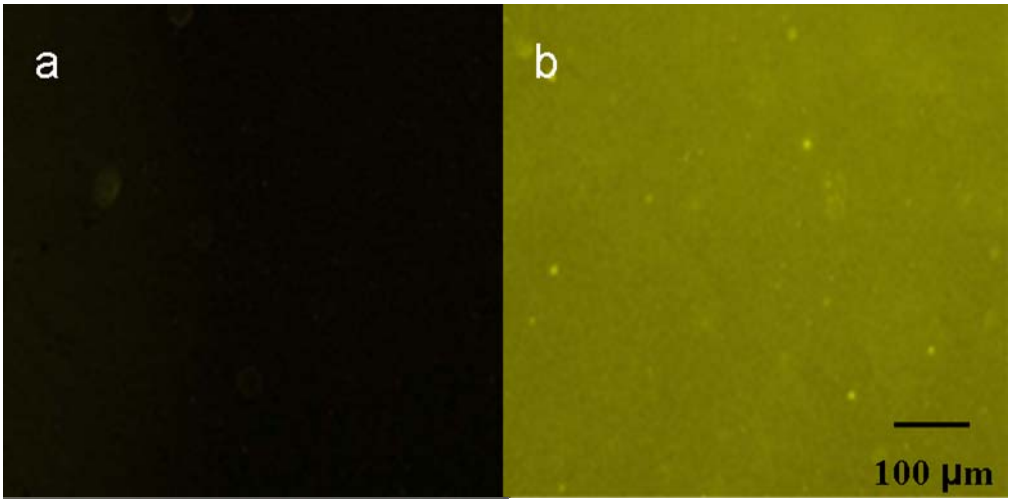

Figure 4-6. Fluorescence images of (a) NP2 and (b) MP2 with Lucifer Yellow CH labeling.

4.3.2 Application of DNA hybridization

Figure 4-7 (a) and (b) shows the NP2 and the MP2 surfaces after exposure to EDAC, then Oligo 1 with subsequent hybridization with Oligo 2. The NP2 surface shows a slight fluorescence, which is most likely due to non-specific DNA adsorption of the FAM-labeled Oligo2. However, Figure 4-7 (b) shows an increase in the observed intensity of the Oligo1/UDA-modified PDMS hybridized with the Oligo2. Analysis of the images using a line scan of intensity profile is shown in Figure 3-7 (c) and (d) as a dotted line. For the purpose of comparing fluorescence intensity on NP2 and MP2 surfaces, the fluorescence intensity values on the different glass slides were normalized. As a result, the average fluorescence intensity along the dotted line for the Oligo 1/NP2 surface hybridized with Oligo 2 was 30.0 ± 9.7 (Figure 4-7 (c)) while for the Oligo1/UDA-modified PDMS hybridized with Oligo 2 this value was 44.6 ± 5.9 (Figure 4-7 (d)). An increase in intensity of 1.3 times after DNA hybridization was thus observed, indicating successful PDMS surface modification and DNA hybridization. The bright spots observed in both Figure 4-7 (a) and (b) may be due to scattering centers or surface asperities with increased fluorescence in these regions.

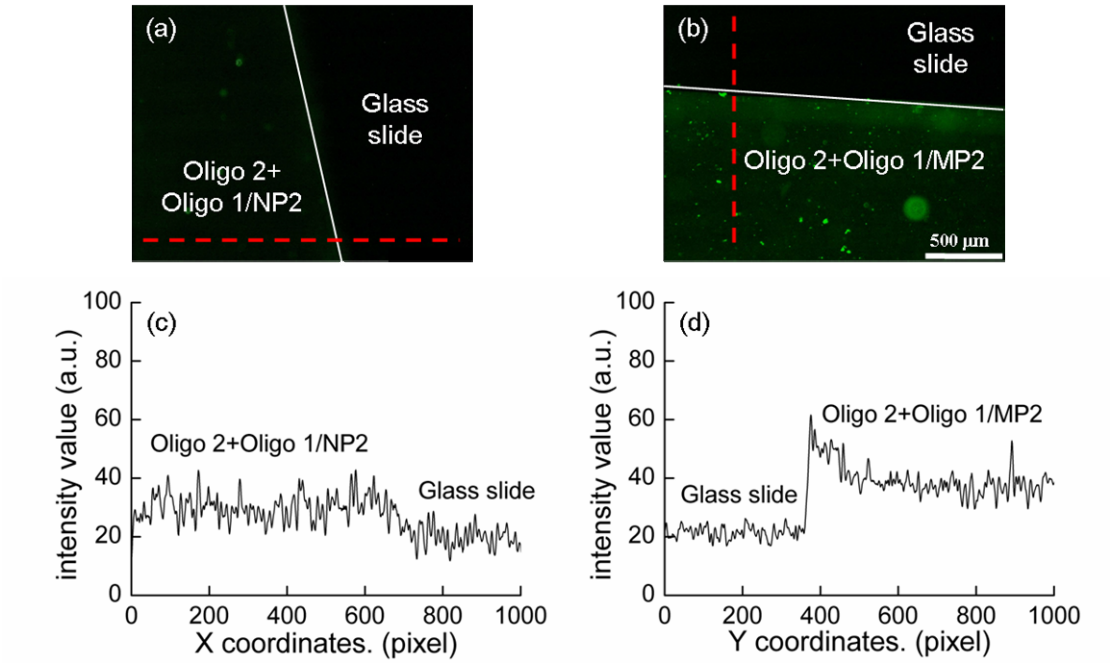

Figure 4-7. Fluorescence microscopy images of (a) Oligo 1/NP2 and (b) Oligo 1/MP2 after DNA hybridization with Oligo2. (c) shows the line intensity profile, marked as dotted lines, of Oligo 1/NP2 (from left to right) and (d) the Oligo 1/MP2 (from top to bottom) after DNA hybridization with Oligo 2. The samples were placed on a glass slide for microscopy imaging.

As a control, an MP2 surface was reacted with EDAC, then reacted with Oligo2 instead of Oligo1. Analysis of this surface showed fluorescence from non-specific adsorption only (intensity value: 17.0 ± 12.2), which confirmed that the covalent immobilization of Oligo1 was required for sequence-specific hybridization. Furthermore, fluorescein-labeled non-complementary DNA Oligo3 was used as a control and hybridized on an Oligo1/MP2 surface. As expected, only a small amount of fluorescence was observed from non-specific binding (intensity value: 23.1 ± 9.6).

Compared with other techniques [8, 174] used on PDMS surfaces for DNA hybridization, there are some limitations when real DNA samples are to be analyzed using our current technique. This is because dye labeling must be carried out on the target DNA before analysis.

4.4 Conclusion

Typically, in order to surface-functionalize native PDMS, the prepolymer is cured, and then functionalized using a variety of wet and physical chemistries. Here, we show a simpler 1-step method. PDMS surfaces were successfully functionalized with carboxyl groups by curing a mixture of PDMS and 2 wt % UDA on a 3-mercaptopropanoic acid modified gold slide. This method is potentially amenable to a wide range of diverse functionalities that can be introduced on the PDMS surface by simple deposition of mixtures of prepolymer and functionalized molecules on either a hydrophobic or hydrophilic template. The improved wettability of the MP2 was confirmed by water contact angle data, which was interpreted by the presence of the characteristic carboxyl peaks in the FTIR-ATR spectrum of MP2 and a C 1s high-resolution peak at 290.0 eV corresponding to O–C=O groups in the XPS spectrum of MP2. The successful attachment of Lucifer Yellow CH on MP2 surface further demonstrated the reactivity of the introduced carboxylic acid groups on the MP2 surface.

The pendent carboxyl groups formed at the PDMS surface were covalently linked to an amino-terminated oligonucleotide capture probe. A FAM-labeled complementary oligonucleotide strand was then successfully hybridized to the surface.

CHAPTER 5 HYDROPHILIZATION OF PDMS BY COMBINATION OF SOXHLET-EXTRACTION AND PLASMA TREATMENT

The content of this chapter is based on references [31].

5.1 Introduction

In recent years, PDMS has been widely employed in microfluidics due to its relatively low cost, easy fabrication and optical transmission characteristics [27, 28]. However, its high hydrophobicity and hydrophobic recovery after surface hydrophilization represent undesirable properties. Therefore, surface modification of PDMS is paramount in order to improve PDMS wettability for microfluidic applications. In practice, PDMS surfaces modified with functional groups are also needed, for example, in order to facilitate immobilization of biological species [97].

Various methods have been employed to render PDMS surfaces hydrophilic. For example, hydroxyl groups have been generated on PDMS surfaces *via* ultraviolet/ozone (UVO) treatment [37]. In addition, amino groups have been introduced onto PDMS surfaces *via* CVD polymerization [40] or silanization [61]. Another example of introducing –COOH moieties onto PDMS surfaces was performed *via* UV-induced polymerization of AAc [19, 97]. Compared with the former modification techniques, plasma polymerization has an obvious advantage in that it requires shorter modification times. Several research groups [30, 33] have utilized a plasma of AAc to coat PAAc onto a previously Ar-pretreated PDMS surface specifically to introduce –COOH moieties onto the surface. However, no further modification of these surfaces has been reported.

Here, we present a PDMS surface modification method by using 2-step Ar and AAc plasma treatment. In addition, in order to prevent quick hydrophobic recovery by rearrangement of uncured PDMS oligomers, the native PDMS was Soxhlet-extracted with hexane before plasma modification to remove the uncured PDMS oligomers. The PDMS surfaces were characterized using WCA, FTIR-ATR spectroscopy, AFM and XPS. We then report on the covalent attachment of 5´-amino-terminated oligonucleotides to the MP3 surfaces and further DNA hybridization with fluorescently tagged complementary oligonucleotides, as determined by fluorescence microscopy.

5.2 Experimental section

The details of the materials and chemicals used, preparation of NP3 and MP3 samples, surface characterization of sample surfaces and the application of DNA hybridization were all detailed in Chapter 2, except for the experiments described below.

5.2.1 WCA

The WCA measurements were performed as described in Chapter 2. However, the PDMS samples were stored in air in order to observe the effects of aging times on the WCA value.

5.2.2 Stability experiment

The MP3 sample was monitored over time at room temperature and/or 50 ºC in water, PBS (pH 4.8 and/or pH 7.4) and HEPES buffer (pH 7.4) to investigate the stability of the applied surface modification. FTIR-ATR spectra were obtained after 0.5 h, 3 h and 17 h to monitor the intensity of the carboxyl peak of PAAc (at 1715 cm^{-1}) on the modified PDMS surfaces. These conditions were chosen as they are typical of normal hybridization conditions. Each surface was then analyzed using FTIR-ATR spectroscopy.

5.2.3 AFM

A piece of hexane Soxhlet-extracted PDMS was half covered with a clean microscope

cover slide, and then exposed to the 2-step plasma process with Ar and then AAc. The microscope cover slide was then removed and the PDMS surface imaged using AFM. AFM imaging was performed as described in Chapter 2.

5.2.4 Fluorescence labeling study

To quantify the fluorescence intensity, the NP3 and MP3 after reacting with EDAC and Lucifer Yellow CH dipotassium salt dye were placed on glass slides and examined under an IX 81 inverted fluorescence microscope (Olympus, Japan). A line scan on each sample was performed and analyzed using ImageJ software V1.34 to produce an intensity profile.

5.3 Results and discussion

To optimize the AAc plasma conditions, a series of different operational pressures and treatment times were tested. Then FTIR-ATR spectroscopy was then carried out on these surfaces to monitor the intensity of COOH peak at 1715 cm^{-1} [19]. The settings used for the FTIR-ATR analysis are described in Chapter 2. As shown in Figure 5-1, when the AAc plasma treatment time was 5 min, the operational pressures were set at 0.1 mbar, 0.2 mbar, 0.3 mbar to 0.4 mbar, respectively. The highest intensity of COOH peak in the FTIR-ATR spectra was observed when using 0.2 mbar. Then, the operational pressure was set at 0.2 mbar, and various treatment times (0.5 min, 1 min, 2 min, 3 min, 4 min, 5 min and 10 min) were applied. As shown in Figure 5-2, the intensity of the COOH peak increased with increasing treatment time, and the highest intensity was observed after 5 min of treatment. At longer treatment times, the intensity of the COOH peak decreased again. Therefore the combination of 0.2 mbar for the operational pressure and 5 min for the treatment time was selected as the optimal condition of AAc plasma for our further work.

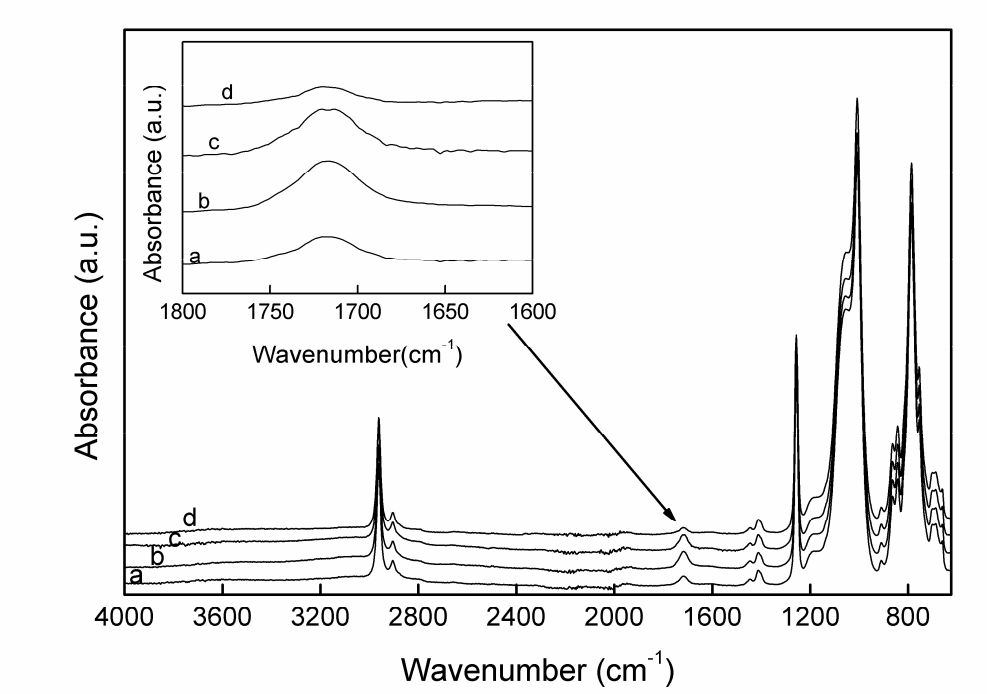

Figure 5-1. FTIR-ATR spectra of AAc plasma modified PDMS with different operational pressures ((a) 0.1 mbar, (b) 0.2 mbar, (c) 0.3 mbar,and (d) 0.4 mbar,) and fixed 5 min treatment time on an Ar pretreated surface (0.7 mbar, 0.5 min).

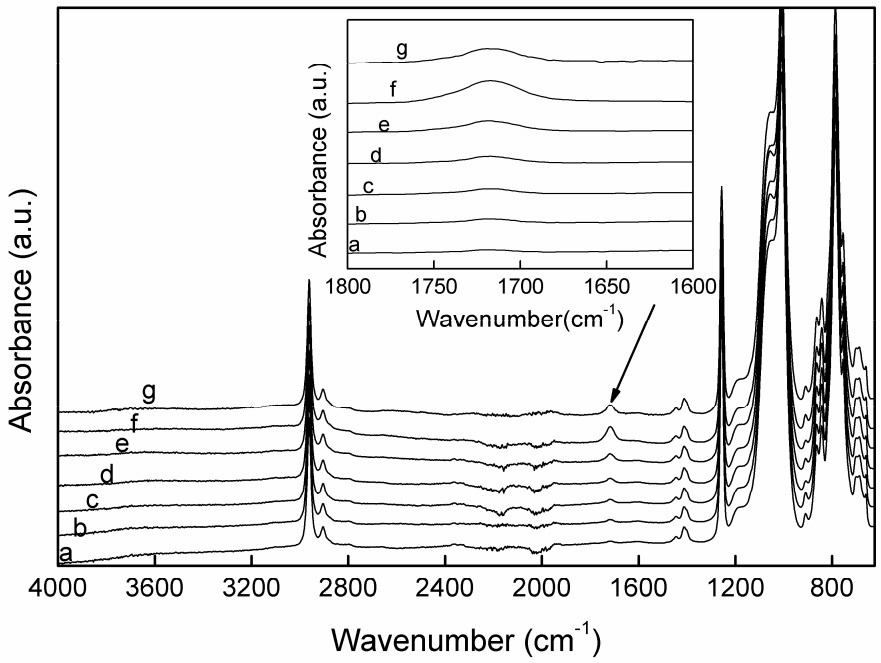

Figure 5-2. FTIR-ATR spectra of AAc plasma modified PDMS with different treatment times ((a) 0.5 min, (b) 1 min, (c) 2 min, (d) 3 min, (e) 4 min, (f) 5 min and (g) 10 min) and fixed 0.2 mbar operational pressure on an Ar pretreated surface (0.7 mbar, 0.5 min).

5.3.1 Surface characterization of PDMS surfaces

5.3.1.1 WCA measurements

WCA measurements are the preferred method to characterize surface wettability. According to Figure 5-3, the WCA of NP3 was ~110º and was stable for at least one month in air. After the one-step Ar plasma treatment (0.5 min at 0.7 mbar) of the NP3 surface, the WCA value dramatically decreased to ~22º. When AAc plasma treatment for 5 min at 0.2 mbar was subsequently performed on this surface, the WCA increased to ~30º. Although the surface wettability was improved by this 2-step plasma treatment, hydrophobic recovery took place in air and the WCA value reverted back to approximately 100º within 1 wk. In order to improve the hydrophilic stability, Soxhlet-extraction with hexane was performed on the NP3 samples prior to the Ar and AAc 2-step plasma treatment. The improved surface wettability and stability in air storage is shown in Figure 5-1. The WCA decreased dramatically to 32 ± 2º and then increased to 50º in the first day, remaining stable in the range of 50º to 60º over the next week. Even after 30 d storage in air, the WCA value on the MP3 surface was still much lower (78º) than for the NP3 surface (110º) and other plasma treated PDMS surfaces without previous Soxhlet-extraction (>100º). The hydrophilic recovery on PDMS surfaces is generally attributed to the migration of uncured PDMS oligomers from the bulk to the surface and the mechanical recovery of PDMS after ion attachment [115]. In our work, the NP3 samples were extracted with hexane to remove the uncured oligomers before the 2-step plasma modification, thus minimizing hydrophobic recovery. The WCA value on the MP3 surface was similar to the value from Barbier *et al.*' work [30], where the WCA was 50º ~ 60º measured after a 3-step plasma modification, which involved an Ar, AAc and finally a He plasma, but the stability of the WCA was not studied in this work.

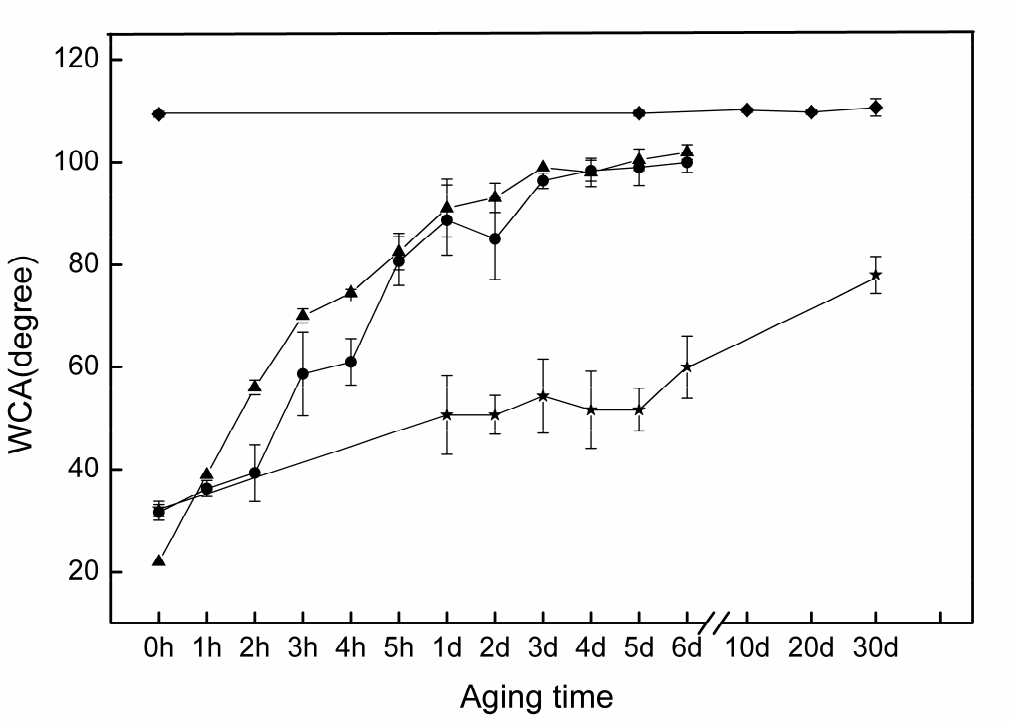

Figure 5-3. WCA versus aging time for PDMS samples in air. Diamond: NP3; triangle: Ar plasma treated NP3; circle: Ar and then AAc plasma treated NP3; pentagram: MP3 in air.

5.3.1.2 FTIR-ATR spectroscopy

FTIR-ATR spectroscopy was carried out to interpret the outcome of the WCA measurements and to confirm the functionalization of the PDMS surface by AAc plasma treatment. Figure 5-4 (a) shows the FTIR-ATR spectrum of the NP3 surface indicating the absence of carboxyl moieties in the region between 1600 and 1800 cm^{-1}, which is in accordance with the literature [37, 164]. From Figure 5-4 (b), it is clear that the MP3 has different spectral features with the appearance of one broad characteristic carboxyl peak at 1715 cm^{-1} corresponding to carboxyl groups. This clearly indicates that carboxyl groups were successfully introduced onto the PDMS surface after plasma polymerization. The large reduction in WCA after surface modification is due to the introduced COOH groups.

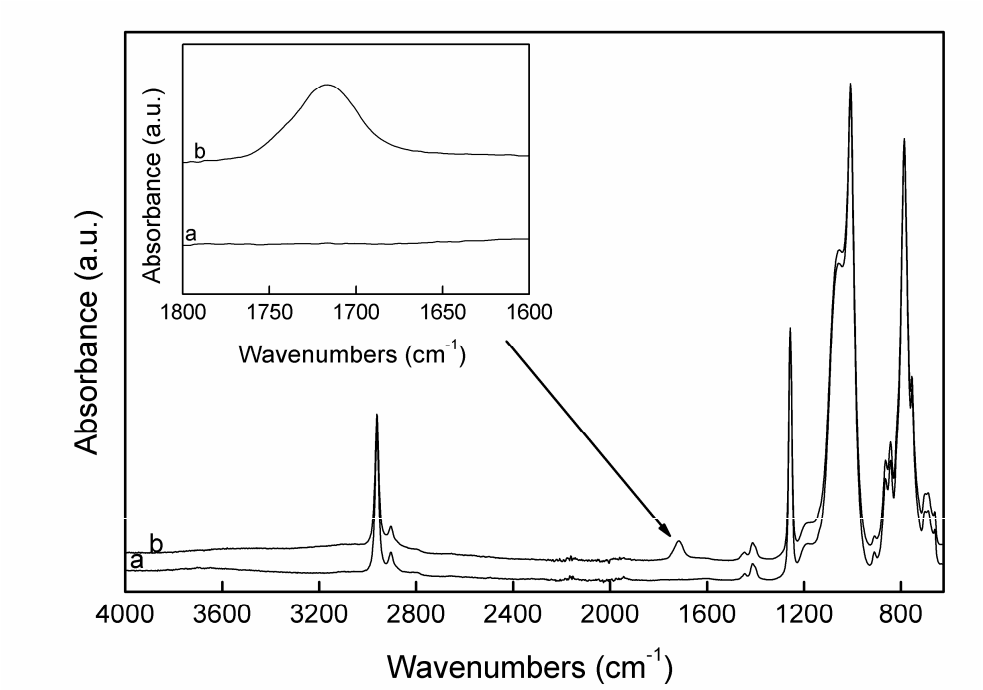

Figure 5-4. FTIR-ATR spectra of (a) NP3 and (b) MP3.

5.3.1.3 XPS

XPS was carried out to investigate the change of surface chemistry upon plasma modification. Table 5-1 shows that the 2-step plasma treatment on the native PDMS surface led to a significant increase in oxygen content (from 27.3 % to 33.8 %) whereas the silicon content showed reverse behaviour (decreased from 28.3 % to 24.2 %). The change in trends of oxygen and silicon content is in good agreement with the Ar/AAc 2-step plasma modified PDMS without previous Soxhlet-extraction [33]. The percentage of carbon on the PDMS surface after plasma modification showed a slight decrease from 44.4 % to 42.0 %, while no change in carbon content was found on the Ar/AAc 2-step plasma modified PDMS without previous Soxhlet-extraction [33]. This difference may be caused by the removal of uncured PDMS oligomers after applying the Soxhlet-extraction step before plasma treatment.

Table 5-1. Chemical compositions of the surface of NP3 and MP3 within the depth of information of XPS.

	C (%)	O (%)	Si (%)
NP3	44.4	27.3	28.3
MP3	42.0	33.8	24.2

Figures 5-5 (a and b) show a fit of the C 1s peaks taken from a high resolution XPS scan of the Soxhlet-extracted NP3 and MP3 surfaces, respectively. The XPS results indicate only one peak at 285.00 eV, corresponding to C-H/C-C on the extracted NP3 surface (Figure 5-5 (a)). However, after the 2-step plasma modification the C 1s became more complex with the appearance of three new peaks at 285.87 eV, 287.37 eV and 289.91 eV, originating from C-O, C=O and O-C=O, respectively (Figure 5-5 (b)). The same peaks have also been observed in previous work by Jafari *et al.* [175] when treating polyethylene films with a plasma mixture of Ar and AAc. Figure 5-5 (b) shows that after the 2-step plasma modification, the percentage of C-H/C-C, C-O, C=O and O-C=O was 72 %, 21 %, 4 % and 4 %, respectively. Here, the most interesting feature is the COOH peak, as this is the functionality required to form potential amide linkages with amino-terminated moieties for further surface modification or applications. The presence of the COOH groups explains the reduction in WCA after plasma polymerization.

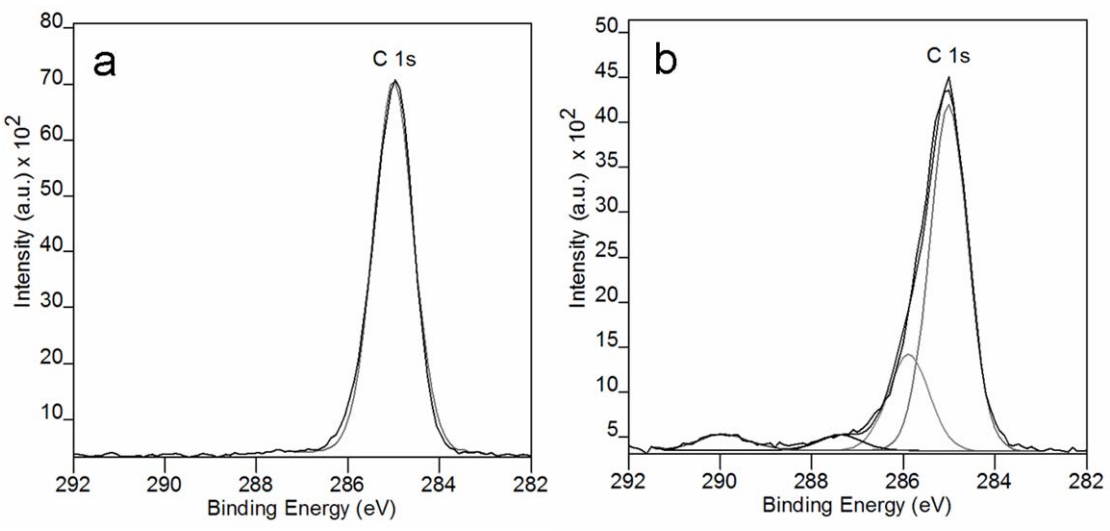

Figure 5-5. High resolution XPS C 1s spectra of (a) Soxhlet-extracted NP3 and (b) MP3.

5.3.1.4 Stability experiments

FTIR-ATR spectroscopy was carried out to confirm the stability of the MP3 surface in MilliQ water and buffers (PBS (pH 4.8/pH 7.4) and HEPES (pH 7.4)) at room temperature and/or 50 ºC (Figure 5-6). Clearly, the carboxyl peaks still remained on the MP3 surface after storage in all cases (Figure 5-6 (a) for MilliQ water, Figure 5-6 (b) for PBS (pH 4.8), Figure 5-6 (c) for PBS (pH 7.4) and Figure 5-6 (d) for pH 7.4 HEPES buffer). Furthermore, the intensities of the 1715 cm^{-1} peak remained stable over a 17 h period, although there was a moderate decrease observed in the case of the PBS (pH 7.4) (Figure 5-6 (c)) and HEPES buffer (Figure 5-6(d)) at 50 ºC.

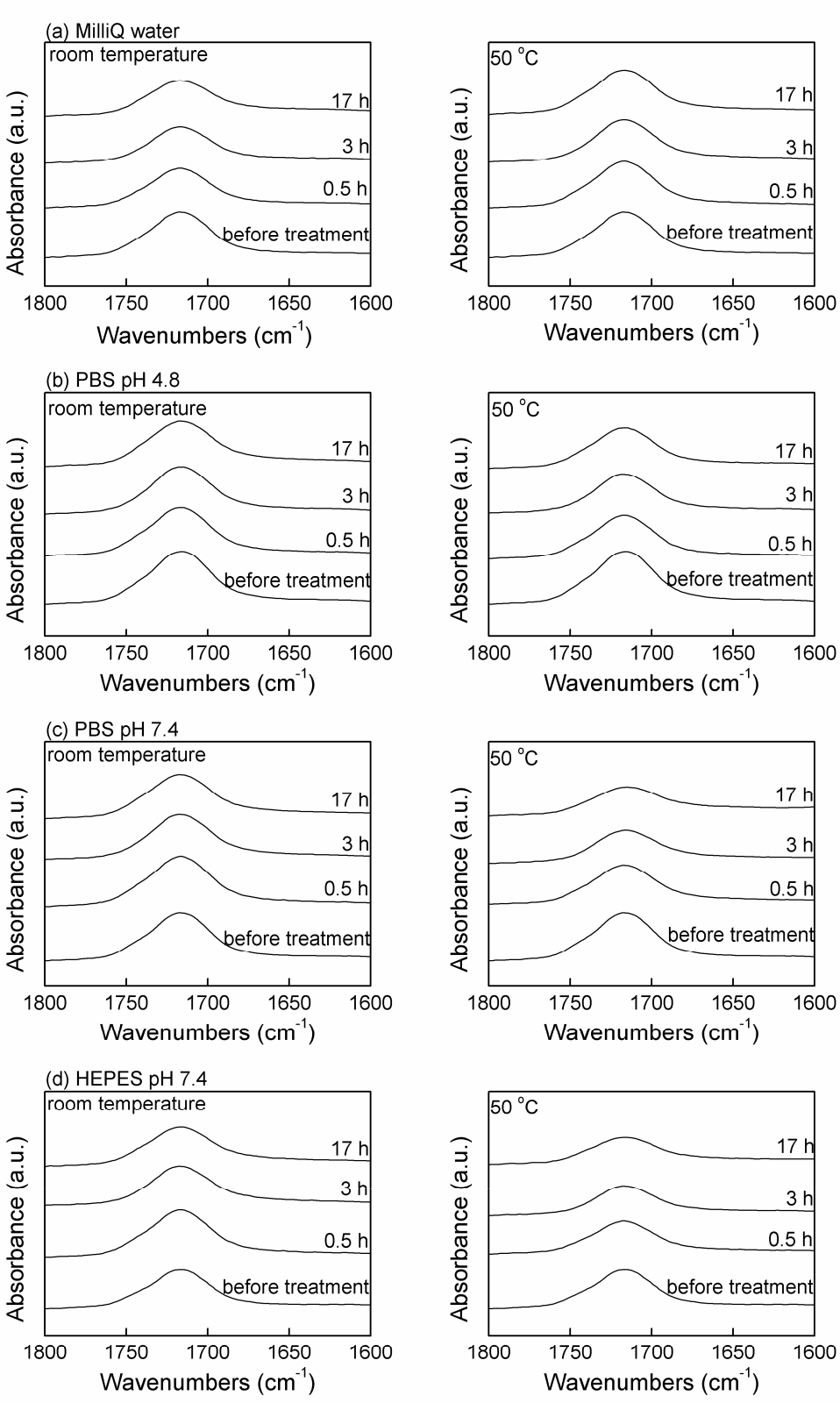

Figure 5-6. Stability of the carboxyl peak in the FTIR-ATR spectra of MP3 immersed in: (a) MilliQ water, (b) PBS (pH 4.8), (c) PBS (pH 7.4) and (d) HEPES buffer (pH 7.4) for 0.5 h, 3 h and 17 h at room temperature and/or 50 ºC.

5.3.1.5 AFM

Based on the WCA, FTIR-ATR and XPS spectra presented previously, it can be concluded that the successful deposition of PAAc was performed onto the PDMS surface. AFM was then used to investigate the difference in surface topography after plasma modification. Figure 5-7 (a) and (b) show the surface topography of Soxhlet-extracted NP3 and MP3, respectively. Clearly, the topography of the MP3 (Figure 5-7 (b)) is significantly different from the NP3 (Figure 5-7 (a)). The RMS surface roughness increased from 1.4 nm ± 0.1 for the NP3 to 4.0 nm ± 3.4 for the MP3 surface. The increased roughness after plasma modification was likely to be due to the etching effect of plasma treatment [176] and/or the deposition of the PAAc polymer layer [177]. In addition, the PDMS sample became slightly thinner after 2-step plasma treatment, which was probably due to an etching effect from plasma treatment [178]. In order to more fully understand the effect of this 2-step plasma treatment on the surface topography, further work needs to be carried out.

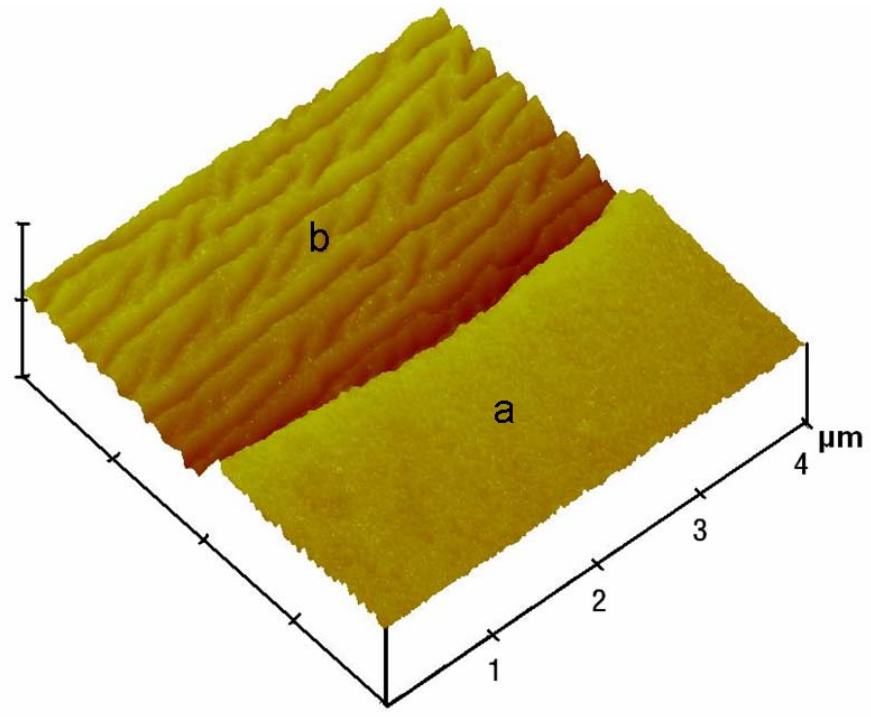

Figure 5-7. AFM images (4 × 4 µm^2) of (a) Soxhlet-extracted NP3 and (b) MP3. The Z scale is 70 nm.

5.3.1.6 Fluorescence labeling study

To demonstrate the reactivity of carboxylic acid groups on the MP3 surface, Lucifer

Yellow CH dye was coupled to the carboxylic acid groups *via* EDAC carbodiimide coupling. The reaction process has been illustrated in Scheme 3-1. The fluorescence microscopy images clearly demonstrate yellow fluorescence across the MP3 surface (Figure 5-8 (b)), indicating the dye has successfully attached to the carboxy-functionalized PDMS surface. However, no fluorescence was detected on the NP2 surface (Figure 5-8 (a)) after incubation with EDAC and Lucifer Yellow CH dye. In addition, analysis of the images using a line scan of intensity profile is shown in Figure 5-8 (c). For the purpose of comparing fluorescence intensity on NP3 and MP3 surfaces, the fluorescence intensity values on the different glass slides were normalized. As a result, the average fluorescence intensity for the NP3 surface was 23 ± 0.3 while for the MP3 this value was 51 ± 3.7. An increase in intensity of 2.2 times after Lucifer yellow CH dye labeling was thus observed, indicating successful PDMS surface modification and Lucifer yellow CH dye attachment. The higher intensity fluorescence observed at the edge of MP3 may result from the physical adsorption of dye onto the rough cross section surface.

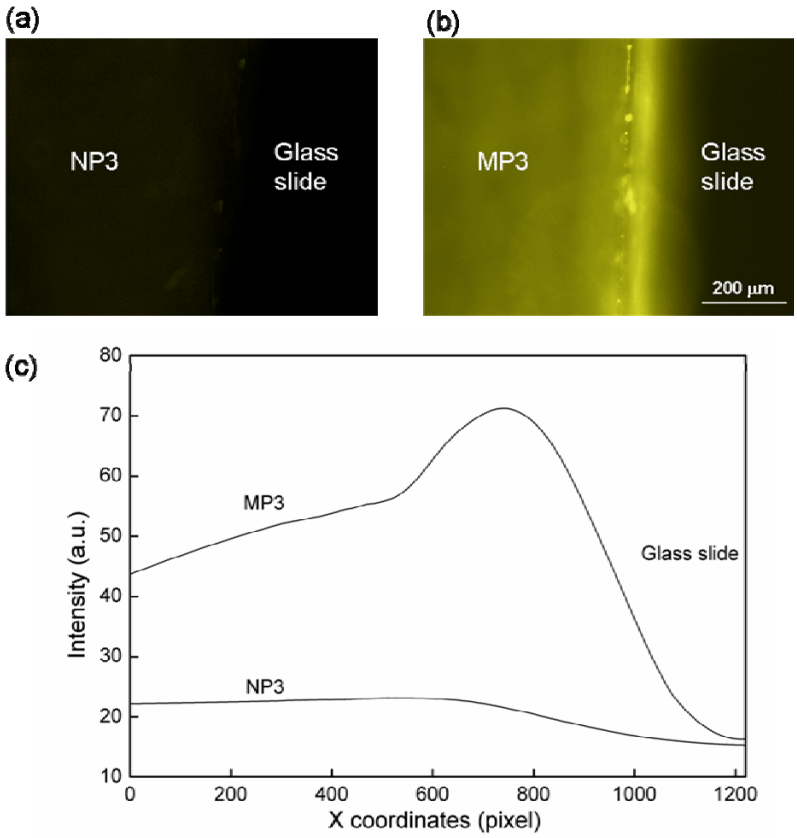

Figure 5-8. Fluorescence images of (a) NP3 and (b) MP3 with Lucifer Yellow CH dye labeling, and (c) the line intensity profile of images (a) NP3 and (b) MP3 (from left to right). The samples were placed on a glass slide for microscopy imaging.

5.3.2 Application of DNA hybridization

In the process of DNA hybridization, amino-terminated DNA (Oligo1) was reacted with the carboxyl groups on the MP3 surface using carbodiimide chemistry. Subsequent to covalent attachment of Oligo1, a FAM-labeled complementary DNA single strand (Oligo2) was hybridized. Figure 5-9 (a) shows a Soxhlet-extracted NP3 surface after DNA hydridization. Clearly, there is no obvious green fluorescence, indicating no attachment of the FAM-labeled Oligo2 to the surface. This is expected as Soxhlet-extracted NP3 does not have any carboxyl groups on its surface for the initial tethering of Oligo1. Figure 5-9 (b) shows the MP3 surface after attachment of the Oligo1 and subsequent hybridization with Oligo2. The whole surface was covered with bright green fluorescence, which is indicative of successful surface modification and DNA hybridization. Analysis of the images using a line scan of the fluorescence intensity profile is also shown in Figure 5-9 (c). For the purpose of comparing fluorescence intensity on the NP3 and MP3 surfaces, the fluorescence intensity values on the different glass slides were normalized. As a result, the average fluorescence intensity for the MP3 surface (50 ± 3.4) was around 2.4 times more than the value for the NP3 surface (21 ± 2.4), indicating successful PDMS surface modification and DNA hybridization on the PAAc modified PDMS surface. As shown in Table 5-2, the MP3 surface that had been reacted with EDAC followed by Oligo2, which lacked the amino-terminus, did not show fluorescence confirming that the covalent immobilization of Oligo1 was required for sequence-specific hybridization. In addition, FAM-labeled non-complementary single strand DNA (Oligo3) was incubated with the Oligo1 modified surface. As expected, no green fluorescence was observed.

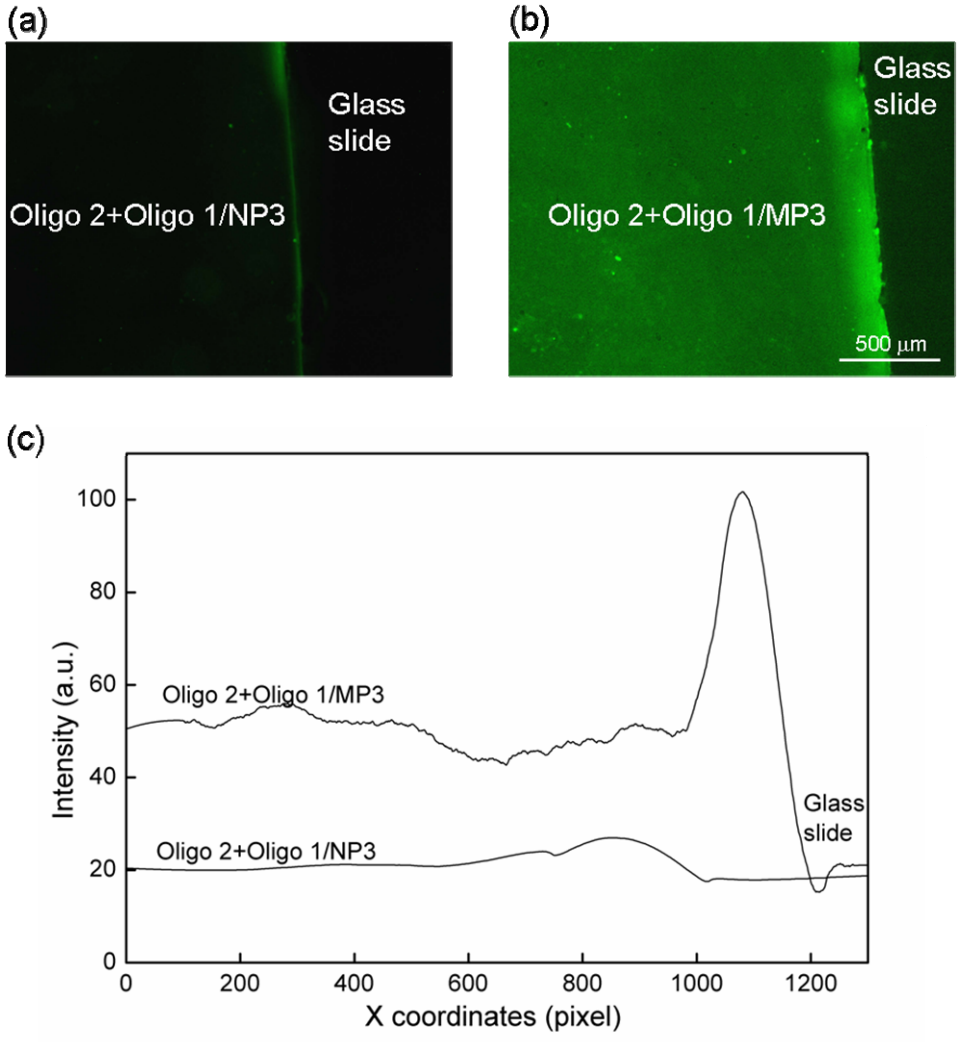

Figure 5-9. Fluorescence images of (a) Oligo 1/Soxhlet-extracted NP3 and (b) Oligo 1/MP3 after DNA hybridization with Oligo 2. (c) shows the line intensity profile of Oligo 1/Soxhlet-extracted NP3 and Oligo 1/MP3 after DNA hybridization with Oligo 2 (from left to right). The samples were placed on a glass slide for microscopy imaging.

Table 5-2. Fluorescent microscopy results of DNA hybridization on two different surfaces using different Oligo combinations.

Surfaces (Oligo)	Fluorescence observed
Soxhlet-extracted NP3 (Oligo1 and Oligo2)	no
MP3 (Oligo1 and Oligo2)	yes
MP3 (Oligo2)	no
MP3 (Oligo1 and Oligo3)	no

The technique used here for DNA hybridization is the same as described in chapter 4. Amino-terminated oligonucleotides were attached onto the COOH-functionalized PDMS

surface *via* amide linkages, and then FAM-labeled complementary oligonucleotides were hybridized with the amino-terminated oligonucleotides. Fluorescence measurement of the FAM-labeled complementary oligonucleotides was then carried out using a fluorescence microscope. Compared with other techniques [8, 174] using DNA hybridization on PDMS surfaces, there are some limitations in this current work because in order to analyze real samples the target DNA must be labeled before analysis.

5.4 Conclusion

In this chapter, we report on a simple 2-step plasma modification of PDMS in which the PDMS was first Soxhlet-extracted with hexane then exposed to an Ar then an AAc plasma. FTIR-ATR spectra show the successful functionalization of the surface with carboxyl groups (1715 cm^{-1}) which were stable in MilliQ water, PBS and HEPES buffer for up to 17 h. Furthermore, XPS data showed two peaks due to oxidized carbon after plasma treatment, one peak clearly from COOH functionalities. The presence of carboxyl groups in the FTIR-ATR and XPS spectra of the modified PDMS confirmed the decreased in the WCA values observed. The stability of the MP3 after storage in air was also confirmed by the WCA data. In addition, fluorescence microscopy showed the successful Lucifer yellow CH dye attachment, which further demonstrated the reactivity of the introduced carboxyl groups on the MP3 surface. Finally, DNA hybridization of a FAM-labeled oligonucleotide was successfully performed on the MP3 surface. This new PDMS surface modification method has future applications in the development of novel DNA microarrays and PDMS microfluidic devices.

CHAPTER 6 APTAMER SENSOR FOR COCAINE USING MINOR GROOVE BINDER BASED ENERGY TRANSFER (MBET)

The content of this chapter is based on reference [169].

6.1 Introduction

Cocaine, or benzoylmethylecgonine, is a common illicit drug encountered by law enforcement, border protection and forensic science authorities [179, 180]. Current field tests for cocaine are either presumptive and require confirmatory analysis in the laboratory or necessitate high levels of training for effective operation [181]. Chemical sensors for cocaine which are simple to operate and still offer high sensitivity and specificity are therefore required. A range of chemical sensors has been developed in recent years involving fluorescence [182-190], colorimetric [191-199], chemiluminescence [200-202], electrochemical [195, 203-215], surface-enhanced Raman scattering [216-218], surface plasmon resonance [209, 219] and surface acoustic wave [220, 221] based transducers. Fluorescence- and colorimetric-based sensors are particularly desirable due to the simple detection procedures involved [194].

Stojanovic et al. [182] were the first to report the use of aptamers for the detection of cocaine in fluorescence-based sensors. Aptamers are nucleic acid based receptors that are obtained through a combinatorial selection process known as systematic evolution of ligands by exponential enrichment (SELEX) [222, 223]. These molecules have significant advantages over antibodies, such as convenient synthesis and chemical modification, high affinity even to small molecular targets and resistance to biodegradation [192, 200, 204, 224]. Among fluorescence-based aptamer sensors, fluorescence resonance energy transfer

(FRET)-based aptamer sensors are particularly attractive for cocaine detection because of the inherent sensitivity of FRET to detect conformation-associated change in donor/acceptor dye separation [186]. In the presence of cocaine, FRET between fluorescein and dabcyl dye both attached to the aptamer was stimulated by the formation of a ligand-induced binding pocket based on terminal stem-closure [182, 183]. Quantum dot (QD)-stimulated FRET with organic dyes on DNA aptamers was recently reported for cocaine detection [185, 225]. Furthermore, Cy5 labeled cocaine aptamers were hybridized with complementary DNA attached to gold nanoparticles. In the presence of cocaine, the aptamer strands were released resulting in deactivation of FRET between the gold nanoparticles and Cy5, and recovery of Cy5 fluorescence [186].

It is generally acknowledged that microfluidic devices are particularly useful for the implementation of lab-on-a-chip sensors due to reduced sample and reagent consumption, shorter analysis times and increased levels of automation [11]. Hilton *et al.* [189] first used a PDMS/glass based microchamber packed with aptamer-functionalized microbeads as a FRET-based sensor for cocaine detection.

Here, we demonstrate an optical cocaine sensor where a cocaine-sensitive aptamer labeled with FITC changes conformation from a partial single-stranded oligonucleotide with a short hairpin to a double-stranded T junction, thereby trapping cocaine. The double-strand specific DNA minor groove binder Hoechst 33342 binds to the double-stranded stem allowing the dye, upon excitation at 360 nm, to instigate energy transfer to FITC. The result of this effect, which we term minor groove binder based energy transfer (MBET), is green fluorescence at 520 nm. To our knowledge, this is the first time using a minor groove binder and a fluorescent dye as a donor/acceptor pair on an aptamer sensor.

We also demonstrate the MBET cocaine sensor on a PDMS surface for potential integration into microfluidic devices. We fabricate a carboxy-functionalized PDMS surface by simply curing a mixture of 2 wt % UDA and PDMS prepolymer on a gold-coated glass slide, which had been pretreated with a hydrophilic SAM of MPA, as described in Chapter 2 (Scheme 2-2). FITC labeled 5'-amino-terminal single-stranded DNA aptamers were then covalently attached to the UDA modified PDMS surface *via* amide linkages (Scheme 6-1).

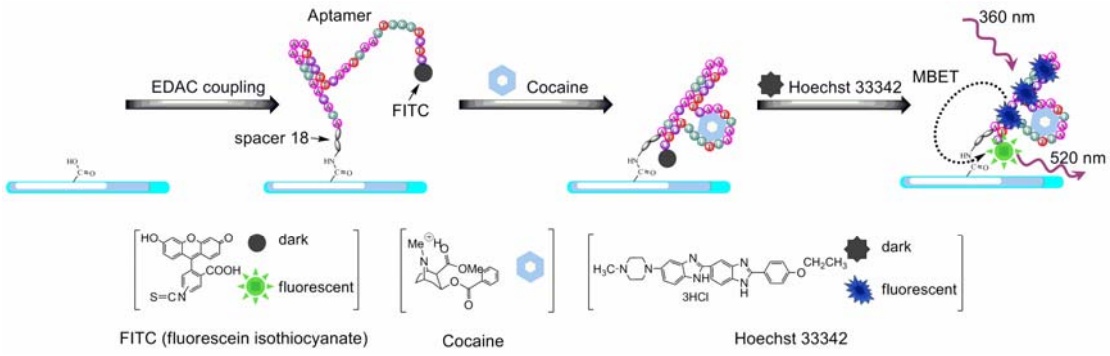

Scheme 6-1. Schematic illustration of MBET aptamer sensors for cocaine detection on a MP2 surface.

6.2 Experimental section

6.2.1 Material and Chemical

Cocaine was obtained from Forensic Science, Adelaide, South Australia, Australia. All other chemicals were purchased from Sigma-Aldrich (USA). The aptamer sequence used here was based on a literature sequence [183, 185] and was adapted to suit our application. 5′-amino-(spacer18)$_2$AGACAAGGAAAATCCTTCAATGAAGTGGGTCTC-FITC-3′ was purchased from GeneWorks Pty Ltd (Australia). The buffers were prepared as detailed in Chapter 2.

6.2.2 PDMS Sample Preparation

The MP2 samples were prepared as described in Chapter 2. Briefly, the PDMS (10:1 weight ratio of base and curing agents) and 2 wt % UDA were thoroughly mixed and degassed to remove air bubbles and then poured onto a hydrophilic gold slide, which was pre-coated with a MPA monolayer. The sample was left on the bench under ambient condition for 24 h and then cured at 80 ºC for 2 h. Following this, the sample was immersed in MilliQ water for 4 h so that the MP2 could be easily peeled off from the gold substrate. The MP2 sample was finally rinsed sequentially with MilliQ water and ethanol and then dried under a stream of nitrogen (Scheme 2-2). NP2 smaples without UDA was used as a control.

6.2.3 MBET aptamer sensor for cocaine detection in solution

To optimize the temperature protocol for cocaine detection using the FITC-labeled cocaine aptamer, three parallel experiments were performed. (a) A solution containing aptamer (100 nM) and cocaine (100 nM) in Tris buffer (pH 8.4) was maintained at room temperature for 20 min; (b) A solution containing aptamer (100 nM) and cocaine (100 nM) in Tris buffer (pH 8.4) was heated at 80 ºC for 10 min, and then cooled to 4 ˚C in the fridge for 10 min; (c) A solution containing aptamer (100 nM) and cocaine (100 nM) in Tris buffer (pH 8.4) was heated at 80 ºC for 10 min, and then cooled to room temperature for 10 min. Hoechst 33342 (100 nM) was then added into the above three aptamer/cocaine solutions and reacted for 30 min. Fluorescence emission spectra from aptamer/cocaine/Hoechst solutions were collected at room temperature on a Cary-Eclipse fluorescence spectrometer from Varian (Australia). The fluorescence spectrometer was set to an excitation wavelength of 360 nm and emission was monitored at 520 nm. In addition, fluorescence of solutions of aptamer (100 nM), Hoechst 33342, cocaine, aptamer/cocaine, aptamer/Hoechst, cocaine/Hoechst solutions was measured.

6.2.4 MBET aptamer sensor for cocaine detection on PDMS surface

The protocol for detecting cocaine using the MP2 sample can be divided into three steps. Step 1: the preparation of an aptamer-modified PDMS surface. MP2 surfaces were first exposed to EDAC (0.4 M) in PBS buffer (pH 4.8) for 30 min (followed by washing with PBS buffer (pH 4.8)), and then aptamer (10 μM) in PBS buffer (pH 7.4) for 2 h (followed by washing with PBS buffer (pH 7.4)). Step 2: the bonding between the aptamer and cocaine. The aptamer-modified PDMS surfaces from step 1 were immersed into cocaine solutions with different concentrations (0.1 μM, 1 μM, 2 μM, 3 μM, 4 μM, 5 μM, 10 μM prepared in PBS buffer (pH 7.4)), then kept at 80 ºC for 10 min, and finally cooled at room temperature for 10 min (followed by washing with PBS buffer (pH 7.4)). Step 3: the activation and readout of the MBET system. Cocaine/aptamer-modified PDMS surfaces were exposed to Hoechst 33342 (20 μM) in Tris buffer (pH 8.4) for 30 min, and then rinsed with the Tris buffer (pH 8.4) and dried under a stream of nitrogen gas. The dried PDMS surfaces were then imaged under an IX81 inverted fluorescence microscope from Olympus (Japan) using a custom filter (excitation at 360-370 nm and emission at 510-550 nm). All

images were taken with a 1 s exposure and fluorescence levels were quantified using Image J software.

6.3 Results and discussion

6.3.1 MBET aptamer sensor for cocaine detection in solution

En route to developing an aptamer sensor for cocaine detection on the PDMS surface, we first tested the performance of the MBET based detection in solution. In our system (as shown in Scheme 2), an partial single-stranded aptamer with a short hairpin labeled with FITC forms a characteristic T-structure in the presence of cocaine, resulting in the formation of an aptamer/cocaine complex [185]. Hoechst 33342 selectively binds to the double-stranded stem, bringing it within the Förster radius of the FITC dye on the aptamer. Upon excitation at 360 nm, MBET between the Hoechst 33342 donor and the FITC acceptor results in fluorescence emission at 520 nm.

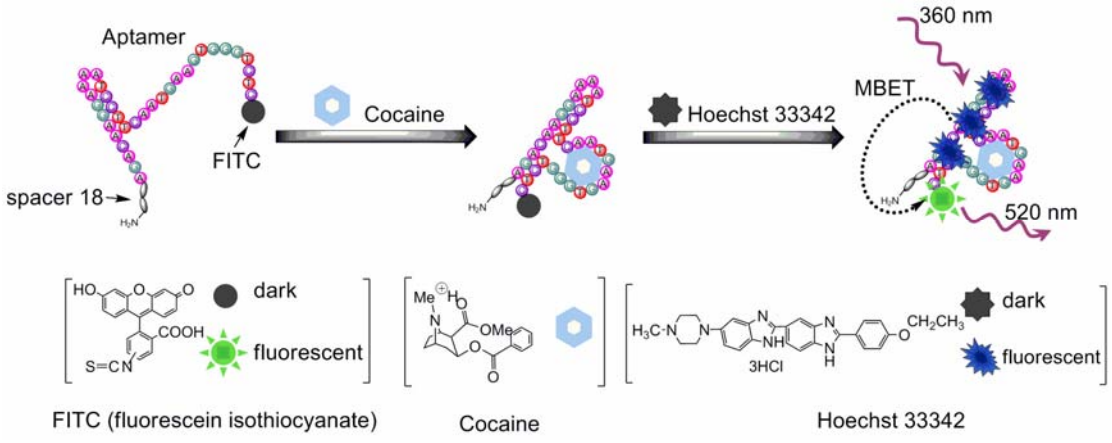

Scheme 6-2. Schematic illustration of fluorescence resonance energy transfer MBET aptamer sensors for cocaine detection in solution.

Three parallel experiments were performed to optimize the incubation conditions for aptamer-based cocaine detection: (a) a solution containing aptamer and cocaine was maintained at room temperature for 20 min; (b) a solution containing aptamer and cocaine was heated at 80 ºC for 10 min and then cooled to 4 ˚C in the fridge for 10 min; (c) a solution containing aptamer and cocaine was heated to 80 ºC for 10 min, and then

maintained at room temperature for a further 10 min. Hoechst 33342 dye was then added to the three solutions. Fluorescence emission spectra over the range of 400 nm to 600 nm, upon excitation at 360 nm, were collected from the three aptamer/cocaine/Hoechst 33342 solutions, as shown in Figure 6-1. A fluorescein emission peak at 520 nm was observed in all cases. However, it is evident that the fluorescence intensity is affected by different treatment conditions. The (b and c) aptamer/cocaine/Hoechst 33342 solutions, having undergone heating and cooling steps, showed a higher intensity fluorescein emission than (a) without the heating and cooling. For the (c) aptamer/cocaine/Hoechst 33342 solutions, after slow cooling to room temperature, showed a higher intensity than (b) aptamer/cocaine/Hoechst 33342 solutions cooled in the fridge. These results show that the heating and slow cooling assisted in aptamer re-conformation and binding to cocaine to form a T-junction structure.

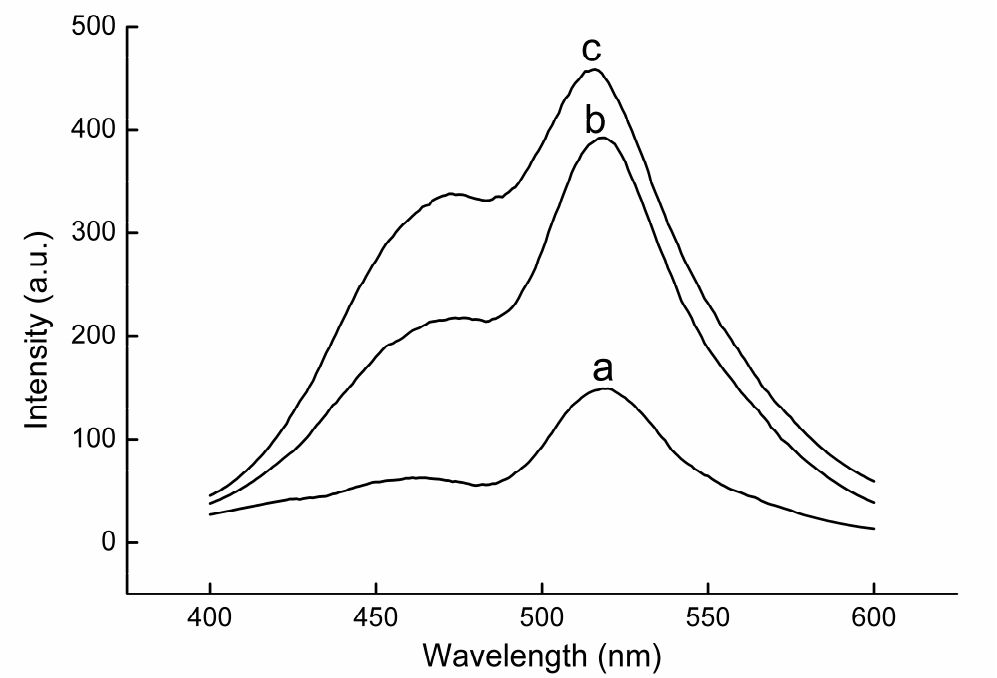

Figure 6-1. Fluorescence emission spectra upon excitation at 360 nm recorded for solutions of aptamer/cocaine/Hoechst 33342 after different incubation protocols: (a) A solution containing aptamer (100 nM) and cocaine (100 nM) in Tris buffer (pH 8.4) was then maintained at room temperature for 20 min; (b) A solution containing aptamer (100 nM) and cocaine (100 nM) in Tris buffer (pH 8.4) was heated at 80 ºC for 10 min, and then cooled in a fridge to 4 ˚C for 10 min; (c) A solution containing aptamer (100 nM) and cocaine (100 nM) in Tris buffer (pH 8.4) was heated at 80 ºC for 10 min, and then cooled to room temperature for 10 min. Hoechst 33342 (100 nM) was then added into the above three aptamer/cocaine solutions and incubated for 30 min.

Fluorescence spectra of solutions of aptamer, cocaine, Hoechst 33342, aptamer/cocaine, aptamer/Hoechst 33342 and cocaine/Hoechst 33342 only after heating and slow cooling steps at 360 nm excitation were also acquired (Figure 6-2). No fluorescein emission was observed except for the solution of aptamer/Hoechst 33342, where weak MBET fluorescence indicates the short hairpin structure of the aptamer in the absence of cocaine. Nevertheless, the fluorescence level was more than four times lower than in the presence of cocaine. Having proven the principle of the MBET-based detection in solution, the next step was to implement the sensor on the PDMS surface.

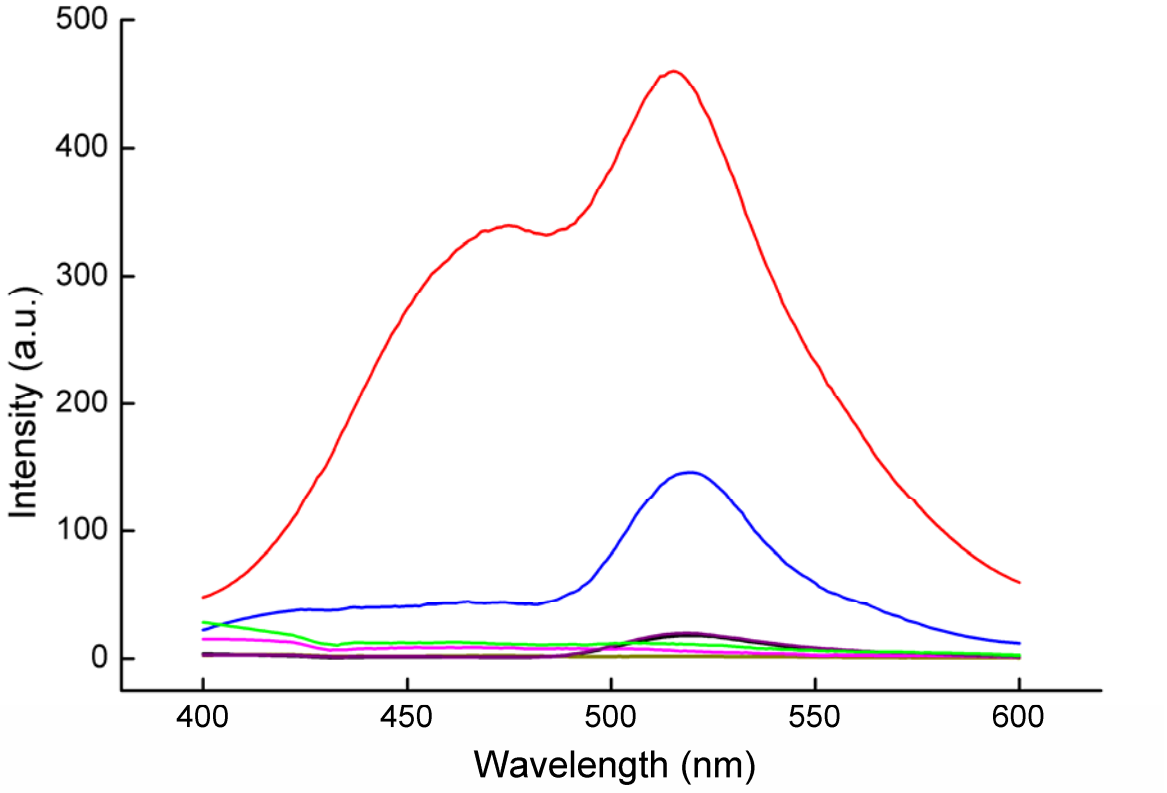

Figure 6-2. Fluorescence emission spectra recorded from different solutions (black: aptamer, yellow: cocaine, pink: Hoechst, purple: aptamer/cocaine, blue: aptamer/Hoechst 33342, green: cocaine/Hoechst 33342, red: aptamer/cocaine/Hoechst 33342) using the same temperature protocol as in Figure 1 (c) (heating at 80 ºC for 10 min, then cooling to room temperature over 10 min).

6.3.2 MBET aptamer sensor for cocaine detection on an aptamer-modified PDMS surface

A PDMS surface functionalized with carboxylic acid groups was first prepared to allow

covalent attachment of aptamers. The templating procedure has been described briefly in Chapter 2.

The MP2 surface was reacted with 5'-amino-terminal cocaine aptamer using carbodiimide coupling. The thus fabricated aptamer sensor was then used for cocaine detection under the optimized treatment conditions (heating at 80 ºC for 10 min, and then cooling to room temperature for another 10 min), followed by incubation with Hoechst 33342 dye (Scheme 6-1). Using a custom filter in a fluorescence microscope, the aptamer-modified PDMS surface was excited at 360 - 370 nm and fluorescence emission from 510 nm to 550 nm was collected. As shown in Figure 6-3, cocaine concentrations ranging from 0.1 μM to 10 μM were readily detected using the aptamer sensor. Fluorescence intensity increased rapidly with increasing cocaine concentration from 0.1μM to 5 μM, and then remained almost constant when the cocaine concentrations increased further from 5 μM to 10 μM. For comparison, the same process was repeated for aptamers incubated on a NP2 surface, reacted with aptamer under identical reaction conditions as for the MP2, exposed to cocaine solution and then Hoechst 33342. The results showed negligible fluorescence emission over the entire concentration range from 0.1 μM to 10 μM. The fluorescence intensity (I) on the MP2 surfaces correlated linearly with the cocaine concentration (C) over the range of 0.1 μM to 5 μM (Figure 6-3 insert). The linear regression equation was: $I = 4.4665C + 3.8598$, and the correlation coefficient was 0.9854. The detection limit for cocaine was 0.34 μM (S/N = 3), which is better than many existing aptamer sensors for cocaine detection [184, 194, 203, 216, 225]. This high sensitivity of cocaine detection is most likely due to the inherent sensitivity of FRET used to detect conformation-associated changes in this particular aptamer.

Another advantage of this MBET aptamer sensor for cocaine detection on the surface is the reduced sensor cost due to the use of PDMS, instead of gold nanoparticles or gold electrodes [195, 200, 203, 205, 206, 212, 213, 215]. The detection time used for this MBET aptamer sensor is ~ 50 min, including incubating the sensor with cocaine at 80 ºC for 10 min, then cooling to room temperature for another 10 min, and followed by incubation of the whole sensor with Hoechst 33342 dye for 30 min. This time is a little longer than the reported colorimetric based cocaine sensor (40 min)[210].

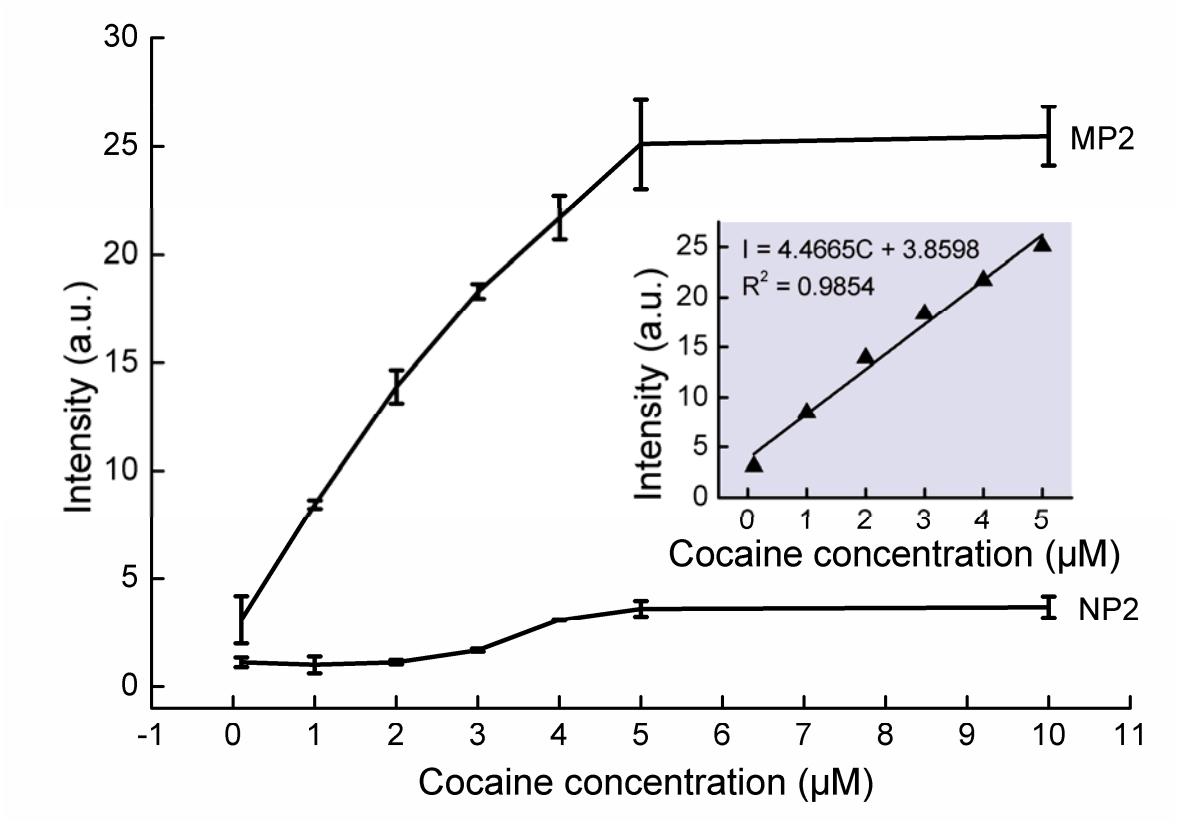

Figure 6-3. MBET response using a 510-550 nm bandpass filter for the aptamer-based sensor to cocaine at varying concentrations on NP2 and MP2 surfaces after functionalization with aptamer and incubation with cocaine and Hoechst 33342. The insert shows a plot of fluorescence intensity for the aptamer-based sensor against the cocaine concentrations.

6.4 Conclusion

In conclusion, a MBET aptamer sensor for cocaine detection was successfully implemented. The exposure of the aptamer sensor to solutions containing cocaine resulted in a conspicuous change of aptamer conformation from a partial single-stranded DNA with a short hairpin to double-stranded T-junction, facilitating MBET between the FITC-labeled 3′-end of the aptamer and Hoechst 33342 bound to the hairpin's stem. The sensor had a detection limit of 0.34 μM. This allowed us to implement an aptamer sensor for cocaine on a PDMS surface, which can potentially be integrated into a microfluidic device.

CHAPTER 7 FABRICATION OF PDMS-BASED MICROFLUIDIC DEVICES

7.1 Introduction

PDMS-based microfluidic devices combine the advantages of polymeric materials and micro-scale devices, as described in Chapter 1. The typical fabrication process of PDMS-based microfluidic devices follows the following steps [226]: The first step is the fabrication of a master. This involves creating a design using a computer-aided design (CAD) program, printing a photomask and producing a master using standard photolithography techniques. The second step is replication of a microstructured PDMS sample from a master using soft-lithography. Conveniently this technique does not require routine access to a clean room which increases manufacturing time and reduces cost. The last step is sealing the PDMS replica to a flat surface to form microchannel. For native PDMS-based microfluidic devices, sealing can be accomplished by using van der Waals forces upon contact for reversible sealing or O_2 plasma treatment for irreversible sealing [227, 228]. Complications arise when this sealing is required to be performed post surface hydrophilization. It has been previously reported [40, 41] that modified PDMS-based microchannels can be sealed by coating the two PDMS slides with two complementary polymers, such as poly(4- aminomethyl-*p*-xylylene-*co*-*p*-xylylene) and poly(4-formyl-*p*-xylylene-*co*-xylylene) or PGMA and PAS *via* the CVD technique. However, this sealing method is only suitable for two PDMS slides with complementary moieties on either side.

Here, we demonstrate the possibility of using two existing simple sealing methods for modified PDMS-based microfluidic devices, involving thermal bonding for native PDMS and MP2-based microfluidic devices, and plasma assisted bonding for MP3-based microfluidic devices. The reactive carboxyl groups were verified to be present in the MP2 and MP3-based microchannels by the increase of μ_{eo} and yellow fluorescence after incubation with EDAC and Lucifer Yellow CH dye compared to the native PDMS

microchannel.

7.2 Experimental section

The experimental details have been described in section 2.6, Chapter 2.

7.3 Results and discussion

7.3.1 Fabrication of PDMS-based microfluidic devices

Native PDMS microchannels were produced using standard soft-lithography techniques. After that, thermal bonding was used for microfluidic devices made out of native PDMS. Here, 80 ºC for 20 min was used to prepare the two partly cured PDMS slides before bringing them into contact to allow for bonding. The bonding of the native PDMS-based microfluidic device was formed *via* hydrosilylation reaction between uncured PDMS base and curing agent on the two PDMS parts.

For preparing MP2 slides, a long curing time (1 d at room temperature and then 2 h at 80 ºC) was used, but, the adding of UDA consumed a portion of the PDMS curing agent *via* the hydrosilylation reaction (Scheme 7-1), resulting in an excess of unreacted PDMS base agent left in the PDMS matrix. When thermal bonding was applied between one incompletely cured native PDMS slide and one MP2 slide, bonding *via* hydrosilylation between the uncured PDMS curing agent from the native PDMS slide and the unconsumed PDMS base agent from the MP2 slide occurred. It is possible that the same reaction might also occur between the uncured PDMS base agent from the native PDMS slide and unconsumed UDA from the MP2 slide.

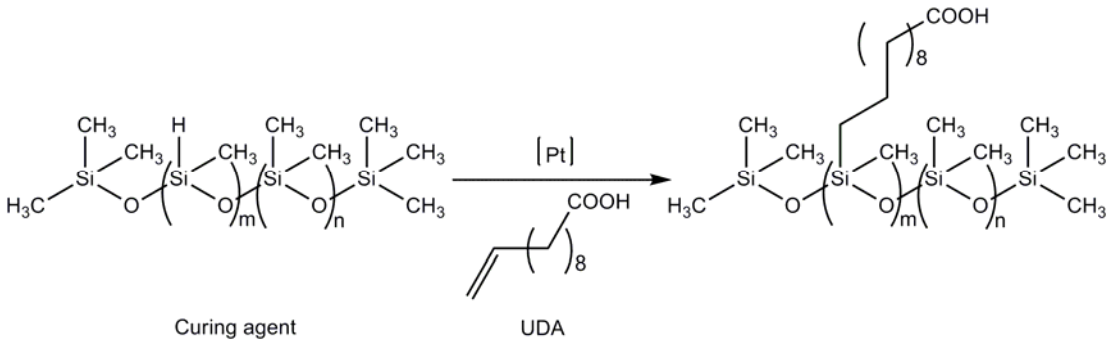

Scheme 7-1. The hydrosilylation reaction between PDMS curing agent and UDA.

Plasma assisted bonding is the most common technique for irreversible sealing of native PDMS-based microfluidic devices [79, 229]. The mechanism of the standard O_2 plasma assisted bonding is thought to occur due to the repeated units of –O-Si$(CH_3)_2$- in the PDMS being converted into surface silanol groups (-OH) at the expense of methyl groups (-CH_3) on exposure to plasma [229]. These silanol groups then can condense with appropriate groups (-OH, -COOH or R-CO-R) on another surface to yield Si-O-Si bonds after loss of a water molecule, when two PDMS slides are brought into conformal contact [226]. To verify that the O_2 plasma assisted bonding is also feasible for fabrication of MP3-based microfluidic devices, the peaks of carboxyl groups and hydroxyl groups on MP3 surface were monitored by FTIR-ATR spectroscopy after two 10 sec O_2 plasma (0.2 mbar) treatments (as described in Chapter 2). As shown in Figure 7-1 (b), the carboxyl peak at 1715 cm^{-1} was not only retained on the MP3 surface after O_2 plasma, but also had higher intensity than the original peak for MP3 (Figure 7-1 (a)), indicating that the O_2 plasma had not degraded the PAAc layer on the surface. This effect could also be achieved by employing an Ar plasma [30]. In addition, a characteristic broad peak, corresponding to hydroxyl groups [230, 231], was observed in the spectrum of MP3 after O_2 plasma at around 3000-3700 cm^{-1} wavenumbers, which was absent on MP3 surface (Figure 7-1 (a)). The presence of carboxyl and hydroxyl groups on MP3 surface after O_2 plasma treatment makes it, in principle, feasible to seal MP3-based microchannels using O_2 plasma assisted bonding.

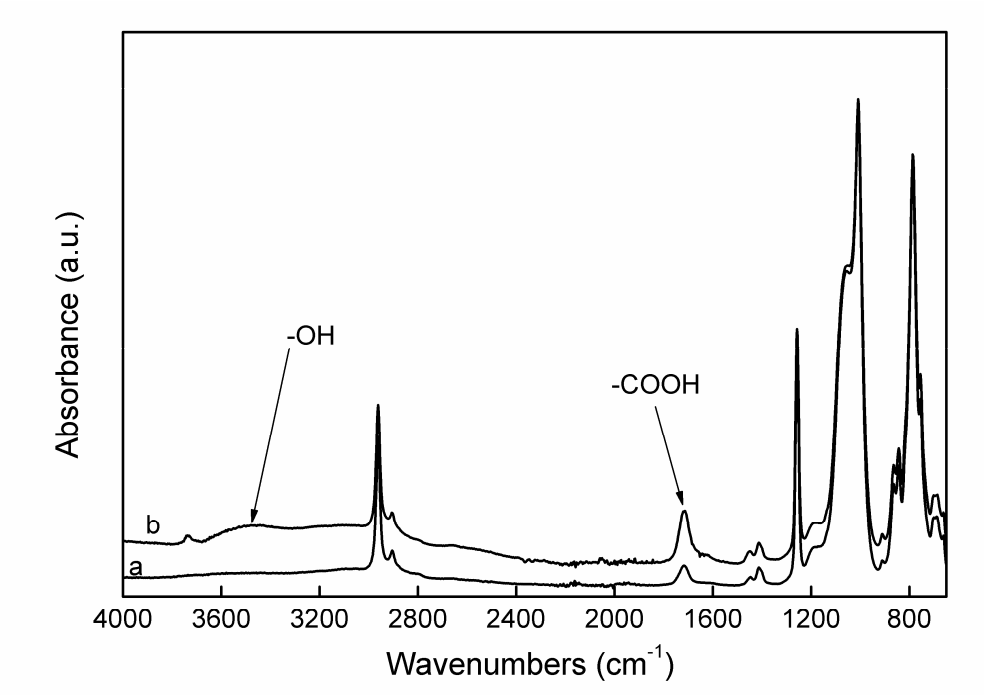

Figure 7-1. FTIR-ATR spectra of (a) MP3 and (b) MP3 after 10 sec O_2 plasma (0.2 mbar).

7.3.2 EOF measurements

Prior to measurement of μ_{eo}, the approach developed by Ren *et al.* [32] was adopted to identify significant Joule heating by determining whether the relationship between the current and voltage was linear. Here, the current at different voltages (100 to 1000 V) was measured in native PDMS-based microchannel. For 10 mM PBS buffer (pH 8.2), the current (I) was correlated linearly with the voltage (V) for voltages less than 300 V (Figure 7-2). Therefore, a 100 V voltage was used in all EOF measurement.

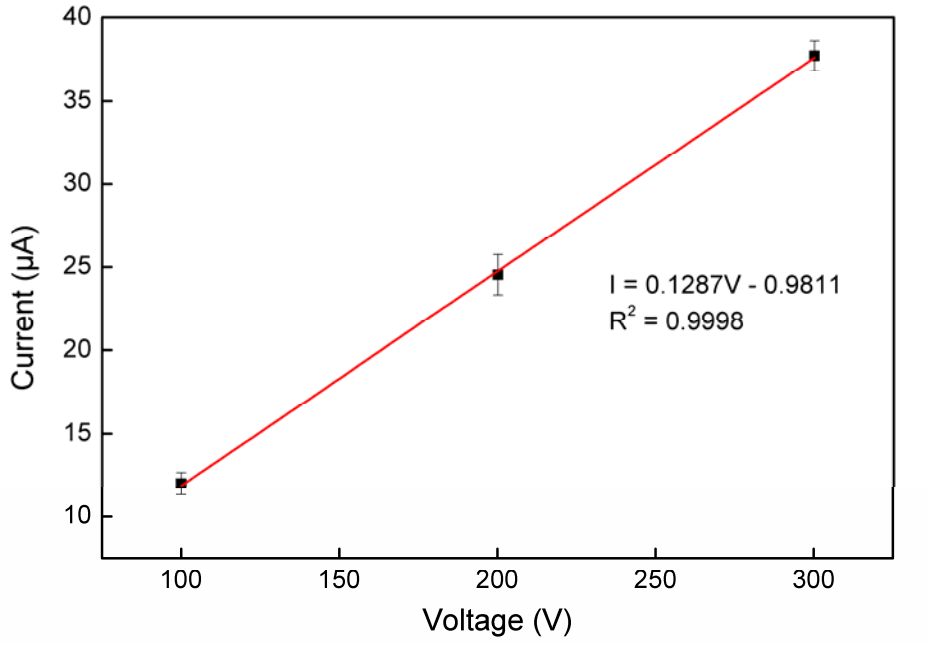

Figure 7-2. Linear relationship between the measured current value and the applied voltage in native PDMS-based microchannel (3 cm length microchannel, measurement performed in 10 mM pH 8.2 PBS buffer).

A typical current monitoring method was used to measure the EOF values in microchannels (3 cm), as described in Chapter 2, where a 20 mM PBS buffer (pH 8.2) was replaced by a 10 mM PBS buffer (pH 8.2) due to the generation of EOF in the microchannel when a voltage of 100 V was applied. As shown in Figure 7-3, the measured μ_{eo} in a native PDMS-based microchannel was approximately 2.95×10^{-4} cm^2/V s. Although the native PDMS was not expected to have an EOF because it is composed of repeating $–OSi(CH_3)_2O-$ groups, similar EOF values was found by many research groups [25, 29, 32, 47]. The origin of the surface charge on native PDMS surface is not known, however, possible explanations include impurities in the PDMS such as the crosslinking agent or silica fillers [32] or physisorbed cations within the Stern layer [165]. After surface modification, the μ_{eo} in MP2 and MP3-based microchannels increased to 3.50×10^{-4} cm^2/Vs and 4.70×10^{-4} cm^2/Vs, respectively. This is in agreement with the literature where higher EOF's were obtained on PDMS surfaces carrying negative charges [32, 33, 63]. Here, the higher EOF values observed in MP2 and MP3-based microchannels were due to the deprotonated carboxylate functionalities present on the surface of the PDMS at pH 8.2. This higher EOF in modified microchannels is useful in the application of analyte separations, where increased EOF translates into decreased migration times of the analytes and consequently increased speed of the separations [64]. However, it is noticeable that the

current along the microchannels gradually increased with time, and this same problem has previously been observed in 2-acrylamido-2-methyl-1-propanesulfonic acid (AMPS)-modified microchannels [135]. This phenomenon may be caused by the electrolysis and evaporation of the buffer for long running times [85]. The higher EOF value observed in MP3-based microchannel might be a result of the higher density of negatively charged carboxyl groups within the microchannel, compared to a MP2-based microchannel.

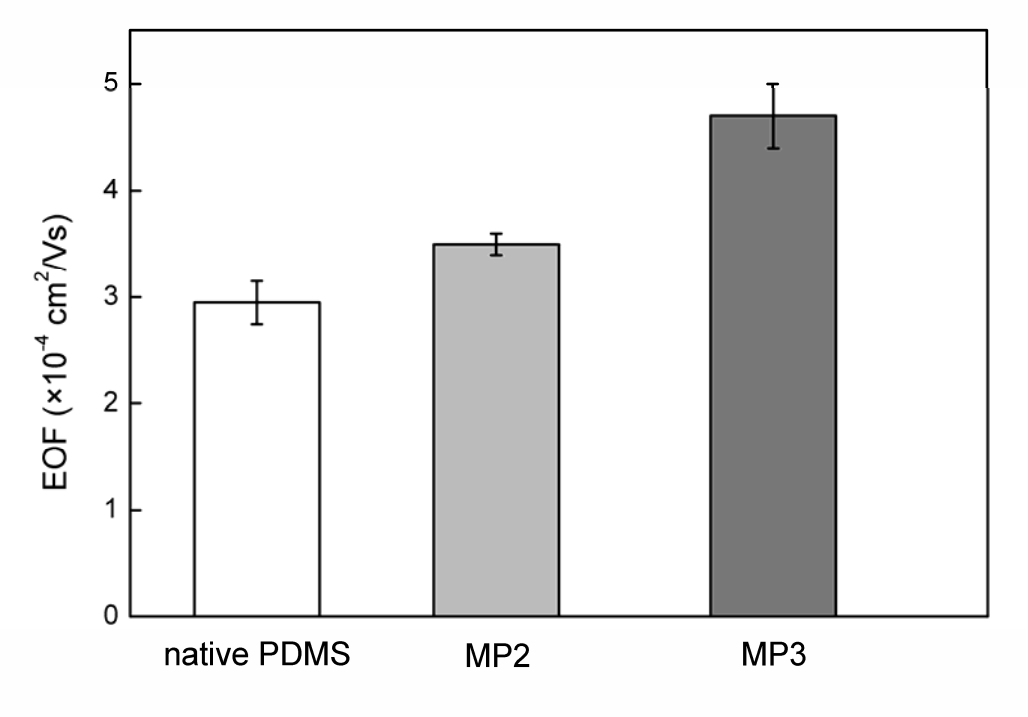

Figure 7-3. EOF values of native PDMS, MP2 and MP3-based microfluidic device. (n=3).

7.3.3 Fluorescence labeling inside microchannels

In principle, only carboxyl groups that come in direct contact with another PDMS slide are consumed during the bonding process, and the carboxyl groups that are located within the microchannels remain available for further applications. To test whether carboxyl groups within microchannels still maintain their typical reactivity after the curing process, Lucifer Yellow CH dye was coupled to the carboxyl groups *via* carbodiimide coupling. The reaction process is illustrated in Scheme 3-1. Figure 7-4 (b and c) shows yellow fluorescence across the MP2 and MP3-based microchannels, indicating that the dye has successfully attached onto the carboxyl functionalized PDMS microchannels. However, no

fluorescence was detected on the native PDMS-based control microchannel (Figure 7-4 (a)) after incubation with EDAC and subsequently Lucifer Yellow CH dye. In addition, analysis of the images using a line scan of the intensity profile is shown in Figure 7-4 (d). For the purpose of comparing fluorescence intensity inside the microchannels, the fluorescence intensity values on the bulk PDMS were normalized. As a result, the average fluorescence intensity in the native PDMS-based microchannel was 6 ± 0.7, while for the MP2 and MP3-based microchannels this value was 40 ± 5.1 and 36 ± 8.3, respectively. The increase in intensity of 6.7 and 6 times after Lucifer yellow CH dye labeling was thus observed in the MP2 and MP3-based microchannels, respectively. This indicates the presence of active carboxyl groups in the microchannel after bonding and successful Lucifer yellow CH dye labeling in MP2 and MP3-based microchannels. However, a higher intensity fluorescence was observed on the two sides of the MP3-based microchannel compared to uniform fluorescence in MP2-based microchannel. This was attributed to carboxyl groups being present on all four walls of the MP3-based microchannel, but only on one wall of the MP2-based microchannel.

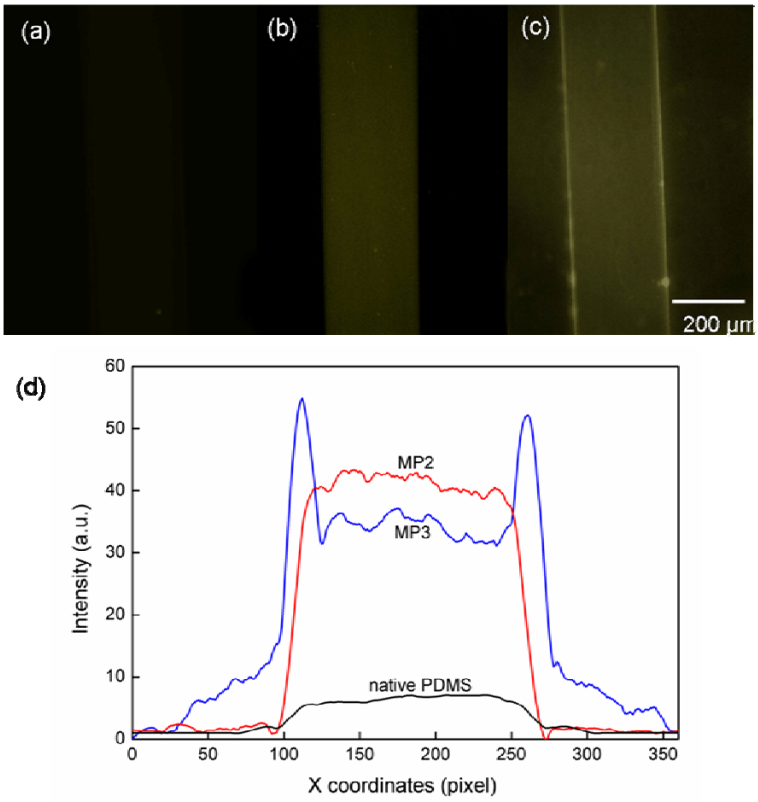

Figure 7-4. Fluorescence images of (a) native PDMS, (b) MP2 and (c) MP3-based microchannels, and (d) the line intensity profile of images (a) native PDMS, (b) MP2 and (c) MP3-based microchannels (from left to right).

7.4 Conclusion

In this chapter, the fabrication of native PDMS, MP2 and MP3-based microfluidic devices was described. The sealing of these devices was accomplished by thermal or plasma assisted bonding techniques. The presence of carboxyl groups in MP2 and MP3-based microchannels after bonding was verified by the increase in the μ_{eo} value, compared to native PDMS. In addition, these carboxyl groups were still available for further surface reactions as shown by the successful attachment of Lucifer Yellow CH dye in MP2 and MP3-based microchannels.

CHAPTER 8 OVERALL CONCLUSIONS AND FUTURE WORK

8.1 Overall conclusions

PDMS is a versatile material for microfluidic devices due to its excellent attributes, including elastomeric properties, biocompatibility, gas permeability, optical transparency, ease of molding into (sub)micrometer features, ease of bonding to itself and glass, relatively high chemical inertia, and low manufacturing costs. In spite of these desirable properties, there is still a main drawback with the implementation of PDMS in microfluidic devices, which is related to its hydrophobic surface. Thus, in order to render PDMS more practical for microfluidic devices, it is necessary to improve PDMS's wettability through surface modification, as well as equip the surface with functional groups for specific applications, which has been the focus of this thesis.

Three different surface modification techniques were employed throughout this thesis to improve the PDMS surface wettability, including 1) thermal assisted hydrosilylation; 2) SAM assisted templating and 3) combination of Soxhlet-extraction and plasma treatment, which were detailed in Chapter 3, Chapter 4 and Chapter 5, respectively. Briefly, in Chapter 3, pre-cured native PDMS was modified by UDA using direct heating with a thin film of UDA at 80 ºC in an oven (referred to as MP1); in Chapter 4, the modified PDMS was achieved by curing a mixture of 2 wt % UDA in PDMS prepolymer on a MPA-coated gold slide (referred to as MP2); in Chapter 5, a 2-step plasma modification was applied on a PDMS surface in which the PDMS was first Soxhlet-extracted with hexane then exposed to an Ar then an AAc plasma (referred to as MP3).

WCA measurements showed that the WCA values decreased from 110º for native PDMS to 71º, 91º and 32º for MP1, MP2 and MP3, respectively. The results indicate that the wettability of the PDMS surfaces was improved after those modifications, particularly

for MP3. The change in chemical properties of the PDMS after modification was investigated using FTIR-ATR spectroscopy. A characteristic peak at 1715 cm^{-1}, corresponding to carboxyl groups was observed in all MP1, MP2 and MP3 spectra, with this peak being absent in the native PDMS spectra. Further, to test the stability of each functionalization this peak was monitored over time after MP1, MP2 and MP3 surfaceswere placed in either water or PBS buffer. Surface modification was also verified using XPS, streaming zeta-potential analysis and AFM. The reactivity of the carboxyl groups on the MP1, MP2 and MP3 surfaces was demonstrated by successfully attaching Lucifer Yellow CH dye *via* carbodiimide coupling, which was then visualized using fluorescence microscopy.

After preparing the carboxyl-functionalized MP2 and MP3 samples, 5´-amino-terminated oligonucleotides were covalently attached to the modified PDMS surface *via* amide linkages (Chapter 4 and 5). Results showed that the covalently tethered oligonucleotides could successfully capture fluorescein-labeled complementary oligonucleotides *via* hybridization, which was visualized using fluorescence microscopy.

In addition, in Chapter 6 the MP3 surface (prepared using SAM assisted templating) was used to implement an aptamer sensor for cocaine. FITC labeled 5'-amino-terminal single-stranded DNA aptamers were covalently immobilized onto the MP3 surface *via* amide linkages. The exposure of the aptamer-linked MP3 to solutions containing cocaine resulted in a conspicuous change of aptamer conformation from a partial single-stranded DNA with a short hairpin to double stranded T-junction, facilitating MBET between the FITC labeled 3´-end of the aptamer and Hoechst 33342 dye bound to the double-stranded stem. The MBET technique has been described here for the first time. This sensor was shown to exhibit a detection limit of 0.34 μM. The successful detection of cocaine on the aptamer-linked MP3 surface has potential for use in PDMS-based microfluidic devices. In addition, this aptamer sensor was also successfully implemented for cocaine detection in solution.

At the end of this thesis (Chapter 7), the fabrication of native and modified PDMS-based microfluidic devices was presented. Thermal and plasma-assisted bonding were successfully used to seal native PDMS, MP2-based and MP3-based microchannels. Moreover, the reactive carboxyl groups were verified to remain present within the MP2

and MP3-based microchannels after bonding. This was determined by an increase in the μ_{eo} measured *via* a current monitoring method, compared to native PDMS-based microchannel. In addition, the carbodiimide coupling of the carboxyl groups with Lucifer Yellow CH dye showed yellow fluorescence within the microchannel, in contrast to the microchannel made from native PDMS.

In summary, PDMS surfaces were successfully functionalized with carboxyl groups using three different techniques (Chapter 3, 4 and 5), which rendered PDMS more practical for analytical applications, such as DNA hybridization and cocaine detection. The carboxyl groups remained within the modified PDMS-based microchannels after bonding and were demonstrated to be available for amino-terminated molecular coupling. This approach will allow for further modification and subsequent applications, such as biomolecular separations, immunoassays and cell culturing.

8.2 Future work

Future work arising from the thermal assisted hydrosilylation surface modification method could include optimization of the PDMS base-to-curing agent ratio to obtain the maximum available SiH groups for hydrosilylation with UDA. Aside from UDA, other olefins with various functional groups could be another focus for future work.

In addition, the thermal-assisted hydrosilylation surface modification method requires longer treatment times compared with the plasma treatment method in this thesis. However, this method may be enhanced by improving the reaction rate. This requires future detailed kinetic studies into the bonding reaction between the UDA and the PDMS surface. If the kinetic study proves that the reaction is diffusion controlled, then the treatment time may be drastically shortened by, for example, agitation.

Future work could be carried out on the combination of Soxhlet-extraction and plasma treatment. Surface modification could include introducing other functional groups onto the PDMS surface by using other plasma sources. Futher investigation of the surface topography after different treatment times is also desirable, as this will be helpful in undertanding how the AAc molecules are deposited onto the surface.

Further applications of the three modified PDMS surfaces and the microfluidic devices based on these modified PDMS fabricated in this thesis could also be pursued. Solid-phase polymerase chain reactions (SP-PCRs) might be a good choice for the next step due to the proved successful attachment of oligonucleotides onto these modified PDMS surface. In addition, the quantitative determination of the functional groups on these modified PDMS surfaces will also need to be investigated.

Future work with cocaine detection using the MBET-based aptamer sensor should focus on the optimization of the detection time. In addition, future work to fully understand the reason why this sensor showed a better detection limit, compared to some other reported sensors, is also desirable.

Future work arising from chapter 7 should focus on the applications of these fabricated microfluidic devices. DNA hybridization could be a good choice for the first application in microchannels, due to the successful performance on open PDMS surfaces.

REFERENCES

[1] Zhou, J. W., Ellis, A. V., Voelcker, N. H., *Electrophoresis* 2010, *31*, 2-16.

[2] Zhou, J. W., Khodakov, D. A., Ellis, A. V., Voelcker, N. H., *Electrophoresis* 2012, *33,* 89-104.

[3] Simpson, P. C., Roach, D., Woolley, A. T., Thorsen, T., Johnston, R., Sensabaugh, G. F., Mathies, R. A., *Proc. Natl. Acad. Sci. USA.* 1998, *95*, 2256-2261.

[4] Liu, Y., Ganser, D., Schneider, A., Liu, R., Grodzinski, P., Kroutchinina, N., *Anal. Chem.* 2001, *73*, 4196-4201.

[5] Chen, X., Cui, D. F., Wang, L., Wang, M., Zhao, Q., *Int. J. Nonlin. Sci. Num.* 2002, *3*, 211-214.

[6] Lee, S. J., Lee, S. Y., *Appl. Microbiol. Biotechnol.* 2004, *64*, 289-299.

[7] Toriello, N. M., Liu, C. N., Mathies, R. A., *Anal. Chem.* 2006, *78*, 7997-8003.

[8] Kim, S., Chen, L. X., Lee, S., Seong, G. H., Choo, J., Lee, E. K., Oh, C. H., *Anal. Sci.* 2007, *23*, 401-405.

[9] Heyries, K. A., Loughran, M. G., Hoffmann, D., Homsy, A., Blum, L. J., Marquette, C. A., *Biosens. Bioelectron.* 2008, *23*, 1812-1818.

[10] Liu, H. B., Ramalingam, N., Jiang, Y., Dai, C. C., Hui, K. M., Gong, H. Q., *Sens. Actuator B-Chem.* 2009, *135*, 671-677.

[11] Erickson, D., Li, D. Q., *Anal. Chim. Acta* 2004, *507*, 11-26.

[12] Henares, T. G., Mizutani, F., Hisamoto, H., *Anal. Chim. Acta* 2008, *611*, 17-30.

[13] Liu, Y. J., Rauch, C. B., *Anal. Biochem.* 2003, *317*, 76-84.

[14] Swickrath, M. J., Shenoy, S., Mann, J. A., Belcher, J., Kovar, R., Wnek, G. E., *Microfluid. Nanofluid.* 2008, *4*, 601-611.

[15] Hashimoto, M., Barany, F., Soper, S. A., *Biosens. Bioelectron.* 2006, *21*, 1915-1923.

[16] Kempitiya, A., Borca-Tasciuc, D. A., Mohamed, H. S., Hella, M. M., *Appl. Phys. Lett.* 2009, *94*, 064106.

[17] Lee, G. B., Chen, S. H., Huang, G. R., Sung, W. C., Lin, Y. H., *Sens. Actuator B-Chem.* 2001, *75*, 142-148.

[18] Wang, Y., Vaidya, B., Farquar, H. D., Stryjewski, W., Hammer, R. P., McCarley, R. L., Soper, S. A., *et al.*, *Anal. Chem.* 2003, *75*, 1130-1140.

[19] Hu, S. W., Ren, X. Q., Bachman, M., Sims, C. E., Li, G. P., Allbritton, N., *Anal. Chem.* 2002, *74*, 4117-4123.

[20] Wang, B., Abdulali-Kanji, Z., Dodwell, E., Horton, J. H., Oleschuk, R. D., *Electrophoresis* 2003, *24*, 1442-1450.

[21] Leclerc, E., Sakai, Y., Fujii, T., *Biotechnol. Prog.* 2004, *20*, 750-755.

[22] García, C. D., Dressen, B. M., Henderson, A., Henry, C. S., *Electrophoresis* 2005, *26*, 703-709.

[23] Zhang, Q., Xu, J. J., Chen, H. Y., *Electrophoresis* 2006, *27*, 4943-4951.

[24] Mehta, G., Kiel, M. J., Lee, J. W., Kotov, N., Linderman, J. J., Takayama, S., *Adv. Funct. Mater.* 2007, *17*, 2701-2709.

[25] Liang, R. P., Gan, G. H., Qiu, J. D., *J. Sep. Sci.* 2008, *31*, 2860-2867.

[26] Wu, M. H., *Surf. Interface Anal.* 2009, *41*, 11-16.

[27] Mata, A., Fleischman, A. J., Roy, S., *Biomed. Microdevices* 2005, *7*, 281-293.

[28] van Poll, M. L., Zhou, F., Ramstedt, M., Hu, L., Huck, W. T. S., *Angew. Chem. Int. Ed. Engl.* 2007, *46*, 6634-6637.

[29] Vickers, J. A., Caulum, M. M., Henry, C. S., *Anal. Chem.* 2006, *78*, 7446-7452.

[30] Barbier, V., Tatoulian, M., Li, H., Arefi-Khonsari, F., Ajdari, A., Tabeling, P., *Langmuir* 2006, *22*, 5230-5232.

[31] Zhou, J. W., Ellis, A. V., Voelcker, N. H., *J. Nanosci. Nanotechno.* 2010, *10*, 7266-7270.

[32] Ren, X., Bachman, M., Sims, C., Li, G. P., Allbritton, N., *J. Chromatogr. B* 2001, *762*, 117-125.

[33] Martin, I. T., Dressen, B., Boggs, M., Liu, Y., Henry, C. S., Fisher, E. R., *Plasma Process. Polym.* 2007, *4*, 414-424.

[34] Tan, H. M. L., Fukuda, H., Akagi, T., Ichiki, T., *Thin Solid Films* 2007, *515*, 5172-5178.

[35] Tan, S. H., Nguyen, N. T., Chua, Y. C., Kang, T. G., *Biomicrofluidics* 2010, *4*, 032204.

[36] Priest, C., Gruner, P. J., Szili, E. J., Al-Bataineh, S. A., Bradley, J. W., Ralston, J., Steele, D. A.*, et al.*, *Lab Chip* 2011, *11*, 541-544.

[37] Efimenko, K., Wallace, W. E., Genzer, J., *J. Colloid Interface Sci.* 2002, *254*, 306-315.

[38] Chen, H. Y., Lahann, J., *Anal. Chem.* 2005, *77*, 6909-6914.

[39] Chen, H. Y., Elkasabi, Y., Lahann, J., *J. Am. Chem. Soc.* 2006, *128*, 374-380.

[40] Chen, H. Y., McClelland, A. A., Chen, Z., Lahann, J., *Anal. Chem.* 2008, *80*, 4119-4124.

[41] Xu, J. J., Gleason, K. K., *Chem. Mater.* 2010, *22*, 1732-1738.

[42] Niu, Z. Q., Gao, F., Jia, X. Y., Zhang, W. P., Chen, W. Y., Qian, K. Y., *Colloid Surf. A-Physicochem. Eng. Aspects* 2006, *272*, 170-175.

[43] Feng, J. T., Zhao, Y. P., *Biomed. Microdevices* 2008, *10*, 65-72.

[44] Zhang, Q., Xu, J. J., Liu, Y., Chen, H. Y., *Lab Chip* 2008, *8*, 352-357.

[45] Patrito, N., McLachlan, J. M., Faria, S. N., Chan, J., Norton, P. R., *Lab Chip* 2007, *7*, 1813-1818.

[46] Wang, A. J., Xu, J. J., Zhang, Q., Chen, H. Y., *Talanta* 2006, *69*, 210-215.

[47] Qiu, J. D., Hu, P. F., Liang, R. P., *Anal. Sci.* 2007, *23*, 1409-1414.

[48] Wang, A. J., Xu, J. J., Chen, H. Y., *Electroanal.* 2007, *19*, 674-680.

[49] Wang, W., Zhao, L., Zhou, F., Zhu, J. J., Zhang, J. R., *Talanta* 2007, *73*, 534-539.

[50] Wang, A. J., Xu, J. J., Chen, H. Y., *J. Chromatogr. A* 2006, *1107*, 257-264.

[51] Wang, A. J., Xu, J. J., Chen, H. Y., *J. Chromatogr. A* 2007, *1147*, 120-126.

[52] Schmolke, H., Demming, S., Edlich, A., Magdanz, V., Büttgenbach, S., Franco-Lara, E., Krull, R.*, et al.*, *Biomicrofluidics* 2010, *4*, 044113.

[53] Schrott, W., Nebyla, M., Přibyl, M., Šnita, D., *Biomicrofluidics* 2011, *5*, 014101.

[54] Kuo, C. H., Wang, J. H., Lee, G. B., *Electrophoresis* 2009, *30*, 3228-3235.

[55] Bauer, W. A. C., Fischlechner, M., Abell, C., Huck, W. T. S., *Lab Chip* 2010, *10*, 1814-1819.

[56] Roman, G. T., Hlaus, T., Bass, K. J., Seelhammer, T. G., Culbertson, C. T., *Anal. Chem.* 2005, *77*, 1414-1422.

[57] Roman, G. T., Culbertson, C. T., *Langmuir* 2006, *22*, 4445-4451.

[58] Orhan, J. B., Parashar, V. K., Flueckiger, J., Gijs, M. A. M., *Langmuir* 2008, *24*, 9154-9161.

[59] Abate, A. R., Lee, D., Do, T., Holtze, C., Weitz, D. A., *Lab Chip* 2008, *8*, 516-518.

[60] Slentz, B. E., Penner, N. A., Lugowska, E., Regnier, F., *Electrophoresis* 2001, *22*, 3736-3743.

[61] Sui, G. D., Wang, J. Y., Lee, C. C., Lu, W. X., Lee, S. P., Leyton, J. V., Wu, A. M*., et al.*, *Anal. Chem.* 2006, *78*, 5543-5551.

[62] Sofla, A. Y. N., Martin, C., *Lab Chip* 2010, *10*, 250-253.

[63] Roman, G. T., Carroll, S., McDaniel, K., Culbertson, C. T., *Electrophoresis* 2006, *27*, 2933-2939.

[64] Roman, G. T., McDaniel, K., Culbertson, C. T., *Analyst* 2006, *131*, 194-201.

[65] Dou, Y. H., Bao, N., Xu, J. J., Meng, F., Chen, H. Y., *Electrophoresis* 2004, *25*, 3024-3031.

[66] Kim, J. A., Lee, J. Y., Seong, S., Cha, S. H., Lee, S. H., Kim, J. J., Park, T. H., *Biochem. Eng. J.* 2006, *29*, 91-97.

[67] Huang, B., Wu, H. K., Kim, S., Zare, R. N., *Lab Chip* 2005, *5*, 1005-1007.

[68] He, T., Liang, Q., Zhang, K., Mu, X., Luo, T., Wang, Y., Luo, G., *Microfluid. Nanofluid.* 2011, *10*, 1289-1298.

[69] Liu, B. F., Ozaki, M., Hisamoto, H., Luo, Q. M., Utsumi, Y., Hattori, T., Terabe, S., *Anal. Chem.* 2005, *77*, 573-578.

[70] Kang, J. Z., Yan, J. L., Liu, J. F., Qiu, H. B., Yin, X. B., Yang, X. R., Wang, E. K., *Talanta* 2005, *66*, 1018-1024.

[71] Xu, Y. H., Li, J., Wang, E. K., *J. Chromatogr. A* 2008, *1207*, 175-180.

[72] Xu, Y. H., Jiang, H., Wang, E. K., *Electrophoresis* 2007, *28*, 4597-4605.

[73] Qin, M., Wang, L. K., Feng, X. Z., Yang, Y. L., Wang, R., Wang, C., Yu, L*., et al.*, *Langmuir* 2007, *23*, 4465-4471.

[74] Wang, R., Yang, Y. L., Qin, M., Wang, L. K., Yu, L., Shao, B., Qiao, M. Q*., et al.*, *Chem. Mater.* 2007, *19*, 3227-3231.

[75] Mikhail, A. S., Ranger, J. J., Liu, L. H., Longenecker, R., Thompson, D. B., Sheardown, H. D., Brook, M. A., *J. Biomater. Sci.-Polym. Ed.* 2010, *21*, 821-842.

[76] Alauzun, J. G., Young, S., D'Souza, R., Liu, L., Brook, M. A., Sheardown, H. D., *Biomaterials* 2010, *31*, 3471-3478.

[77] Zhou, J. W., Voelcker, N. H., Ellis, A. V., *Biomicrofluidics* 2010, *4*, 046504.

[78] van Poll, M. L., Khodabakhsh, S., Brewer, P. J., Shard, A. G., Ramstedt, M., Huck, W. T. S., *Soft Matter* 2009, *5*, 2286-2293.

[79] Wang, B., Oleschuk, R. D., Horton, J. H., *Langmuir* 2005, *21*, 1290-1298.

[80] Miyaki, K., Zeng, H. L., Nakagama, T., Uchiyama, K., *J. Chromatogr. A* 2007, *1166*, 201-206.

[81] Wang, A. J., Feng, J. J., Fan, J., *J. Chromatogr. A* 2008, *1192*, 173-179.

[82] Wang, B., Chen, L., Abdulali-Kanji, Z., Horton, J. H., Oleschuk, R. D., *Langmuir* 2003, *19*, 9792-9798.

[83] Matsubara, Y., Murakami, Y., Kobayashi, M., Morita, Y., Tamiya, E., *Biosens. Bioelectron.* 2004, *19*, 741-747.

[84] Diaz-Quijada, G. A., Wayner, D. D. M., *Langmuir* 2004, *20*, 9607-9611.

[85] Wu, D. P., Zhao, B. X., Dai, Z. P., Qin, J. H., Lin, B. C., *Lab Chip* 2006, *6*, 942-947.

[86] Zhang, Z. W., Feng, X. J., Luo, Q. M., Liu, B. F., *Electrophoresis* 2009, *30*, 3174-3180.

[87] Moorcroft, M. J., Meuleman, W. R. A., Latham, S. G., Nicholls, T. J., Egeland, R. D., Southern, E. M., *Nucleic Acids Res.* 2005, *33*, *e*75.

[88] Zhang, Z. W., Feng, X. J., Xu, F., Liu, X., Liu, B. F., *Electrophoresis* 2010, *31*, 3129-3136.

[89] Séguin, C., McLachlan, J. M., Norton, P. R., Lagugné-Labarthet, F., *Appl. Surf. Sci.* 2010, *256*, 2524-2531.

[90] Cortese, G., Martina, F., Vasapollo, G., Cingolani, R., Gigli, G., Ciccarella, G., *J. Fluorine Chem.* 2010, *131*, 357-363.

[91] Schneider, M. H., Willaime, H., Tran, Y., Rezgui, F., Tabeling, P., *Anal. Chem.* 2010, *82*, 8848-8855.

[92] Liao, C. Y., Su, Y. C., *Biomed. Microdevices* 2010, *12*, 125-133.

[93] Lin, H. H., Chang, S. C., Su, Y. C., *Microfluid. Nanofluid.* 2010, *9*, 1091-1102.

[94] Ma, D., Chen, H. W., Li, Z. M., He, Q. H., *Biomicrofluidics* 2010, *4*, 044107.

[95] Hoffman, J. M., Ebara, M., Lai, J. J., Hoffman, A. S., Folch, A., Stayton, P. S., *Lab Chip* 2010, *10*, 3130-3138.

[96] Fiddes, L. K., Chan, H. K. C., Lau, B., Kumacheva, E., Wheeler, A. R., *Biomaterials* 2010, *31*, 315-320.

[97] Wu, H. L., Zhai, J. J., Tian, Y. P., Lu, H. J., Wang, X. Y., Jia, W. T., Liu, B. H.*, et al.*, *Lab Chip* 2004, *4*, 588-597.

[98] Hu, S. W., Ren, X. Q., Bachman, M., Sims, C. E., Li, G. P., Allbritton, N. L., *Anal. Chem.* 2004, *76*, 1865-1870.

[99] Ebara, M., Hoffman, J. M., Stayton, P. S., Hoffman, A. S., *Radiat. Phys. Chem.* 2007, *76*, 1409-1413.

[100] Sugiura, S., Imano, W., Takagi, T., Sakai, K., Kanamori, T., *Biosens. Bioelectron.* 2009, *24*, 1135-1140.

[101] Völcker, N., Klee, D., Höcker, H., Langefeld, S., *J. Mater. Sci-Mater. M.* 2001, *12*, 111-119.

[102] Xiao, D., Hui Zhang, Wirth, M., *Langmuir* 2002, *18*, 9971-9976.

[103] Xiao, D. Q., Van Le, T., Wirth, M. J., *Anal. Chem.* 2004, *76*, 2055-2061.

[104] Tugulu, S., Klok, H. A., *Macromol. Symp.* 2009, *279*, 103-109.

[105] Lillehoj, P. B., Wei, F., Ho, C. M., *Lab Chip* 2010, *10*, 2265-2270.

[106] Geissler, A., Vallat, M. F., Fioux, P., Thomann, J. S., Frisch, B., Voegel, J. C., Hemmerlé, J.*, et al.*, *Plasma Process. Polym.* 2010, *7*, 64-77.

[107] Yeh, P. Y., Rossi, N. A. A., Kizhakkedathu, J. N., Mu, C. A., *Microfluid. Nanofluid.* 2010, *9*, 199-209.

[108] Li, M., Kim, D. P., *Lab Chip* 2011, *11*, 1126-1131.

[109] Wu, D. P., Luo, Y., Zhou, X. M., Dai, Z. P., Lin, B. C., *Electrophoresis* 2005, *26*, 211-218.

[110] Xiao, Y., Yu, X. D., Wang, K., Xu, J. J., Huang, J., Chen, H. Y., *Talanta* 2007, *71*, 2048-2055.

[111] Makamba, H., Hsieh, Y. Y., Sung, W. C., Chen, S. H., *Anal. Chem.* 2005, *77*, 3971-3978.

[112] Sung, W. C., Chen, H. H., Makamba, H., Chen, S. H., *Anal. Chem.* 2009, *81*, 7967-7973.

[113] Makamba, H., Kim, J. H., Lim, K., Park, N., Hahn, J. H., *Electrophoresis* 2003, *24*, 3607-3619.

[114] Peterson, S. L., McDonald, A., Gourley, P. L., Sasaki, D. Y., *J. Biomed. Mater. Res. Part A* 2005, *72A*, 10-18.

[115] Bodas, D., Khan-Malek, C., *Sens. Actuat. B* 2007, *123*, 368-373.

[116] Hillborg, H., Ankner, J. F., Gedde, U. W., Smith, G. D., Yasuda, H. K., Wikström, K., *Polymer* 2000, *41*, 6851-6863.

[117] Hillborg, H., Gedde, U. W., *Polymer* 1998, *39*, 1991-1998.

[118] Bausch, G. G., Stasser, J. L., Tonge, J. S., Owen, M. J., *plasmas and polymers* 1998, *3*, 23-34.

[119] Ozdemir, M., Yurteri, C. U., Sadikoglu, H., *Crit. Rev. Food Sci. Nutr.* 1999, *39*, 457-477.

[120] Wong, I., Ho, C. M., *Microfluid. Nanofluid.* 2009, *7*, 291-306.

[121] Berdichevsky, Y., Khandurina, J., Guttman, A., Lo, Y. H., *Sens. Actuator B-Chem.* 2004, *97*, 402-408.

[122] Choy, K. L., *Prog. Mater. Sci.* 2003, *48*, 57-170.

[123] Lee, J. N., Park, C., Whitesides, G. M., *Anal. Chem.* 2003, *75*, 6544-6554.

[124] Wu, Z., Hjort, K., *Lab Chip* 2009, *9*, 1500-1503.

[125] Zhou, J., Yan, H., Ren, K., Dai, W., Wu, H., *Anal. Chem.* 2009, *81*, 6627-6632.

[126] Sharma, V., Dhayal, M., Govind, Shivaprasad, S. M., Jain, S. C., *Vacuum* 2007, *81*, 1094-1100.

[127] Schneider, M. H., Tran, Y., Tabeling, P., *Langmuir* 2011, *27*, 1232-1240.

[128] Cortese, B., Piliego, C., Viola, I., D'Amone, S., Cingolani, R., Gigli, G., *Langmuir* 2009, *25*, 7025-7031.

[129] Hattori, K., Sugiura, S., Kanamori, T., *Biotechnol. J.* 2010, *5*, 463-469.

[130] Mosadegh, B., Tavana, H., Lesher-Perez, S. C., Takayama, S., *Lab Chip* 2011, *11*, 738-742.

[131] Winton, B. R., Ionescu, M., Dou, S. X., Wexler, D., Alvarez, G. A., *Acta Mater.* 2010, *58*, 1861-1867.

[132] Shao, Y. P., Brook, M. A., *J. Mater. Chem.* 2010, *20*, 8548-8556.

[133] Thangawng, A. L., Swartz, M. A., Glucksberg, M. R., Ruoff, R. S., *Small* 2007, *3*, 132-138.

[134] Thorslund, S., Lindberg, P., Andrén, P. E., Nikolajeff, F., Bergquist, J., *Electrophoresis* 2005, *26*, 4674-4683.

[135] Sung, W. C., Huang, S. Y., Liao, P. C., Lee, G. B., Li, C. W., Chen, S. H., *Electrophoresis* 2003, *24*, 3648-3654.

[136] Wu, D. P., Qin, J. H., Lin, B. C., *Lab Chip* 2007, *7*, 1490-1496.

[137] Nakajima, H., Yagi, M., Kudo, Y., Nakagama, T., Shimosaka, T., Uchiyama, K., *Talanta* 2006, *70*, 122-127.

[138] Hu, G. Q., Gao, Y. L., Sherman, P. M., Li, D. Q., *Microfluid. Nanofluid.* 2005, *1*, 346-355.

[139] Jang, Y. H., Oh, S. Y., Park, J. K., *Enzyme Microb. Technol.* 2006, *39*, 1122-1127.

[140] Ko, S., Kim, B., Jo, S. S., Oh, S. Y., Park, J. K., *Biosens. Bioelectron.* 2007, *23*, 51-59.

[141] Xiang, Q., Hu, G. Q., Gao, Y. L., Li, D. Q., *Biosens. Bioelectron.* 2006, *21*, 2006-2009.

[142] Pereira, A. T., Novo, P., Prazeres, D. M. F., Chu, V., Conde, J. P., *Biomicrofluidics* 2011, *5*, 014102.

[143] Harris, D. C., *Quantitative chemical analysis,* W.H. Freeman, New York c1999.

[144] Landers, J. P., *Handbook of capillary electrophoresis,* CRC Press, Boca Raton c1994.

[145] Dodge, A., Brunet, E., Chen, S. L., Goulpeau, J., Labas, V., Vinh, J., Tabeling, P., *Analyst* 2006, *131*, 1122-1128.

[146] Wang, L., Sun, B., Ziemer, K. S., Barabino, G. A., Carrier, R. L., *J. Biomed. Mater. Res. A* 2010, *93A*, 1260-1271.

[147] Zhou, J., McInnes, S. J. P., Md Jani, A. M., Ellis, A. V., Voelcker, N. H., *Proceedings of the SPIE,* Melbourne 2008, *7267(726719),* 1-10.

[148] Olah, A., Hillborg, H., Vancso, G. J., *Appl. Surf. Sci.* 2005, *239*, 410-423.

[149] Hook. A. L., t*hesis 'Patterned and switchable surfaces for biomaterial applications',* Flinders Uni, Australia 2008.

[150] Fowkes, F. M., *Contact Angle, Wettability, and Adhesion*, Advanceds in Chemistry, ACS 1964.

[151] Kiuru, M., Alakoski, E*., Mater. Lett. 2*004, *58*, 2213-2216.

[152] Ma, M., Hill, R. M., Lowery, J. L., Fridrikh, S. V., Rutledge, G. C., *Langmuir* 2005, *21*, 5549-5554.

[153] Petronis, ar, nas, Berntsson, K., Gold, J., Gatenholm, P., J. *Biomater. Sci.-Polym. Ed.* 2000, *11*, 1051-1072.

[154] Barber, A. H., Cohen, S. R., Wagner, H. D., *Phys. Rev. Lett.* 2004, *92*, 186103.

[155] Kossen, N. W. F., Heertjes, P. M., *Chem. Eng. Sci.* 1965, *20*, 593-599.

[156] Kane, S. R., Ashby, P. D., Pruitt, L. A., *J. Biomed. Mater. Res. Part B* 2009, *91B*, 613-620.

[157] Schnyder, B., Lippert, T., Kotz, R., Wokaun, A., Graubner, V. M., Nuyken, O., *Surf. Sci.* 2003, *532*, 1067-1071.

[158] Elimelech, M., Chen, W. H., Waypa, J. J., *Desalination* 1994, *95*, 269-286.

[159] Hunter, R. J., Zeta potential in colloid science: principles and applications, Academic Press, London 1981.

[160] Karkhaneh, A., Mirzadeh, H., Ghaffariyeh, A. R., *J. Appl. Polym. Sci.* 2007, *105*, 2208-2217.

[161] Stone, H. A., Stroock, A. D., Ajdari, A., *Annu. Rev. Fluid Mech.* 2004, *36*, 381-411.

[162] Luo, Y. Q., Huang, B., Wu, H., Zare, R. N., *Anal. Chem.* 2006, *78*, 4588-4592.

[163] Morent, R., De Geyter, N., Leys, C., Gengernbre, L., Payen, E., *Surf. Interface Anal.* 2008, *40*, 597-600.

[164] Bodas, D., Khan-Malek, C., *Microelectron. Eng.* 2006, *83*, 1277-1279.

[165] Wang, D., Oleschuk, R. D., Horton, J. H., *Langmuir* 2008, *24*, 1080-1086.

[166] Elimelech, M., Omelia, C. R., *Colloid Surf.* 1990, *44*, 165-178.

[167] Sprague, E. D., Duecker, D. C., Larrabee, C. E., *J. Colloid Interface Sci.* 1983, *92*, 416-421.

[168] Asseline U., Thuong, N. T., Current Protocols in Nucleic Acid Chemistry 2002, Unit 4.10.

[169] Zhou, J. W., Ellis, A. V., Kobus, H., Voelcker, N. H., *Anal. Chim. Acta* 2012, *719,* 76-81.

[170] Seo, J., Lee, L. P., *Sens. Actuator B-Chem.* 2006, *119*, 192-198.

[171] Xiao, Y., Yu, X. D., Xu, J. J., Chen, H. Y., *Electrophoresis* 2007, *28*, 3302-3307.

[172] Gu, X. H., Yang, C. Q., *Res. Chem. Intermed.* 1998, *24*, 979-996.

[173] Vinod, T. P., Chang, J. H., Kim, J., Rhee, S. W., *B. Kerean Chem. Soc.* 2008, *29*, 799-804.

[174] Jung, J., Chen, L. X., Lee, S., Kim, S., Seong, G. H., Choo, J., Lee, E. K*., et al.*, *Anal. Bioanal. Chem.* 2007, *387*, 2609-2615.

[175] Jafari, R., Tatoulian, M., Morscheidt, W., Arefi-Khonsari, F., *React. Funct. Polym.* 2006, *66*, 1757-1765.

[176] Kim, H. T., Jeong, O. C., *Microelectron. Eng.* 2011, *88*, 2281-2285.

[177] Pinto, S., Alves, P., Matos, C. M., Santos, A. C., Rodrigues, L. R., Teixeira, J. A., Gil, M. H., *Colloid Surf. B-Biointerfaces* 2010, *81*, 20-26.

[178] Balakrisnan, B., Patil, S., Smela, E., *J. Micromech. Microeng.* 2009, *19*. 047002.

[179] Ritz, M. C., Lamb, R. J., Goldberg, S. R., Kuhar, M. J., *Science* 1987, *237*, 1219-1223.

[180] Avois, L., Robinson, N., Saudan, C., Baume, N., Mangin, P., Saugy, M., *Br. J. Sports Med.* 2006, *40*, 16-20.

[181] Ortuño, J., De La Torre, R., Segura, J., Camí, J., *J. Pharmaceut. Biomed.* 1990, *8*, 911-914.

[182] Stojanovic, M. N., de Prada, P., Landry, D. W., *J. Am. Chem. Soc.* 2000, *122*, 11547-11548.

[183] Stojanovic, M. N., de Prada, P., Landry, D. W., *J. Am. Chem. Soc.* 2001, *123*, 4928-4931.

[184] Shlyahovsky, B., Li, D., Weizmann, Y., Nowarski, R., Kotler, M., Willner, I., *J. Am. Chem. Soc.* 2007, *129*, 3814-3815.

[185] Zhang, C. Y., Johnson, L. W., *Anal. Chem.* 2009, *81*, 3051-3055.

[186] Zhang, J., Wang, L. H., Zhang, H., Boey, F., Song, S. P., Fan, C. H., *Small* 2010, *6*, 201-204.

[187] He, J. L., Wu, Z. S., Zhou, H., Wang, H. Q., Jiang, J. H., Shen, G. L., Yu, R. Q., *Anal. Chem.* 2010, *82*, 1358-1364.

[188] Wu, C. C., Yan, L., Wang, C. M., Lin, H. X., Wang, C., Chen, X., Yang, C. J., *Biosens. Bioelectron.* 2010, *25*, 2232-2237.

[189] Hilton, J. P., Nguyen, T. H., Pei, R. J., Stojanovic, M., Lin, Q., *Sens. Actuator A-Phys.* 2011, *166*, 241-246.

[190] Ma, C. P., Wang, W. S., Yang, Q., Shi, C., Cao, L. J., *Biosens. Bioelectron.* 2011, *26*, 3309-3312.

[191] Stojanovic, M. N., Landry, D. W., *J. Am. Chem. Soc.* 2002, *124*, 9678-9679.

[192] Liu, J. W., Lu, Y., *Angew. Chem.-Int. Edit.* 2006, *45*, 90-94.

[193] Liu, J. W., Mazumdar, D., Lu, Y., *Angew. Chem.-Int. Edit.* 2006, *45*, 7955-7959.

[194] Liu, J. W., Lee, J. H., Lu, Y., *Anal. Chem.* 2007, *79*, 4120-4125.

[195] Elbaz, J., Shlyahovsky, B., Li, D., Willner, I., *Chembiochem* 2008, *9*, 232-239.

[196] Zhang, J., Wang, L. H., Pan, D., Song, S. P., Boey, F. Y. C., Zhang, H., Fan, C. H., *Small* 2008, *4*, 1196-1200.

[197] Zhu, Z., Wu, C. C., Liu, H. P., Zou, Y., Zhang, X. L., Kang, H. Z., Yang, C. J.*, et al.*, *Angew. Chem.-Int. Edit.* 2010, *49*, 1052-1056.

[198] Xia, F., Zuo, X. L., Yang, R. Q., Xiao, Y., Kang, D., Vallee-Belisle, A., Gong, X.*, et al.*, *Proc. Natl. Acad. Sci. U. S. A.* 2010, *107*, 10837-10841.

[199] Du, Y., Li, B. L., Guo, S. J., Zhou, Z. X., Zhou, M., Wang, E. K., Dong, S. J., *Analyst* 2011, *136*, 493-497.

[200] Li, Y., Qi, H. L., Peng, Y., Yang, J., Zhang, C. X., *Electrochem. Commun.* 2007, *9*, 2571-2575.

[201] Li, T., Li, B. L., Dong, S. J., *Chem.-Eur. J.* 2007, *13*, 6718-6723.

[202] Yan, X. L., Cao, Z. J., Lau, C. W., Lu, J. Z., *Analyst* 2010, *135*, 2400-2407.

[203] Baker, B. R., Lai, R. Y., Wood, M. S., Doctor, E. H., Heeger, A. J., Plaxco, K. W., *J. Am. Chem. Soc.* 2006, *128*, 3138-3139.

[204] Li, X. X., Qi, H. L., Shen, L. H., Gao, Q., Zhang, C. X., *Electroanalysis* 2008, *20*, 1475-1482.

[205] White, R. J., Phares, N., Lubin, A. A., Xiao, Y., Plaxco, K. W., *Langmuir* 2008, *24*, 10513-10518.

[206] Sharon, E., Freeman, R., Tel-Vered, R., Willner, I., *Electroanalysis* 2009, *21*, 1291-1296.

[207] Zuo, X. L., Xiao, Y., Plaxco, K. W., *J. Am. Chem. Soc.* 2009, *131*, 6944-6945.

[208] Swensen, J. S., Xiao, Y., Ferguson, B. S., Lubin, A. A., Lai, R. Y., Heeger, A. J., Plaxco, K. W.*, et al.*, *J. Am. Chem. Soc.* 2009, *131*, 4262-4266.

[209] Golub, E., Pelossof, G., Freeman, R., Zhang, H., Willner, I., *Anal. Chem.* 2009, *81*, 9291-9298.

[210] Du, Y., Chen, C. G., Yin, J. Y., Li, B. L., Zhou, M., Dong, S. J., Wang, E. K., *Anal. Chem.* 2010, *82*, 1556-1563.

[211] Abelow, A. E., Schepelina, O., White, R. J., Vallee-Belisle, A., Plaxco, K. W., Zharov, I., *Chem. Commun.* 2010, *46*, 7984-7986.

[212] Hua, M., Tao, M. L., Wang, P., Zhang, Y. F., Wu, Z. S., Chang, Y. B., Yang, Y. H., *Anal. Sci.* 2010, *26*, 1265-1270.

[213] Zhang, H. X., Jiang, B. Y., Xiang, Y., Zhang, Y. Y., Chai, Y. Q., Yuan, R., *Anal. Chim. Acta* 2011, *688*, 99-103.

[214] Du, Y., Chen, C. G., Zhou, M., Dong, S. J., Wang, E. K., *Anal. Chem.* 2011, *83*, 1523-1529.

[215] Cai, Q. H., Chen, L. F., Luo, F., Qiu, B., Lin, Z. Y., Chen, G. N., *Anal. Bioanal. Chem.* 2011, *400*, 289-294.

[216] Chen, J. W., Jiang, J. H., Gao, X., Liu, G. K., Shen, G. L., Yu, R. Q., *Chem.-Eur. J.* 2008, *14*, 8374-8382.

[217] Neumann, O., Zhang, D. M., Tam, F., Lal, S., Wittung-Stafshede, P., Halas, N. J., *Anal. Chem.* 2009, *81*, 10002-10006.

[218] Sanles-Sobrido, M., Rodríguez-Lorenzo, L., Lorenzo-Abalde, S., González-Fernández, Á.,

Correa-Duarte, M. A., Alvarez-Puebla, R. A., Liz-Marzán, L. M., *Nanoscale* 2009, *1*, 153-158.
[219] Munoz, E. M., Lorenzo-Abalde, S., González-Fernández, Á., Quintela, O., Lopez-Rivadulla, M., Riguera, R., *Biosens. Bioelectron.* 2011, *26*, 4423-4428.
[220] Hunt, W. D., Stubbs, D. D., Lee, S. H., *Proc. IEEE* 2003, *91*, 890-901.
[221] Stubbs, D. D., Lee, S. H., Hunt, W. D., *Anal. Chem.* 2003, *75*, 6231-6235.
[222] Ellington, A. D., Szostak, J. W., *Nature* 1990, *346*, 818-822.
[223] Tuerk, C., Gold, L., *Science* 1990, *249*, 505-510.
[224] Madru, B., Chapuis-Hugon, F., Peyrin, E., Pichon, V., *Anal. Chem.* 2009, *81*, 7081-7086.
[225] Freeman, R., Li, Y., Tel-Vered, R., Sharon, E., Elbaz, J., Willner, I., *Analyst* 2009, *134*, 653-656.
[226] McDonald, J. C., Duffy, D. C., Anderson, J. R., Chiu, D. T., Wu, H. K., Schueller, O. J. A., Whitesides, G. M., *Electrophoresis* 2000, *21*, 27-40.
[227] Zhang, C., Xu, J., Ma, W., Zheng, W., *Biotechnol. Adv.* 2006, *24*, 243-284.
[228] McDonald, J. C., Whitesides, G. M., *Accounts Chem. Res.* 2002, *35*, 491-499.
[229] Bhattacharya, S., Datta, A., Berg, J. M., Gangopadhyay, S., *J. Microelectromech. Syst.* 2005, *14*, 590-597.
[230] Maji, D., Lahiri, S. K., Das, S., *Surf. Interface Anal.* 2012, *44,* 62-69.
[231] Sellin, N., Campos, J. S. d. C., *Mater. Res.* 2003, *6*, 163-166.